CHALMERS
UNIVERSITY OF TECHNOLOGY

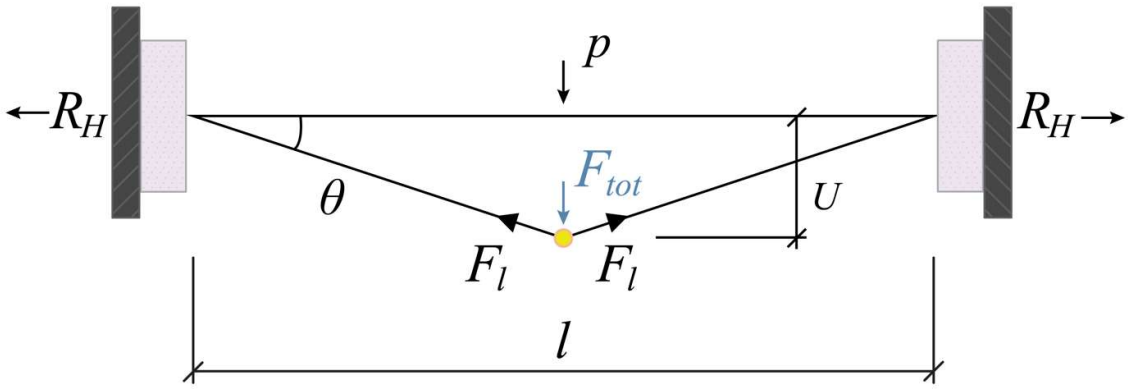

Numerical Modelling of Tensile Membrane action in Reinforced Concrete Beams

Master's thesis in the master's Program Structural Engineering and Building Technology

GIBRAN DIAB
SIWAKORN SANCHUENSAKUL

DEPARTMENT OF ARCHITECTURE AND CIVIL ENGINEERING
DIVISION OF STRUCTURAL ENGINEERING AND BUILDING TECHNOLOGY

CHALMERS UNIVERSITY OF TECHNOLOGY
Gothenburg, Sweden 2024
www.chalmers.se

MASTER'S THESIS ACEX30

Numerical Modelling of Tensile Membrane Action in Reinforced Concrete Beams

Master's Thesis in the Master's Programme Structural Engineering and Building Technology

GIBRAN DIAB
SIWAKORN SANCHUENSAKUL

Department of Architecture and Civil Engineering
Division of Structural Engineering
Concrete Structures
CHALMERS UNIVERSITY OF TECHNOLOGY
Göteborg, Sweden 2024

Numerical Modelling of Tensile Membrane Action in Reinforced Concrete Beams

Master's Thesis in the Master's Programme Structural Engineering and Building Technology

GIBRAN DIAB

SIWAKORN SANCHUENSAKUL

Examensarbete ACEX30
Institutionen för arkitektur och samhällsbyggnadsteknik
Chalmers tekniska högskola, 2024

Department of Architecture and Civil Engineering
Division of Structural Engineering and Building Technology
Concrete Structures
Chalmers University of Technology
SE-412 96 Göteborg
Sweden
Telephone: + 46 (0)31-772 1000

Cover:
A simplified schematic illustration of the tensile membrane action mechanism, characterized by large deformations and the presence of sufficient lateral restraints at the beam supports.

Department of Architecture and Civil Engineering
Göteborg, Sweden, 2024

Numerical Modelling of Tensile Membrane Action in Reinforced Concrete Beams

Master's thesis in the Master's Programme Structural Engineering and Building Technology

GIBRAN DIAB

SIWAKORN SANCHUENSAKUL

Department of Architecture and Civil Engineering
Division of Structural Engineering and Building Technology
Concrete Structures
Chalmers University of Technology

ABSTRACT

Conventional design practices for reinforced concrete (RC) beams primarily focus on ensuring adequate flexural capacity. However, the ultimate load-carrying capacity and deformation limits of these beams can be significantly enhanced through the development of membrane actions if sufficient lateral restraints are provided. Membrane actions include two distinct mechanisms: compressive membrane action (CMA) and tensile membrane action (TMA) or catenary action.

CMA is activated sequentially after the flexural action, as deformations continue to increase. In this stage, the beam's lateral expansion is restrained, inducing compressive membrane forces that enhance the beam's load-bearing capacity. As the RC beams undergo large deformations, the compressive forces shift to tensile forces. At this certain point, TMA is activated, and the reinforcement bars become the load-carrying mechanism for the RC beams.

This thesis investigates the numerical modelling of TMA in RC beams subjected to increasing load at the middle joint of the beam under a static loading condition. An extensive literature review and analysis of previous experimental works were studied to gain insights into TMA. One of the prior experiments was selected to verify the results obtained from the Finite Element program ABAQUS and ensure its capability to accurately capture the TMA behaviour.

In ABAQUS, beam and truss elements were used to model the concrete and reinforcing steel, respectively. Full interaction between concrete and reinforcement bars was assumed. Concrete damaged plasticity model was applied for the concrete, on the other hand, plasticity model was applied for the reinforcing steel.

The results obtained from ABAQUS were compared with the reference experiment before performing a parametric study to explore various factors that could influence the development and behaviour of TMA, including horizontal stiffness, span-depth ratio, and other relevant parameters.

In general, the numerical models demonstrated good agreement with the reference experiment in terms of the load-midspan deflection relationship. Once the numerical models were validated, parametric studies were conducted.

Keywords: reinforced concrete, compressive membrane action, tensile membrane action, catenary action, static loading condition, ABAQUS, concrete damage plasticity

Numerisk Modellering av Spänningsmembranverkan i Armerade Betongbalkar

Examensarbete i Structural Engineering and Building Technology

GIBRAN DIAB

SIWAKORN SANCHUENSAKUL

Arkitektur och Samhällsbyggnadsteknik
Avdelningen för Konstruktionsteknik
Betongbyggnad
Chalmers Tekniska Högskola

SAMMANFATTNING

Konventionella konstruktionsmetoder för armerade betongbalkar (RC) fokuserar främst på att säkerställa tillräcklig böjkapacitet. Böjkapacitet i brottgränstillstånd och deformationsgränserna för dessa balkar kan emellertid avsevärt förbättras genom utvecklingen av membranåtgärder om tillräckliga laterala begränsningar tillhandahålls. Membranåtgärderna innefattar två distinkta mekanismer: tryckmembranverkan (CMA) och dragmembranverkan (TMA).

CMA aktiveras sekventiellt efter böjverkan, eftersom deformationerna fortsätter att öka. I detta skede begränsas balkens laterala expansion, vilket inducerar tryckmembrankrafter som förbättrar balkens bärförmåga. När de betongbalkarna utsätts för stora deformationer, övergår tryckkrafterna till dragkrafter. Vid denna tidpunkt aktiveras TMA, och armeringsjärnen bär hela lasten i balken.

Detta examensarbete undersöker numeriska modelleringen av TMA i betongbalkar som utsätts för ökad belastning på balkens mittled under en statisk belastning. En omfattande litteraturöversikt och analys av tidigare experimentella studier har genomförts för att få ökad förståelse för TMA. Ett av de experimenten valdes för att verifiera resultaten från finita element-programmet ABAQUS och säkerställa dess förmåga att noggrant fånga TMA-beteendet.

I ABAQUS användes 1D balk- och fackverkselement för att modellera betongen respektive armeringsstålet. Full interaktion mellan betongen och armeringsjärnen antogs. En betongskademodell för plasticitet tillämpades för betongen, medan en plasticitetsmodell användes för armeringsstålet.

Resultat från ABAQUS jämfördes med referensexperimentet innan de parametriska studierna utfördes för att undersöka olika faktorer som kan påverka utvecklingen och beteendet hos TMA, inklusive horisontell styvhet, förhållande spännvidd och höjd, samt andra relevanta parametrar.

Generellt sett visade de numeriska modellerna en god överensstämmelse med referensexperimentet vad gäller last-mittledsförskjutning. När de numeriska modellerna hade validerats, genomfördes parametriska studier.

Nyckelord: armerad betong, tryckmembranverkan, dragmembranverkan, statisk belastning, ABAQUS, betong skademodell med plasticitet.

CONTENTS

PREFACE

Numerical modelling of tensile membrane action in reinforced concrete beams has been investigated in this Master's thesis. An extensive literature review and analysis of previous experimental studies were conducted. One of the prior experiments was selected as a benchmark to validate the results obtained from the Finite Element program and ensure its capability to accurately capture the tensile membrane action mechanism. Subsequently, parametric studies were performed to explore various factors that could influence the development and behaviour of tensile membrane action.

The thesis was developed from January to June 2024. The thesis was carried out at the Division of Structural Engineering at Chalmers and in collaboration with Norconsult. The thesis was supervised by Fabio Lozano Mendoza and Morgan Johansson and examined by Joosef Leppänen.

We express our sincere gratitude to Fabio Lozano Mendoza and Morgan Johansson for their valuable supervision, guidance, and continuous support throughout the course of this Master's thesis. Their expertise and insights have been important in shaping the quality of our work. We would also like to thank Joosef Leppänen for his support and encouragement throughout the course of the thesis.

Finally, we would like to express our gratitude to each other for the collaborative efforts, constructive exchange of opinions, and shared knowledge that have contributed to the successful completion of this Master's thesis.

Göteborg June 2024

Gibran Diab

Siwakorn Sanchuensakul

NOTATIONS

Abbreviations

1D	One-dimensional
3D	Three-dimensional
CDP	Concrete damaged plasticity
CMA	Compressive membrane action
DIF	Dynamic increase factor
EC	Eurocode
FE	Finite element
FEA	Finite element analysis
FEM	Finite element model
FIB	Fédération internationale du béton
LVDTs	Linear variable differential transformations
MJD	Middle joint displacement
RC	reinforced concrete
TMA	tensile membrane action
UFC	Unified facilities criteria

Roman upper case letters

A_c	Area of concrete in compression zone
$A_{c,ef}$	Effective area of concrete in tension zone
A_g	Gross area of concrete
A_s	Area of tensile reinforcing steel
A_{sc}	Area of compressive reinforcing steel
E	Modulus of elasticity
E_c	Compressive modulus of elasticity of concrete
E_{c0}	Initial elastic modulus of undamaged concrete
E_{ci}	Tangent modulus of elasticity of concrete
E_{cm}	Compressive modulus of elasticity of concrete; mean value
E_s	Modulus of elasticity of reinforcing steel;
F_c	Compressive force in concrete
F_s	Tensile force in reinforcing steel
F_{sc}	Compressive force in reinforcing steel
G_f	Fracture energy
K	Horizontal stiffness
L	Specimen length
L_{cr}	Critical fracture zone
M_f	Field moment or span moment
M_s	Support moment
N_t	Axial force
P_f	Flexural capacity load

Roman lower case letters

b	Width of beam cross-section
c	Concrete cover
d	Distance to center of tensile reinforcement layer; measured from compression edge of concrete, damage factor
d'	Distance to center of compressive reinforcement layer; measured from compression edge of concrete
e	eccentricity
f	Strength of concrete
f_c	Compressive cylinder strength of concrete
f_{cd}	Compressive cylinder strength of concrete; designed value
f_{ck}	Compressive cylinder strength of concrete; characteristic value
f_{cm}	Compressive cylinder strength of concrete; mean value
f_{ct}	Tensile strength of concrete
f_{ctm}	Tensile strength of concrete; mean value
$f_{ctm,sp}$	Splitting tensile strength of concrete; mean value
f_y	Yield strength of reinforcing steel
f_{yd}	Yield strength of reinforcing steel; designed value
f_{yd}'	Yield strength of compressive reinforcing steel; designed value
f_{yk}	Yield strength of reinforcing steel; characteristic value
f_u	Ultimate tensile strength of reinforcing steel
h	Height of beam cross-section
h_w	Crack band width
$h_{c,ef}$	Effective height of concrete
k_c	Ratio of the second stress invariant on the tensile meridian
l_n	Clear span length
s^{-1}	Strain rate
s_{rm}	Mean crack distance
$s_{r,max}$	Maximum crack distance
u	Deformation or deflection
w	Crack width
x	Distance to neutral axis from compression edge of concrete

Greek letters

ε	Strain
β_R	Stress block factor for the location of the stress resultant
α_R	Stress block factor for the average stress
σ	Stress
μ	Viscosity parameter
ε_c	Compressive strain of concrete
$\varepsilon_{rupture}$	Rupture strain of reinforcing steel
ε_s	Strain of tensile reinforcing steel
ε_{sc}	Strain of compressive reinforcing steel
ε_y	Yield strain of reinforcing steel
ε_u	Ultimate strain of reinforcing steel
ε_{c1}	Compressive strain at peak stress of concrete
ε_{cr}	Cracking strain of concrete
ε_{ct}	Tensile strain of concrete

ε_{cu}	Ultimate compressive strain of concrete at failure
ε_{el}	Elastic strain
ε_{eng}	Engineering strain
ε_{in}	Inelastic strain
ε_{pl}	Plastic strain
ε_{true}	True strain
ε_{uk}	Ultimate reinforcing steel strain
σ_{bo}	Initial equibiaxial compressive yield stress
σ_{co}	Initial uniaxial compressive yield stress
σ_{ct}	Tensile stress of concrete
σ_{eng}	Engineering stress
σ_{true}	True stress
φ	Dilation angle
θ	Rotation
θ_{pl}	Plastic rotation
ϕ	Reinforcing steel diameter
$\rho_{\rho,eff}$	Effective reinforcement ratio
γ_c	Partial factor of concrete
γ_s	Partial factor of reinforcing steel
Δ	Deformation at tensile membrane action capacity

Index

c	Concrete
d	Designed value
cube	Cubic strength of concrete
el	Elastic
I	State I
II	State II
III	State III
in	Inelastic
k	Characteristic value
m	Mean value
pl	Plastic
u	Ultimate
y	Yield

1 Introduction

1.1 Background

The use of reinforced concrete (RC) has been widespread in various structures worldwide, for example, residential buildings, offices, etc. When it comes to RC beams, in typical design scenarios, the structural analysis and design of RC beams are typically based on their ultimate bending capacity. However, in case of accidental design scenarios (e.g., blast loading or progressive collapse), relying only on the ultimate bending capacity may lead to underestimation of the load capacity and deformation capacity of laterally restrained RC beams. This is because the effects of axial forces in the plane, compressive membrane action (CMA) and tensile membrane action (TMA)[1] are not considered. In this thesis, the term *catenary action* is used interchangeably with the term tensile membrane action.

When subjected to transverse loading, RC beams undergo deflection under the applied loads. As the beams deform, the tension face of the concrete cracks and the reinforcement bars are subjected to stretching. In general, the strains on the compression face are lower than the tension face. Therefore, the net tensile strain at the mid-depth causes the beam to elongate, leading to outward lateral displacements, this induces CMA in the plane of RC beams if supports are restrained against outward movement, and it provides ultimate flexural load higher than failure load calculated from yield line theory.

After CMA reaches the peak load, the effect of CMA declines with further deflection rapidly. As RC beams continues to deflect, there comes a critical point where the membrane forces shift from compression to tension. This transition occurs after the concrete has crushed at the compression zone, leaving only the reinforcement bars to carry the applied load. Catenary action develops afterwards as a result of large displacements, and it helps to stabilise the beams and increase the load capacity until the reinforcement bars begin to fracture.

To achieve catenary action, lateral restraint at the supports should be provided and it is important to ensure those supports have sufficient capacity to carry the enhanced reaction forces following the development of catenary action at large deflections. Furthermore, the use of reinforcement bars with high ductility is favourable to utilise the catenary action. Catenary action might have a substantial influence on the structure's ability to delay accidental design load cases.

In order to simulate and analyse the catenary action of RC beams under various boundary conditions, finite element analysis (FEA) offers the ability to capture non-linear behaviour. It allows for efficient investigation of different design parameters, and provides insights into deformations that extend beyond the capabilities of analytical analysis.

1.2 Aim and goals

The aim of this thesis is to gain a better understanding of catenary action of RC structures and to utilize the FEM to simulate catenary action in RC beams subjected to accidental design situations, such as progressive collapse or blast loading.
The main goals of this thesis are:

- To conduct a literature review on the effects of the catenary action in RC beams and slabs.

[1] Also known as catenary action

- To utilize the FEM to simulate catenary action in RC beams and investigate its effect under static loading condition, aiming to enhance the reserve capacity of RC beams.
- To validate the FEM with the reference experimental results.
- To investigate the influence of different factors including span-depth ratio, horizontal stiffness, the viscosity parameter in concrete damaged plasticity model, the fracture energy, and reinforcement ratio.
- To calculate the catenary action capacity with a simplified method, in order to compare with the experiment and numerical models.

1.3 Methodology

To achieve the goals, this thesis includes literature review, analytical studies, and Finite Element (FE) analyses including validation with experimental results and a parametric study to investigate how different parameters influence the results.

The purpose of the literature is to establish a foundational understanding of catenary action in RC beams and how to capture catenary action using FE model. It involves a study of previous experiments, and relevant codes.

Using FEM, this thesis will examine the responses of RC beams with different boundary conditions under static loading condition. The geometry and properties of the RC beams in the validation study are consistent with those utilised in the reference experiment by Yu & Tan (2013), which will be mentioned in Chapter 3. Therefore, the results from the numerical analysis can be compared with the experimental data. After the validation, the study explores the effects of different conditions on the catenary action of RC beams. This approach ensures a comprehensive evaluation of the membrane actions.

The finite element software, ABAQUS/CAE 2023 (Dassault Systèmes, 2023) is utilised for modelling the RC beams and the results are compared with analytical calculations and reference experimental results. The displacement-controlled loading approach will be applied at the midspan of the RC beam to capture the loads- vertical displacement relationship.

1.4 Limitations

The verifications of the FE model in this thesis relied on existing experimental data from previous studies available in the literature, rather than conducting new experiments. The studies provide an understanding for the development process of the simplified approach using a 1D beam element and full interaction between the concrete and reinforcement bars.

The thesis will be limited to single-span elements' behaviour. However, single-span elements can be part of a continuous system where the adjacent spans would provide lateral restraint for the studied span. Other structural forms than one-way element is not considered in the thesis. In the FE model, only beam elements will be utilized.

Despite its significance, the effect of CMA is not accounted for in this thesis, even though CMA can be part of the mechanisms if the lateral restraints are sufficient. The focus is only on the catenary action since it represents the last reserve capacity before failure of RC beams, and the aim is to study in this stage.

The FEA will be limited to static analysis in this thesis.

2 Reinforced Concrete Structures

2.1 Reinforced concrete properties

Reinforced concrete (RC) is a robust and durable composite material that combines the advantageous properties of concrete and steel. The tensile strength of RC is provided by the steel while the concrete is robust in compression and it is able to protect the steel, for example, from corrosion, fire, and chemical degradation.

2.1.1 Concrete

Concrete is a composite material made by combining cement with coarse and fine aggregates. When water is added, it reacts with the cement that causes it to harden and bind the aggregates together, forming a solid material. Concrete exhibits significant variety in its mechanical characteristics as a result of variations in its composition and the conditions that it undergoes during the mixing and curing processes.

2.1.1.1 Concrete compressive behaviour

Concrete is typically characterised by its 28-day strength. For example, strength class C30/37 concrete has a characteristic cylinder strength of 30 MPa at 28 days and a characteristic cube strength of 37 MPa. It is noted that all calculations according to Eurocode 2 (CEN, 2004) are based on the characteristic cylinder strength f_{ck}.

The compressive behaviour of concrete is defined by a stress-strain relationship that is obtained from uniaxial compression tests. Under normal conditions, as the load is applied, the relationship between stress and strain is approximately linear at first indicating elastic behaviour, which means that the material will return to its original form upon the removal of the load. Beyond the elastic phase, the stress- strain curve exhibits nonlinearity, indicating that the concrete begins to exhibit inelastic or plastic behaviour as shown in Figure 2.1. If the load is released during this plastic phase, a permanent deformation will persist.

The plastic region starts when the compressive stress is greater than 0.4 f_{cm} and the total strain is the sum of the elastic strain and plastic strain (Mathern & Yang, 2021). Figure 2.2 illustrates the concrete compressive stress-strain relationship consolidated from FIB Model Code 2010. According to Eurocode 2 (CEN, 2004), the ultimate strain has a constant value of 0.0035.

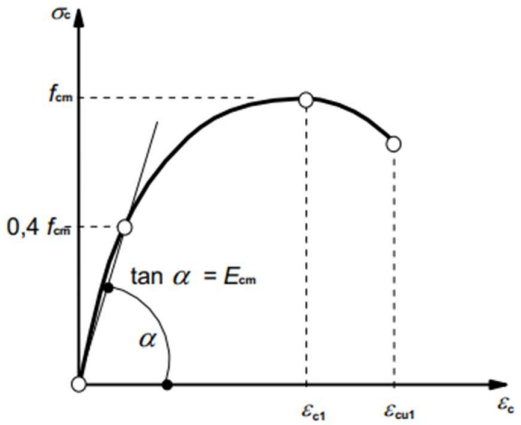

Figure 2.1 Schematic stress-strain relationship for non-linear structural analysis of concrete (CEN, 2004).

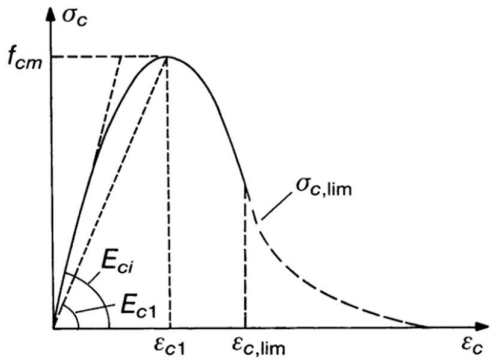

Figure 2.2 Concrete compressive stress-strain relationship according to FIB Model Code 2010.

Eurocode 2 (CEN, 2004) presents various stress-strain relationships for concrete subjected to uniaxial compression. The relation depicted in Figure 2.1 is suitable for non-linear structural analysis. The parameter, ε_{c1}, represents the strain at peak stress, ε_{cu1}, represents the final compressive strain, f_{cm}, represents the mean value of concrete compressive strength.

The modulus of elasticity E of concrete is a measure of its stiffness defined as the slope of the stress-strain curve in the elastic phase, as given by equation 2.1.

$$E = \frac{\sigma}{\varepsilon} \tag{2.1}$$

Commonly, the equation $E = E_{cm}$, is assumed, where E_{cm} is known as the static or secant modulus. The procedure for determining the value of E is described in Eurocode 2 (CEN, 2004).

Mosley, Bungey, and Hulse (2012) state that the measurement for a specific concrete's characteristic is conducted via a static test. In this test, a cylindrical specimen is subjected to a load slightly exceeding one-third of the mean control cube stress ($f_{cm,\text{cube}}$) or 40% of the mean cylinder strength, before being returned to zero stress. This process eliminates the effects of the initial "bedding-in" and minor stress redistributions inside the concrete that occur when it is subjected to a load. Upon reapplying the load, the concrete's response becomes almost perfectly linear. The modulus of elasticity, E_{cm}, is then determined by averaging the slope of the line up to the specified stress level. Eurocode 2 (CEN, 2004) provides an expression for the short-term secant modulus of elasticity, as given by equation 2.2.

$$E_{cm} = 22[\frac{f_{cm}}{10}]^{0.3} \text{ GPa} \tag{2.2}$$

2.1.1.2 Concrete tensile behaviour

The concrete tensile behaviour exhibits a linear elastic stress-strain relationship until the tensile strength, f_{ct}, of the concrete is reached as shown in Figure 2.3a. Following the peak stress, the post-peak softening behaviour is modelled with a bilinear tensile stress against crack width was depicted in Figure 2.3b, in accordance with the FIB Model Code 2010. According to the FIB Model Code 2010, the post-peak softening behaviour is determined by the tensile strength and the fracture energy. The fracture energy, G_f, in [N/m] quantifies the energy required to fracture a unit area of material completely. It essentially measures the amount of energy in order to develop a full crack. G_f is the area under the curve of tensile

stress against crack width, w, and can be calculated using equation 2.3 according to FIB Model Code 2010.

$$G_f = 73 f_c^{0.18} \tag{2.3}$$

where f_c represents the mean compressive strength of concrete in MPa

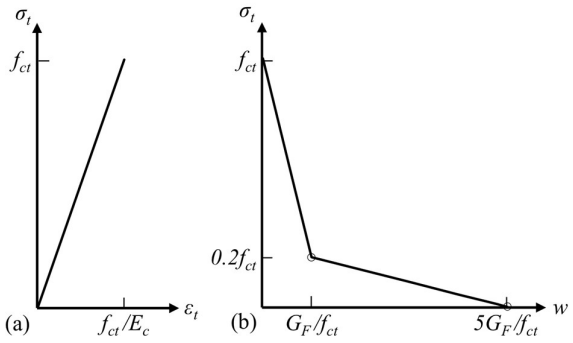

Figure 2.3 Constitutive model for concrete in tension: (a) linear elastic stress-strain relationship for uncracked concrete; (b) bilinear tensile stress-crack width relationship according to fib Model Code 2010, taken from (Mathern & Yang, 2021).

2.1.2 Reinforcement

Engström (2015) explains that the response of reinforcing steel varies based on whether they are hot-rolled steel or cold-worked steel. The yield strength of reinforcing steel ranges from 400 to 600 MPa. The stress-strain curves for different reinforcing steel are shown in Figure 2.4. Hot-rolled bars have a definite yield point whereas the yield point of cold-worked bars is measured by a defined proof stress at a strain of 0.2%.

The Young's modulus, E_s, is usually assumed to be 200 GPa. The yield strength, f_{yk}, and the tensile strength, f_{tk}, are defined respectively as the characteristic value of the yield load, and the characteristic maximum load in direct axial tension, each divided by the nominal cross-sectional area.

According to Eurocode 2 (CEN, 2004), the reinforcement properties can be simplified using bilinear stress-strain relationships as shown in Figure 2.5.

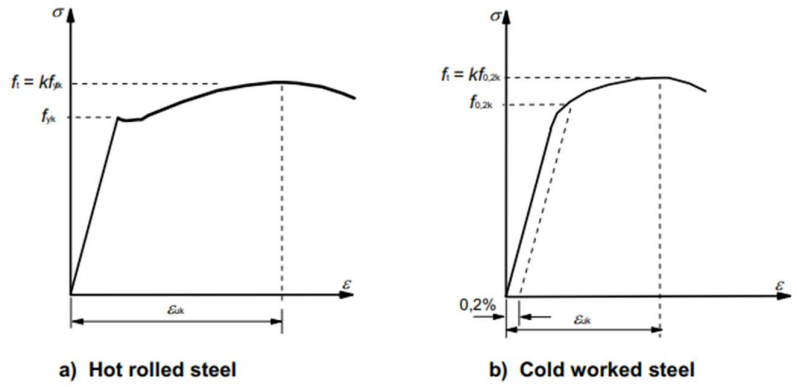

Figure 2.4 Stress-strain diagrams of (a) hot rolled steel and (b) cold worked steel, Eurocode 2 (CEN, 2004).

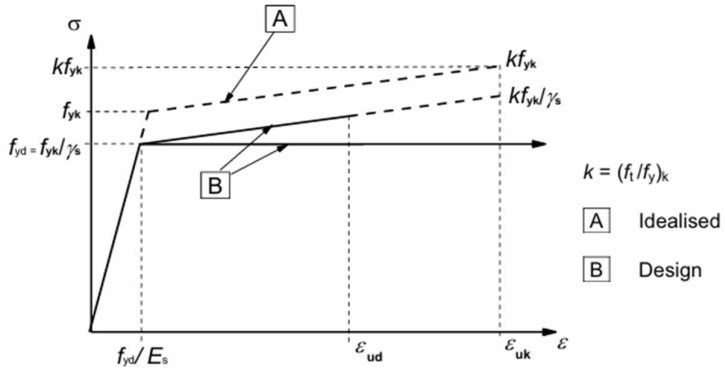

Figure 2.5 Idealised and design stress-strain diagrams for reinforcing steel from Eurocode 2 (CEN, 2004).

The ductility of reinforcement is an important consideration for the design of concrete structures. Ductility refers to the reinforcement's ability to undergo significant deformation before failure, which is crucial for the structural integrity and safety of concrete structures. Eurocode 2 (CEN, 2004) specifies requirements for the ductility of reinforcement materials, including the ratio of tensile strength to yield strength $(f_t/f_y)_k$ and the strain at maximum force, ε_{uk}, ensuring that structures can sustain deformations from loads without sudden failure. Reinforcing steel is classified into 3 different grades based on their ductility and total elongation at maximum force, grade A, B, and C. Reinforcing steel grade C has the highest ductility. This is indicated by its $(f_t/f_y)_k$ ratio which ranges between 1.15 and 1.35 and its total elongation at maximum force of at least 7.5%, meaning the higher these values, the greater the ductility of the reinforcing steel. To utilize the catenary action effectively, the high ductile reinforcing steel is required. Table 2.1 shows the properties of reinforcement according to Eurocode 2.

Table 2.1 Properties of reinforcement according to Eurocode 2 (CEN, 2004).

Product form		Bars and de-coiled rods			Wire Fabrics			Requirement or quantile value (%)
Class		A	B	C	A	B	C	-
Characteristic yield strength f_{yk} or $f_{0,2k}$ (MPa)		400 to 600						5,0
Minimum value of $k = (f_t/f_y)_k$		≥1,05	≥1,08	≥1,15 <1,35	≥1,05	≥1,08	≥1,15 <1,35	10,0
Characteristic strain at maximum force, ε_{uk} (%)		≥2,5	≥5,0	≥7,5	≥2,5	≥5,0	≥7,5	10,0
Bendability		Bend/Rebend test			-			
Shear strength		-			0,3 A f_{yk} (A is area of wire)			Minimum
Maximum deviation from nominal mass (individual bar or wire) (%)	Nominal bar size (mm)							
	≤ 8	± 6,0						5,0
	> 8	± 4,5						

2.2 Analysis methods

The design and analysis of a simply supported, fully restrained or partially restrained RC beam subjected to a concentrated load at midspan differ significantly in terms of their support conditions and the resulting structural behaviour. However, they can be categorized into three primary analytical scenarios, linear elastic analysis, plastic analysis, and non- linear analysis (Engström, 2015). Figure 2.6 illustrates a representative load-deformation curve for these three scenarios.

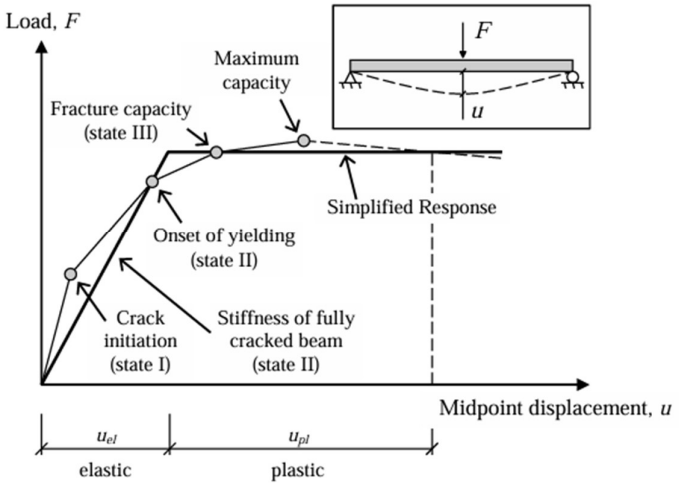

Figure 2.6 Response of a simply supported concrete beam subjected to a concentrated load at midspan, mentioned by (Lozano & Makdesi, 2017).

Linear elastic analysis assumes that materials behave elastically, and their stress-strain relationship is linear, as it is shown in state I in Figure 2.6. This method is applicable as long as the concrete remains uncracked, and the reinforcing steel does not yield. In the ultimate limit state, linear elastic analysis can predict the moment distribution after some plastic distribution has occurred, matching the design's assumptions. This method often starts with

an assumption of uncracked gross concrete sections and ignores reinforcement, to simplify the preliminary and final verifications (Engström, 2015).

When a RC section cracks, its stiffness decreases compared to the uncracked state. The behaviour of these cracked regions is governed by the section's stiffness in state II. The reinforcing steel has a large influence on the structural response. In state III, once the yielding of reinforcement bars at a critical section has initiated, a non-linear analysis should be applied where the actual non-linear properties of materials and the structure's geometry can be considered. A model for a non-linear analysis requires more detailed information about the beam, such as material data, reinforcement arrangement and detailing. It accounts for the non-linear stress-strain relationship of concrete, including cracking, tension stiffening, and yielding of reinforcement.

The plastic analysis is based on the theory of plasticity and assumes that certain regions of the beam exhibit ideally plastic behaviour, where the yield capacity is reached (surpassed its elastic limit) and plastic deformation capacity is theoretically unlimited, state III in Figure 2.6. Plastic analysis is useful for preliminary designs as it allows for the determinations of bending moment capacity from equilibrium equations without assuming member sizing or sectional stiffness (Engström, 2015).

Non-linear analysis can be categorized into first-order and second-order analysis. The second-order analysis additionally considers the effects of structural deflections. However, this method provides a more accurate representation of the structural behaviour in both the service and ultimate limit states by accounting for the progressive changes in stiffness and strength due to cracking and yielding. It considered the most reliable method compared to linear elastic and plastic analyses, especially for detailed final stage designs (Engström, 2015).

2.3 Load conditions (static and dynamic loadings)

RC structures can experience different types of loading conditions that influence their behaviour and performance. These loading conditions are mainly categorized as static loads and dynamic loads. Static loads refer to constant or gradually applied forces. However, dynamic loads are time-varying forces that introduce inertial effects, causing the structure to undergo rapid deformations.

Static loading conditions are evaluated using the principles of equilibrium and strength of materials. Structures subjected to dynamic loading may behave significantly different from its behaviour under static loading conditions. Dynamic loads, particularly those with significant peak values and brief durations referred to as impulse loads, can generate stress waves that propagate throughout a structure and impact its behaviour. An explosion can be an example of dynamic load, it will cause a high peak pressure rapidly. Consequently, the structures will have a different response compared to the structures subjected to a static load.

Another example as shown in Figure 2.7, is when a simply supported beam subjected to the impact of a drop weight hitting the beam with certain speed. The crack patterns and failure modes can be different from those observed under static loading conditions. Inclined shear cracks and cracks at the top of the beam may appear due to the time-dependent boundary conditions created by the wave propagation effects. The boundary conditions under dynamic loading can be viewed as time-dependent fixed supports, where the support locations move towards the ends of the beam at the wave speed in the beam (Johansson, 2000).

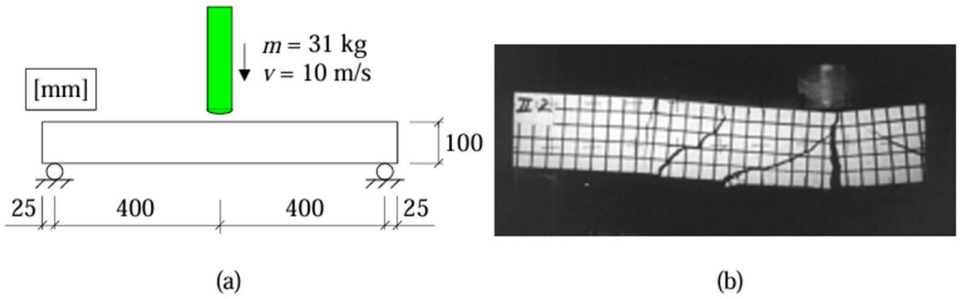

Figure 2.7 (a) Load set-up of simply supported beam with width 100 mm; (b) crack pattern obtained when subjected to the impact of falling drop weight, from (Johansson, 2000).

This highlights the crucial role of time-dependent boundary conditions in dynamic loading scenarios. Unlike static conditions where loads and constraints remain relatively constant, dynamic analyses must consider rapidly changing boundary conditions, particularly in events like blasts or impacts.

In a dynamic analysis, the stiffness of a structure might change as the structure deforms due to the dynamic loading conditions, such as vibrations or impacts, leading to variations in the stiffness matrix. This is particularly relevant when considering non-linear material behaviour, where the relationship between stresses and strains changes as the material yields or undergoes other non-linear responses. This concept is crucial in dynamic analyses, such as those involving explosions or other transient loads, where the boundary conditions, including support constraints and applied loads, can change rapidly with time, influencing the structural response. It underscores the need for complex analytical or numerical methods to accurately predict the behaviour of structures under such conditions, ensuring their safety and integrity.

2.4 Strain rate effects

The strain rate plays a crucial role in impulsive loading, particularly as materials transition into the plastic zone (Zhang & Abedini, 2023). The sensitivity of most structural materials utilized in civil engineering to the loading rate is a critical factor. The properties of materials used in RC structures, including strength, stiffness, and ductility or brittleness, exhibit dependence on the strain rate (Bischoff & Perry, 1991).

Figure 2.8 gives the range of the strain rate for different loading conditions. From this Figure, quasi-static load displays the strain rates ranging approximately 10^{-6} to 10^{-5} s^{-1} whereas the ranges of the strain rates under blast loading are from 10^{2} to 10^{3} s^{-1}. It can be seen that dynamic loadings produce higher strain rates than static loadings.

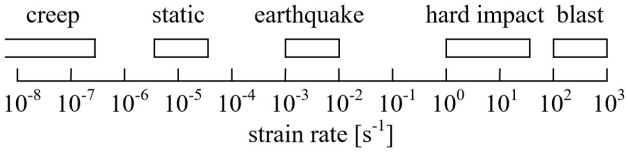

Figure 2.8 The ranges of the strain rate for different loading conditions from (Johansson, 2000).

The significant factor called dynamic increase factor, *DIF*, represents the ratio between the dynamic strength and static strength. This factor is commonly used in conditions involving rapid loading. As shown in Figure 2.9, the compressive strength of concrete at a strain rate close to 10 s^{-1} can be 85% to 100% greater compared to its strength under static load conditions. Nonetheless, the experimental data shows considerable variability, and it has been suggested by some researchers that this inconsistency among different experiments might be due to the testing methods used, (Bischoff & Perry, 1991).

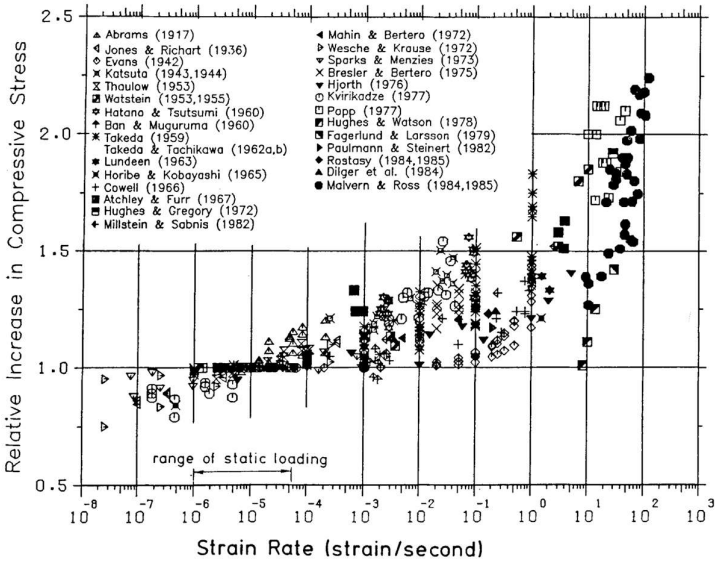

Figure 2.9 Strain rate influence on compressive strength from (Bischoff & Perry, 1991).

Various proposals for concrete in compression is shown in Figure 2.10. Johansson (2000) stated that the relations most widely recognized are found in the CEB-FIB Model Code 1990, which correlates the *DIF* for concrete under tensile and compressive forces with its static compressive strength. Figure 2.11 shows the DIF-strain rate relations for concrete in tension with different proposals.

The strain rate effect in the concrete can be categorized into 2 types, viscous and structural effects as shown in Figure 2.12. Johansson (2000) explained that viscous effects significantly influence crack formation within materials. Under static loading, cracks progress slowly, allowing them to pass strong aggregates and form in the material's weaker zones, e.g water cement paste. Conversely, for higher strain rates if the load velocity is high enough, cracks progress swiftly towards stronger zones instead. As strain rates increase beyond the transition zone, structural effects including inertia forces and confinement start to play a more dominant role in material strength. This is largely because of the inertial forces that emerge at the leading edge of the crack. When concrete is compressed more quickly than its response rate,

the confinement effect occurs, leading to a multiaxial stress state similar to plain strain, which, in turn, enhances the concrete's strength.

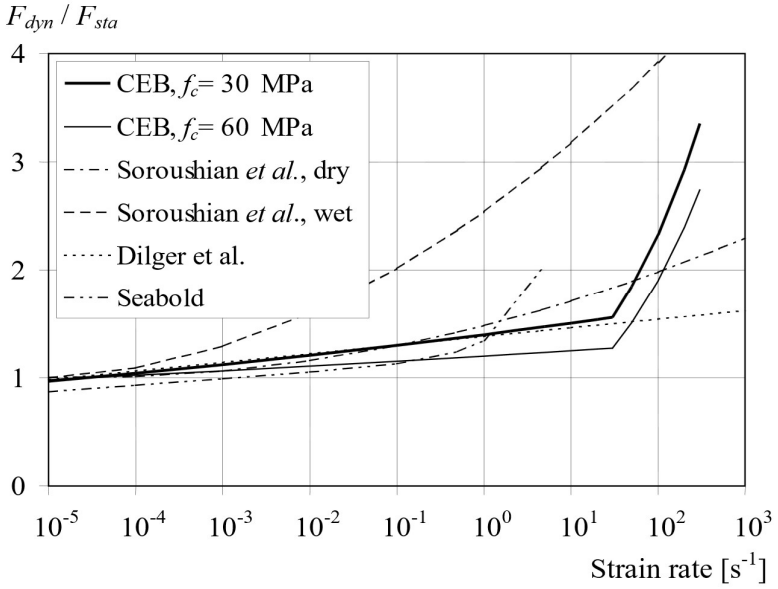

Figure 2.10 Comparison of DIF-strain rate relations for concrete in compression from (Johansson, 2000).

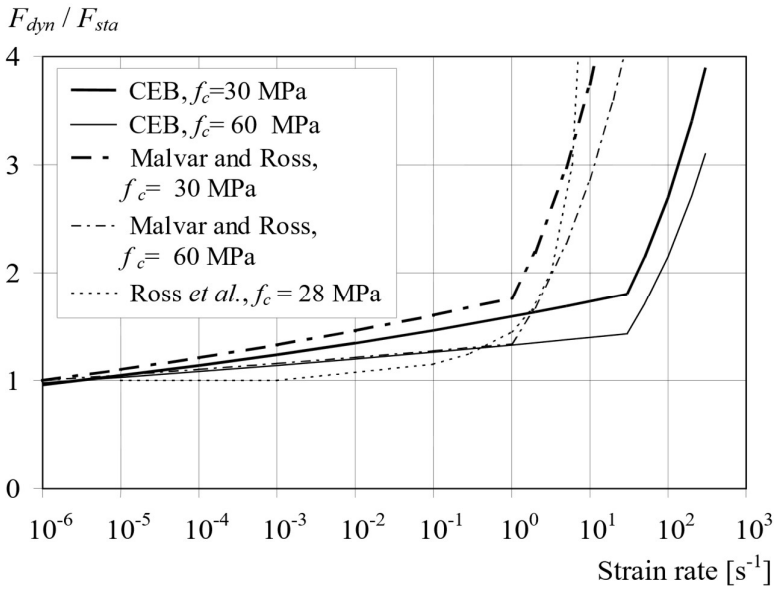

Figure 2.11 Comparison of DIF-strain rate relations for concrete in tension from (Johansson, 2000).

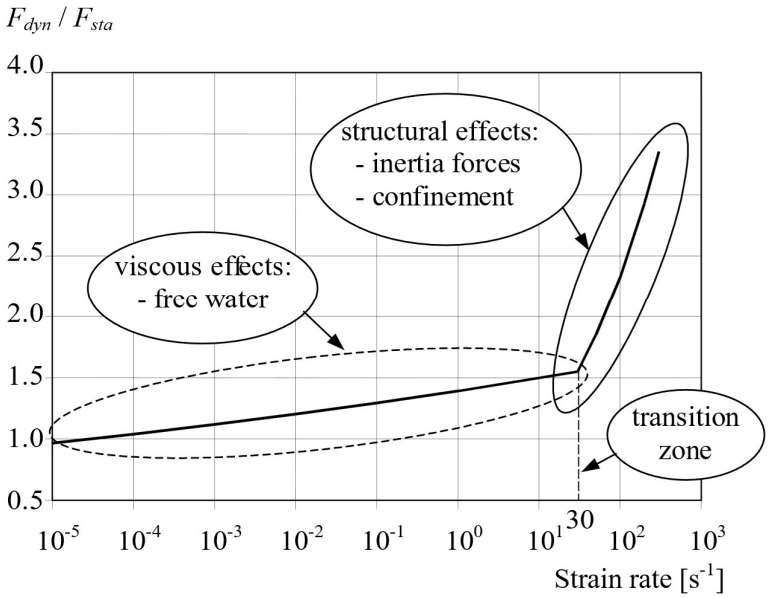

Figure 2.12 Two types of strain rate effects from (Johansson, 2000).

2.5 Plastic hinge and plastic rotation capacity

Plastic rotation capacity and plastic hinge are related concepts in structural engineering, particularly in the analysis and design of structure under ultimate states, but they refer to different aspects of structural behaviour. Whilst plastic hinge is a theoretical model used to represent the spread of plasticity along the member when it reaches its moment capacity at a particular section, the plastic rotation capacity is a measure of the ductility of the member, indicating how much deformation it can sustain in the plastic range before failure (Johansson & Laine, 2009).

Plastic rotation capacity refers to the ability of a structural member to undergo large deformation in rotation beyond the yield limit without significant loss of strength. Therefore, a large plastic rotation capacity is a sought-after property in structures subjected to impulsive loading, it is crucial for ensuring that structures can dissipate energy through large deformations, without experiencing catastrophic failure. A higher plastic rotation capacity indicates better ductility and, generally, a more resilient structure under extreme loading conditions. The plastic rotation capacity is influenced by the materials properties, cracking and tension stiffening, the cross-sectional geometry of the member, the type and amount of reinforcement, and the loading conditions (Johansson & Laine, 2009).

Reinforced concrete members have limited plastic rotation capacity. This limitation can cause the member to fail before the predicted failure mechanism develops. Due to various factors affecting rotation capacity, multiple methods have emerged to predict the plastic behaviour of concrete beams.

A method in Eurocode 2 (CEN, 2004) can be used to estimate a conventional value of the maximum allowed rotation, as it is seen in Figure 2.13 where the definition of plastic rotation capacity has been developed to address the rotation over an inner support within a continuous beam. Furthermore, the length of the rotation is assumed to occur over a length equal to 1.2 times the depth of the section.

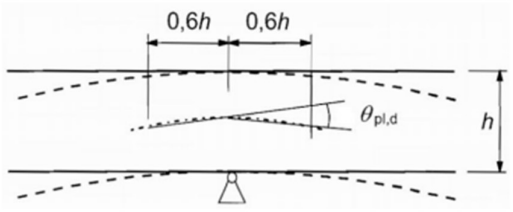

Figure 2.13 Plastic rotational capacity according to Eurocode 2 (CEN,2004).

Eurocode 2 (CEN, 2004) presents a simplified approach using a diagram as shown in Figure 2.14 to evaluate the plastic rotation capacity. This method considers three key factors which are concrete strength, reinforcement class, and the ratio of the compressed zone depth, x, to the effective depth, d.

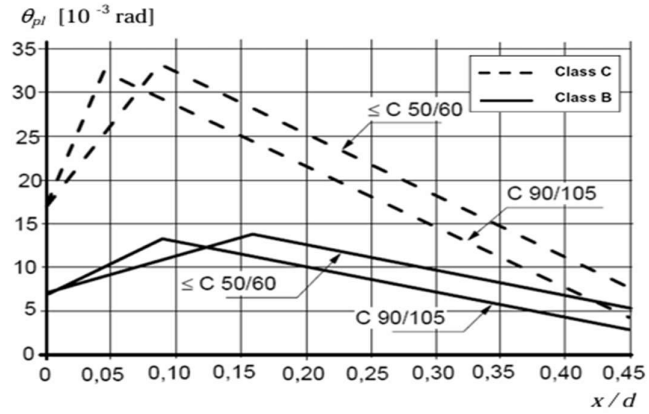

Figure 2.14 Evaluating the plastic rotation capacity according to Eurocode 2 (CEN, 2004).

According to UFC 3-340-02, elements without shear reinforcement, the ultimate deflection is limited to 2 degrees support rotation whereas elements with shear reinforcement are capable to reach 6 degrees support rotation. If the lateral restraint is sufficient and shear reinforcement type is lacing reinforcement as shown in Figure 2.17, the plastic rotation capacity can be increased to 12 degrees (DOD, 2008) as shown in Figure 2.15 and Figure 2.16.

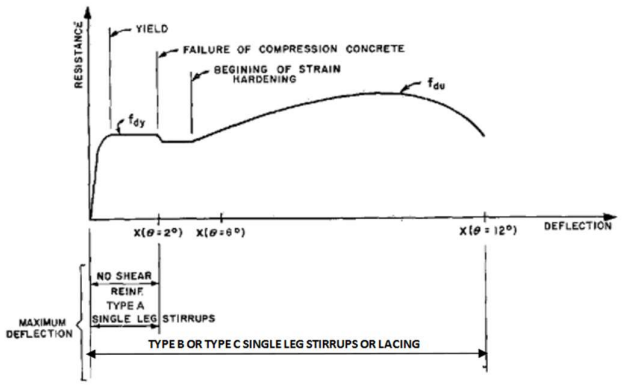

Figure 2.15 Typical load-deflection curve for a reinforced concrete beam from (DOD, 2008).

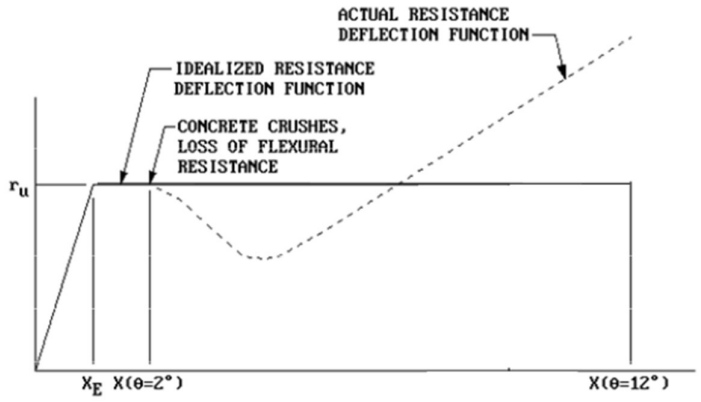

Figure 2.16 Load-deflection curve for large deflections from (DOD, 2008).

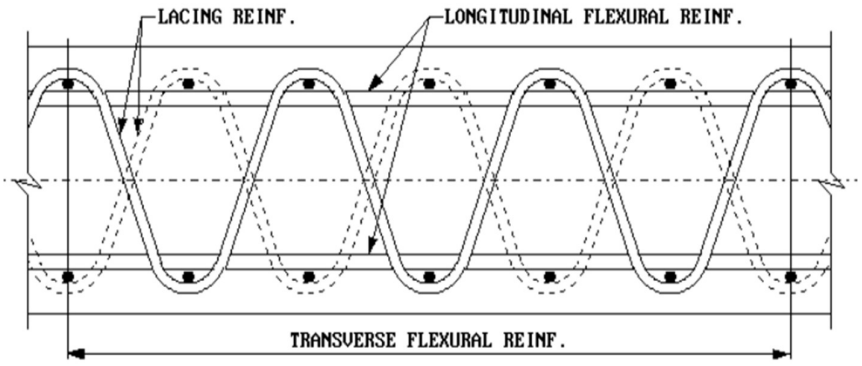

Figure 2.17 Lacing reinforcement from (DOD, 2008).

For a simply supported RC beam with an increased load, the yielding of reinforcements may lead to formation of the plastic hinge, this hinge can be assumed to be concentrated to specific section, as can be seen in Figure 2.18.

The formation of a sufficient number of plastic hinges in a statically indeterminate structure, for example, fixed end supports can lead to the formation of a mechanism, indicating that the structure has reached its load-carrying capacity.

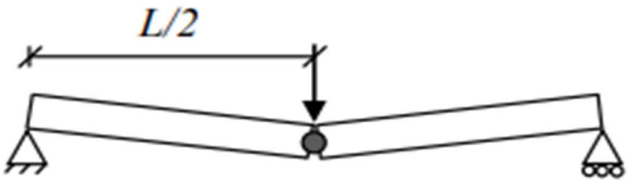

Figure 2.18 Representation of a concentrated plastic hinge.

3 Tensile Membrane Action – (Catenary Action)

3.1 Overview

If a RC beam subjected to an external load has sufficient lateral restraint at the supports, axial forces arise within the beam, leading to the development of membrane action. This membrane action can be either compressive membrane action (CMA) or catenary action (Park, 1964). Membrane action enhances both load and deformation capacities of the beam. Some authors suggest that CMA occurs when the displacement reaches approximately half the section depth, while catenary action occurs when the displacement exceeds the section depth (Smith, 2016a).

The displacement response in a laterally restrained RC beam is shown in Figure 3.1. The different stages are shown sequentially; a) bending or flexural response, b) CMA response, and c) catenary action response. Figure 3.2 illustrates the idealized load-displacement curve under membrane actions of a fully restrained RC beam with a higher amount of top reinforcement at the supports and an unrestrained RC beam. Point A marks the theoretical flexural capacity, where the cracks at critical sections have already appeared. Point B denotes the maximum flexural capacity considering CMA development and the load resistance is enhanced beyond the ultimate bending load predicted using the yield line theory. From point B to C, it can be seen that the load capacity decreases gradually because of crushing of the concrete at the compressive regions. The influence of CMA also diminishes after this point. Point C denotes the initiation of catenary action. From point C to D, there is a change in the axial force within the beam, transitioning from compression to tension and from point D to E, the rupture of the bottom longitudinal reinforcement bars occurs particularly at the middle joint region. This rupture is a result of the applied loads exceeding the capacity of the bottom rebars. After the rupture of the bottom rebars, any further increase in displacement at the middle joint causes the top reinforcing bars to engage in tension. The top rebars contribute to the remaining capacity of the catenary mechanism until they fracture. However, in unrestrained system, where there are no horizontal supports or boundaries, the structural element lacks the necessary restraints to develop the horizontal tensile forces required for catenary action. Therefore, catenary action cannot be utilized.

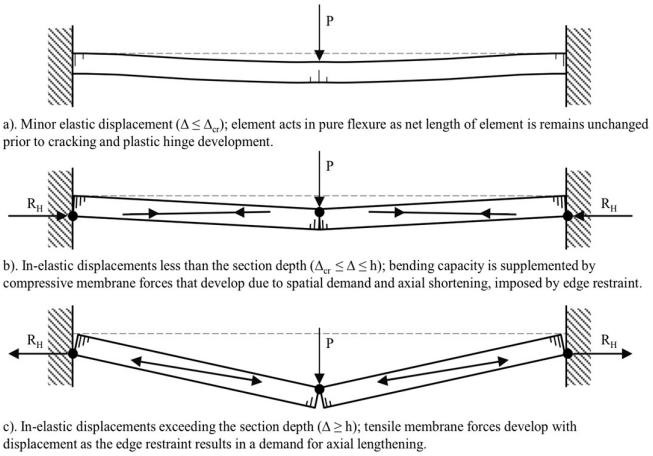

Figure 3.1 Membrane force development in a centrally loaded RC beams, subject to large displacement and rigid lateral restraint from (Smith, 2016a).

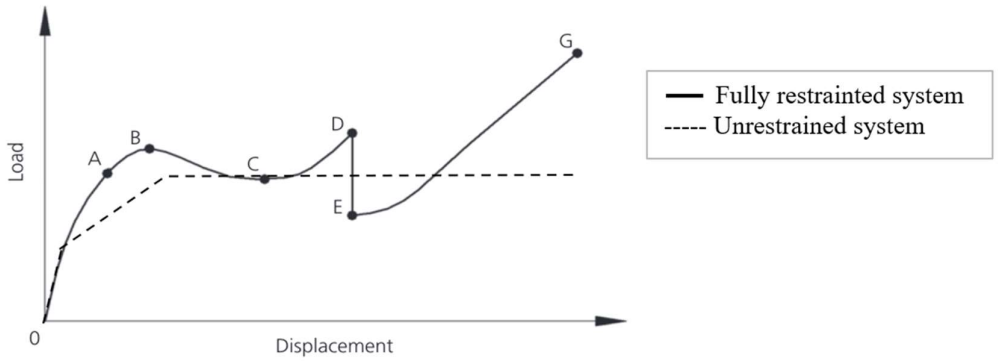

Figure 3.2 Idealized load-displacement curve under membrane actions of a RC beams for fully restrained and unrestrained systems.

Catenary action refers to the mechanism of internal force transfer in a RC beam during large deformation. This typically happens during extreme loading situations like explosions, impacts, or progressive collapses. Under normal service loads, a traditional RC beam primarily resists load through bending, with the concrete under compression and the reinforcing steel under tension. However, under extreme loads causing significant vertical deformations, the beam begins to develop considerable tensile forces along its length, beyond its bending capacity. Catenary action engages the longitudinal reinforcing bars to resist the axial tensile forces.

Although traditional design does not take catenary action into account due to the significant deformations and cracking it causes, it can serve as an alternative method of load transfer that prevents complete collapse under extreme loading conditions if the reinforcement detailing allows for the sufficient ductility.

When a RC beam is subjected to impulsive loading, such as from an explosion or impact, the load is applied very rapidly or with high strain rate. This can cause a significant deformation and possibly the formation of a large deflected shape of the beam. The concrete, which is generally weak in tension, may crack and spall, leaving the steel reinforcement to carry the tensile forces. The steel acts like a stretched membrane.

Catenary action involves extensive deformations and utilizes tensile force to balance the augmented gravity loads. This catenary action can be beneficial for the structural integrity of the beam under extreme loading conditions because it allows the structure to redistribute loads and remain stable even after concrete crushing. It contributes to the overall ductility and toughness of the structure.

According to (Smith, 2016a), catenary action performs effectively under three critical aspects:

- Larger area and ratio of reinforcing steel as the load resistance increases proportionally to the in-plane tensile strength.
- Higher rotational and tensile ductility to undergo large displacement without loss of in-plane strength.
- Sufficient lateral restraint at the beam ends to allow the development of axial tension forces.

3.1.1 Primary and secondary catenary action

Catenary action in RC beams consists of two modes of response, primary and secondary response (Smith, 2016a), as shown in Figure 3.3. Smith explained that the primary response refers to the behaviour characterized by large displacement catenary action that occurs before the failure of the extreme tension reinforcement layer in a structure.

The study suggests that the primary catenary action is concerned only with the initial capacity of the structure to undergo large deformations and resist loads up to a certain limit. The failure of the structure is typically attributed to the yielding or rupture of the tension reinforcement at specific locations known as yield lines and critical sections. In addition, the force developed by the catenary action may be governed by two important factors which are the ultimate tensile strength and ductility of the extreme tension reinforcement or the ultimate bond strength of its anchorage.

Secondary response depicts a stage in the structural behavior following the primary response. Maximum catenary action capacity is found to occur during secondary response when the displacements at the critical sections are beyond the rotation capacity. In this secondary phase, the beam has already undergone significant deformations, the top rebar layer (the extreme tension reinforcement) has failed at the end supports. With the top layer failing, the load is redistributed to other structural elements, such as the bottom rebar layer at the supports, which now becomes critical in carrying the load. This stage demonstrates the reserve strength of the beam, where the remaining reinforcement is mobilized to sustain the loads as shown in Figure 3.3b. The secondary response is vital in the context of structural robustness and resilience as it represents the structure's ability to continue to carry loads and resist collapse after primary load-carrying mechanisms have failed.

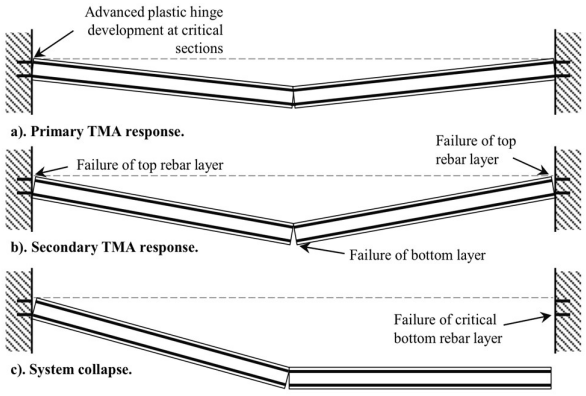

Figure 3.3 (a) primary catenary response, (b) secondary catenary response and (c) system collapse in RC beam by (Smith, 2016a).

3.2 Experimental investigations

The resilience of concrete structures has gained significant attention considering a succession of disastrous events caused by structural failures resulting from unanticipated events like gas explosions and terrorist attacks. These incidents have prompted substantial research efforts focused on creating strong design principles to prevent similar catastrophes. This increased focus has also led to efforts to enhance the structural robustness of buildings to endure unanticipated failures (Gouverneur et al., 2013).

This thesis aims to examine the effect of membrane actions, with a specific focus on catenary action, in enhancing the collapse resistance of RC beams under extreme loading conditions. In order to accomplish this, a sequence of experimental investigations was reviewed and analysed, with a focus on three of them to investigate the response of RC beams and slabs under scenarios that simulate accidental events, such as the sudden removal of a central support.

The phenomenon of catenary action has been investigated and documented since 1964, when Park initially drew attention to it. Numerous prior investigations have been conducted over the years up until the present time (Park, 1964).

The three selected experiments are intended to document the structural response at different loading stages, with a particular focus on the transition from flexural to catenary behaviour.

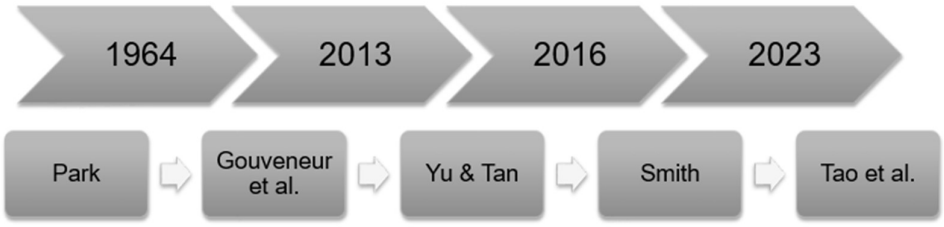

Figure 3.4 Timeline of catenary action studies.

3.2.1 Experiment 1, (Park, 1964)

An investigation by (Park, 1964) was carried out on rectangular RC slabs with edges that were completely restrained against all translations. The setup was designed to simulate the behaviour of inner panels in continuous slab and beam floors, where the surrounding panel's stiffness restricts lateral movement. The slabs were uniformly loaded in order to observe the transition from compressive to tensile membrane action, enabling a consistent distribution of stress and strain throughout the experiment and providing a control setting to analyse the structural behaviour of the slab when exposed to uniform pressure.

The goal of this experiment was to observe and record the shift from compressive membrane action, where the slab initially carried loads through compressive stresses, to tensile membrane action, where the slab primarily carried loads through the reinforcement's tensile strength after significant deflections. Indeed, it was important to understand the behaviour of concrete slabs beyond the reinforcement's yield point and into the post-failure regime.

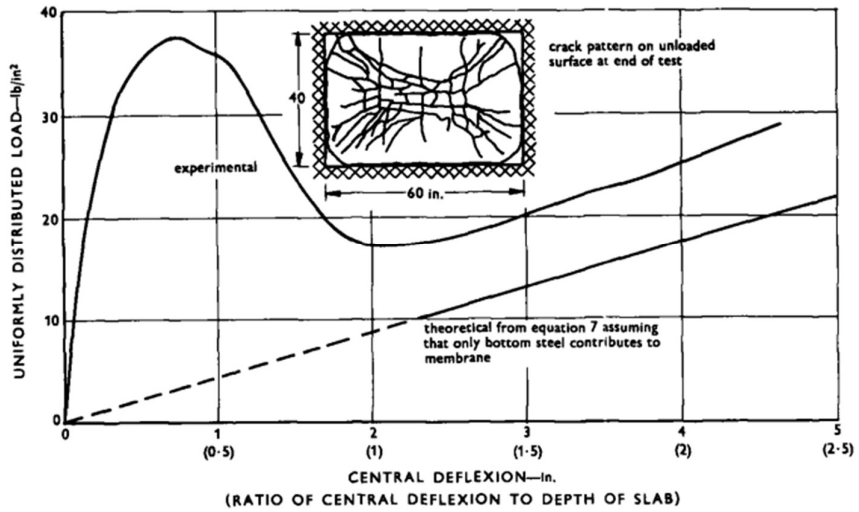

Figure 3.5 Load-deflexion curves and crack pattern of a rectangular slab with fully restrained edges based on (Park, 1964).

Initially, the slab exhibited elastic behaviour, returning to its original state after the load was removed. As the load increased, plastic behaviour was observed, characterised by irreversible deformations.

After substantial deflections and the yielding of steel, the reinforcement began to function as a tensile membrane. This stage is critical as it represents the slab's capacity to carry loads even after undergoing substantial changes due to high stress levels.

Moreover, the crack patterns were documented, offering valuable insights on the distribution of load and the modes of failure in the slabs. Substantial deformations were also recorded, demonstrating the slab's capacity to experience substantial deformation without experiencing catastrophic collapse, see Figure 3.5.

This experiment validated that heavily reinforced slabs have the capacity to withstand loads beyond their maximum bending strength due to the tensile strength of the reinforcement. This finding aligns with the theoretical concept of tensile membrane action discussed in the experiment. These results are not contradictory but rather complement Park's studies, providing in-depth understanding of the load-bearing stages that take place in concrete slabs under uniform loads (Park, 1964).

3.2.2 Experiment 2, (Gouverneur et al., 2013)

An experimental investigation was performed by (Gouverneur et al., 2013b), focusing on the tensile catenary action in a restrained RC slab strip under an accidental situation, the loss of a support, as illustrated in Figure 3.6. The primary objective of the investigation was to assess the strength reserve and robustness of concrete structures when they are subjected to large deformations that can trigger tensile membrane or catenary forces, potentially aiming to increase the structural load-carrying capacity significantly.

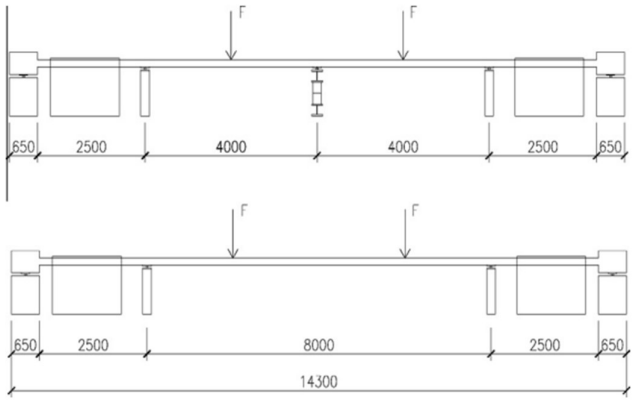

Figure 3.6 Schematic representation of the test set-up before (top) and after (bottom) the removal of the central support by (Gouverneur et al., 2013b).

The experimental setup consisted of slab strips that were longitudinally restrained and subjected to vertical loading. The load was applied by using two identical jacks, each with a capacity of 500 kN. The jacks applied force to the mortar-embedded spreader I-profiles located in the middle of each inner span of the slab sample, simulating the impact of an unintended failure of the central support.

The slab strips were continuously monitored to capture their deformation behaviour, load-carrying capacity, and the development of tensile forces within the slab.

Beyond what would be predicted by small deformation theories, which focus on the behaviour of materials under conditions where deformations are relatively small, there is a significant increase in load-bearing capacity that results from the activation of tensile membrane or catenary forces at large deflections. This experiment revealed a distinct load-displacement behaviour characterized by three phases: elastic bending, yield bending leading to plastic hinge formation, and finally tensile catenary action dominating as the primary load-carrying mechanism at large deflections.

During service load behaviour, before the removal of the central support, the slab showed minimal deflections under service loads, indicating that for normal operating conditions, the structure performs within acceptable limits. Hence, attention in design must be paid to ensuring that under normal conditions, the deflections are kept minimal to maintain structural integrity and serviceability.

However, the focus in this investigation was on the load-deformation response following the removal of the central support, simulating an accidental scenario. The experiment's results were noteworthy in demonstrating the slab's ability to adjust to new load routes once the central support was eliminated. Observations indicated that there was an increase in deflections and the outward movement of edge beams, which suggested that the slab was adapting to the altered structural dynamics. The cracking behaviour was observed and recorded at several load levels as they are shown in Figure 3.6, emphasising the shift from the initial elastic behaviour stage (a) to plastic stage (b), and ultimately to catenary actions at stage (c) as the load increased. This was followed by the rupture of the top reinforcement over the right support at stage (d).

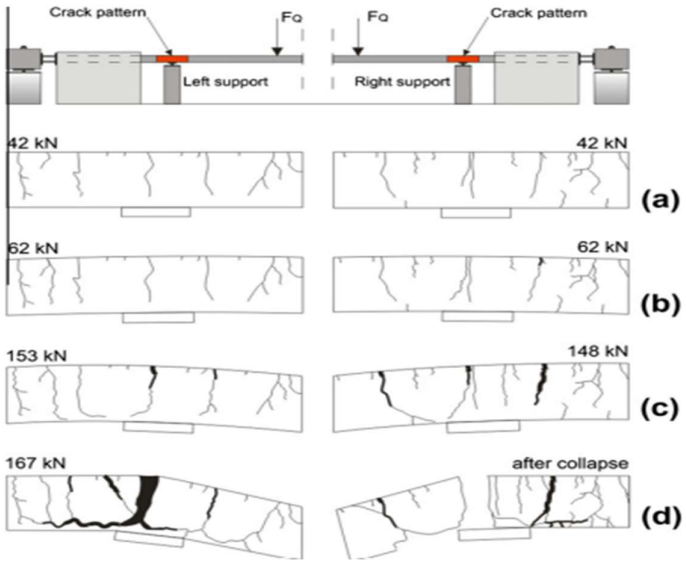

Figure 3.7 Crack patterns at the left and right support zones at different loading stages, from elastic to plastic behaviour and ultimately to failure through catenary action by (Gouverneur et al., 2013b).

This development of catenary action was found to substantially increase the ultimate bearing capacity of the slab strips, allowing them to support loads much greater than their initial design capacity under extreme loading conditions. The post-development of a plastic mechanism where the slab entered the catenary stage, significantly affecting the load-displacement curve due to the tensioning of reinforcing bars and the development of tensile catenary forces, see Figure 3.8.

Lastly, the experiment captured an ultimate load of 180 kN for the slab after removing the centre support. This was three times higher than the load that was determined as the service load for the test situation with central support. Upon removal of the central support, the experimental setup exposed the slab to conditions that significantly altered the initial load distribution, resulting in a further increase of the bending moments. The measured ultimate load of 180 kN, along with a deflection of 645 mm in the centre of the span, demonstrates a decrease from the designed capacity, emphasising the influence of removing support on the structural behaviour.

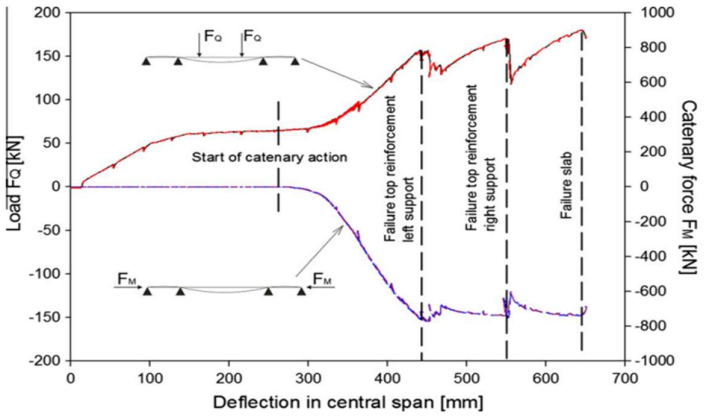

Figure 3.8 Vertical load and catenary action in function of deflections by (Gouverneur et al., 2013b).

3.2.3 Experiment 3, (Yu & Tan, 2013)

In another experimental investigation by Yu and Tan, two one-half scaled specimens were designed and tested under a middle column removal scenario. The specimens consisted of a two-bay beam, a middle joint and two enlarged end columns stubs. The specimens were supported by a statically determinate test rig, and a point load was applied at the top of the middle joint with displacement control until the specimens completely failed. During the tests, catenary action of RC beams was mobilized at large displacements (Yu & Tan, 2013).

This experiment will be the reference experiment for this thesis to be simulated in the FE analysis. It provides a critical test for understanding the progressive collapse resistance of RC beam, by investigating the structural response of RC beam-column setup subjected to a middle column removal scenario. Two different reinforcement arrangements were tested to study the impact of such detailing on the structural behaviour during progressive collapse.

A range of instruments within the experimental setup (see Figure 3.9) were used to ensure accurate observation of the structural behaviour, including linear variable differential transformations (LVDTs) to measure vertical displacements, strain gauges on reinforcing steel, and load cells to measure reaction forces. These instruments provided a detailed observation of deformations, internal forces, and the evolution of failure mechanism. The detailing of beam-column sub-assemblage in this experiment is shown in Figure 3.10.

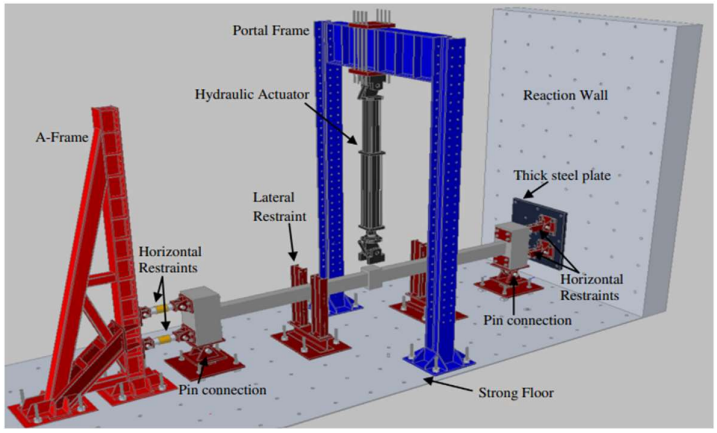

Figure 3.9 Test set-up, simulating the axial restraints, the ends of specimens respectively connected to a steel frame and a reaction wall through two horizontal pin connections with rollers, (Yu & Tan, 2013).

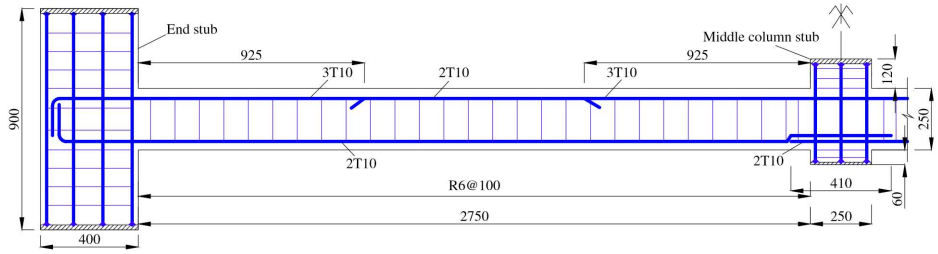

Figure 3.10 Detailing of specimen from (Yu & Tan,2013).

The experiment simulated the sudden removal of a middle column by applying a point load at the top of the middle column joint. By using displacement control, the load was increased incrementally in order to observe the structural response. Simultaneously, data throughout the experiment were assembled aiming to document the response of the RC beam to the increased load and understand the behaviour of structural components at different stages of the loading process.

Initially, the structure exhibited flexural behaviour, and the bending stresses distributed across the beam which led to the formation of plastic hinges at critical points indicated the limits of flexural capacity.

As the loading continued beyond the flexural capacity, the structure showed the ability to redistribute loads and preserve stability through additional mechanisms such as CMA, with a noticeable increase in load carrying capacity at the middle joint interfaces.

The deformation of the structure significantly increased, resulting in a prominent catenary action. This is characterised by the tensile forces acting on the reinforcements.

This development of catenary action played a crucial role in increasing the load-bearing capacity of the structure, determining the importance of tensile membrane action in preventing progressive collapse, as it is shown in Figure 3.11.

The failure observation of the structure was highlighted by significant cracks and large rotations at the middle joint and the beam ends. Notably determining the critical areas in the structure that are responsive to failure under extreme loading conditions.

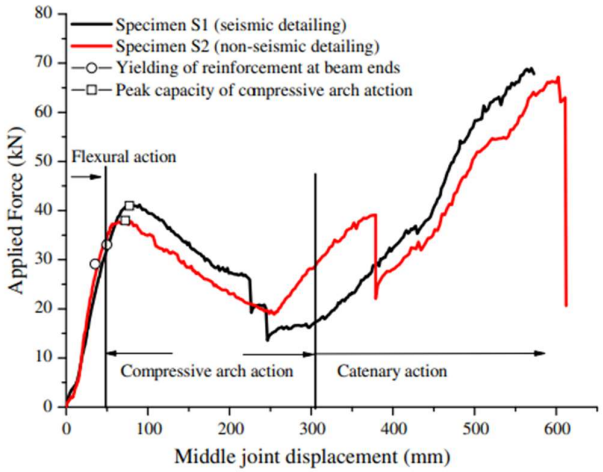

Figure 3.11 Relationship of applied force to the middle joint displacement by (Yu & Tan, 2013).

Chapter 6 will further investigate this experiment through FE analysis, aiming to analyse the findings by simulating a comparable setup in ABAQUS. This analysis will emphasize the significance of flexural action, CMA, and particularly catenary action in enhancing the collapse resistance of reinforced concrete structures.

4 Finite Element Modelling

4.1 Introduction

This chapter delves into the utilisation of a FE program for the creation of a detailed model to describe catenary action in RC beams. This involves detailing model geometry, defining material models, selecting element types and their properties, establishing boundary conditions, and setting other relevant parameters. Experiment 3 by Yu & Tan (2013) as mentioned in Section 3.2.3 was selected as a reference experiment to validate the numerical results before performing the parametric studies to explore various factors that could influence the development and behaviour of catenary action.

Two different boundary conditions were modelled. The first model was designed to closely duplicate the experimental setup which will be seen in Section 4.2. This model was aimed to provide a direct comparison with the experimental results. The second model was created with full restraints at the end of the beam. This model allowed for additional investigations and comparisons under simplified conditions.

The models were simulated using ABAQUS FEA, a software developed by Dassault Systèmes and Simulia Corp. ABAQUS FEA product suite is composed of five core products. For the purposes of this research, "ABAQUS/CAE" or the "Complete ABAQUS Environment" 2023 has been employed. This suite is recognised for its robust and intuitive interface that facilitates the intricate process of model development from conceptual design to the visualization of simulation results.

Nonlinear properties of the concrete and reinforcing steel were applied using concrete damaged plasticity model and plasticity model, respectively. A deformation-controlled approach under a static loading condition was adopted to track the loads-displacement relationship. By controlling deformation rather than load, ABAQUS will calculate the loads, and other quantities that correspond to the prescribed displacement, assuming the system reaches equilibrium under the applied boundary conditions.

ABAQUS has no default units. Hence, the units have to be provided in a consistent system. The units adopted for the models in ABAQUS are shown in Table 4.1.

Table 4.1 Consistent units adopted in ABAQUS/CAE 2023.

Property	Mass	Length	Force	Time	Stress	Energy
Unit	kg	m	N	s	N/m^2	Nm

4.2 Model geometries and properties for the validation study

This section describes the two distinct ABAQUS models developed to simulate RC beam behaviour under different support conditions for the validation study. Two model geometries are considered in this thesis:

1. A RC beam with two end columns and one middle column, with horizontal restraints applied to the end columns. This configuration, denoted as the *spring model*, aims to more accurately represent the experimental setup by Yu & Tan (2013).
2. A RC beam with fixed supports on each side, denoted as *fully restrained* model. This model represents a simplified boundary condition.

Table 4.2 provides the model geometries of two different conditions. In the *fully restrained* model, the span length was taken as the clear span length, representing the distance between the faces of the columns. For the *spring model*, as the end columns were modelled, the span length was taken from the centre to the centre of the columns.

Table 4.2 Model geometries from the reference experiment.

Model	Beam Size (mm)		Span length (mm)	Rebars at the supports		Rebars at the middle joint	
	width, b	depth, h		Top	Bottom	Top	Bottom
Fully Restrained	150	250	5750	3ϕ10	2ϕ10	3ϕ10	2ϕ10
Spring	150	250	6150	3ϕ10	2ϕ10	3ϕ10	2ϕ10

Figure 4.1 shows the dimensions of the model and the boundary conditions, including the middle and end columns with horizontal restraints. The horizontal restraints are represented by two rods at each end column. Additionally, roller supports are located under the end columns, allowing for horizontal movement while preventing vertical displacement. It is noted that a lap splice at the middle joint is not considered.

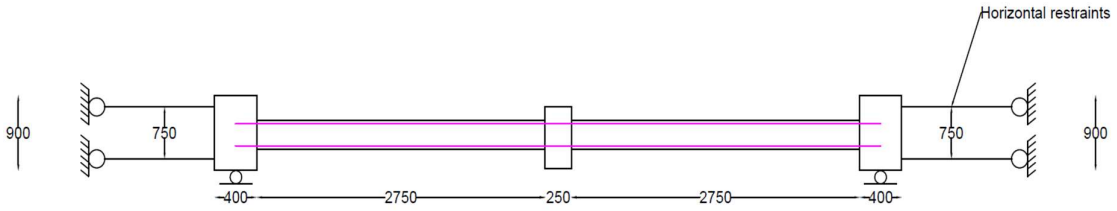

(a) Front view

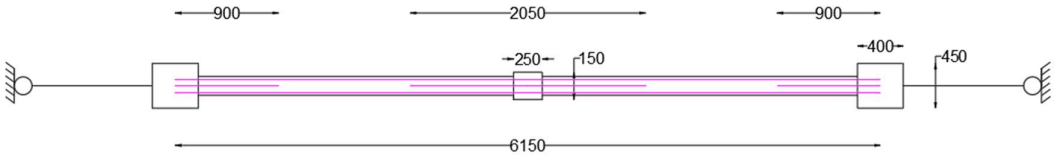

(b) Top view

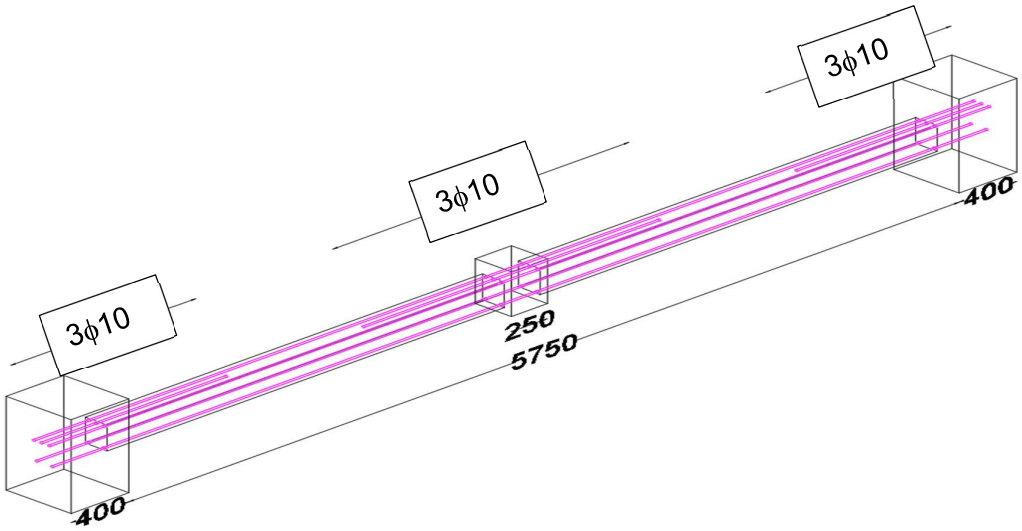

(c) Perspective view

Figure 4.1 The detailing of model geometry (a) Front view, (b) Top view, and (c) Perspective view.

Figure 4.2 to Figure 4.5 illustrates the model geometries in ABAQUS. In Figure 4.2 and 4.4, horizontal line in the middle represents a concrete beam and the top and bottom lines represent top and bottom rebars, respectively. The vertical lines in Figure 4.4 represent the end column stubs. The interactions between the concrete beam and the rebars, as well as the interactions between concrete beam and the end column stubs are discussed in detail Sections 4.4 and 4.5.

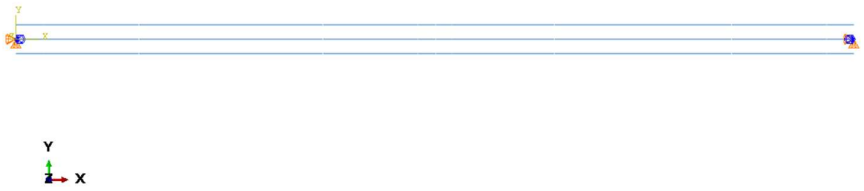

Figure 4.2 ABAQUS model for the fully restrained model including concrete beam, top and bottom rebars.

Figure 4.3 ABAQUS 3D rendering for the fully restrained model.

Figure 4.4 ABAQUS model for the spring model including concrete beam, top and bottom rebars, and end column stubs.

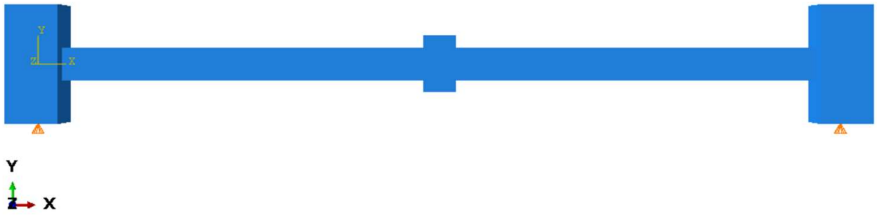

Figure 4.5 ABAQUS 3D rendering for the spring model.

To compare with the experiment by Yu & Tan (2013), the material properties of concrete and rebar tested by authors were selected. There were four concrete specimens with dimensions of 150 mm in diameter and 300 mm in height average values of compressive stress and strain of the concrete were selected.

The reinforcement bar used in the reference experiment were high-yield strength rebar with the nominal diameter of 9.53 in millimetres. The material properties of concrete and rebar according to Yu & Tan (2013) are shown in Table 4.3 and Table 4.4, respectively.

Table 4.3 Material properties of concrete.

Modulus of elasticity [MPa]	Compressive strength, f_c [MPa]	Tensile strength, f_{ct} [MPa]	Poisson's ratio
27663	32.8	2.88	0.2

Table 4.4 Material properties of rebar.

Diameter of rebar, ϕ [mm]	Yield strength, f_y [MPa]	Ultimate strength, f_u [MPa]	Rupture strain [%]
9.53	511	731	12.32

4.3 Element types

Two different element types were used to model the concrete beam, particularly, beam element and truss element.

For the beam element which represents the concrete part as it is shown in Figure 4.6, it is a one-dimensional line element in the x – y plane that has stiffness associated with the

deformation of the line which is the beam´s axis. In ABAQUS, this element corresponds to B21 beam which is a planar beam that uses linear interpolation with 3 degrees of freedoms. The 3 degrees of freedoms for the B21 beam element are:

1. Translational degree of freedom along the X-axis, ux
2. Translational degree of freedom along Y-axis, uy
3. Rotational degree of freedom about Z-axis, rz

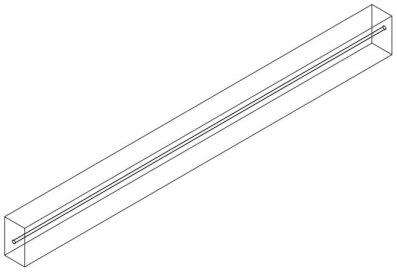

Figure 4.6 A 2- node B21 beam element for the concrete.

The reinforcement bars were modelled in ABAQUS with linear truss element, corresponds to T2D2 with a 2-node linear 2-D truss, see Figure 4.7. Truss elements are constant strain elements as one-dimensional bars that primarily undergo deformation through axial elongation and carry stresses only in the longitudinal direction. These elements have only translational degrees of freedom at each node, and they are connected at their nodes with pin joints, allowing for translational displacements.

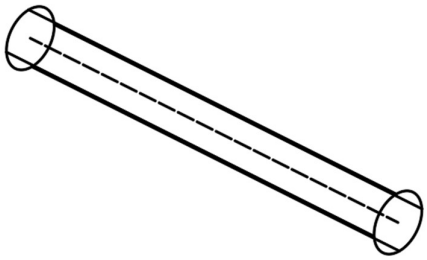

Figure 4.7 A 2-node T2D2 truss element for rebars.

4.4 Boundary conditions

In the *fully restrained model*, fully fixed supports were applied at the end of the concrete beam as shown in Figure 4.2. For the *spring model*, to describe the experiment more accurately, the end columns were included in the model. The vertical restriction due to the roller supports was introduced at the bottom of the end columns, see Figure 4.4. Additionally, the horizontal restraints were modelled using the equivalent stiffness of $1x10^5$ kN/m according to Yu and Tan, 2013 in horizontal direction or X-axis for all 4 nodes as shown in Figure 4.8.

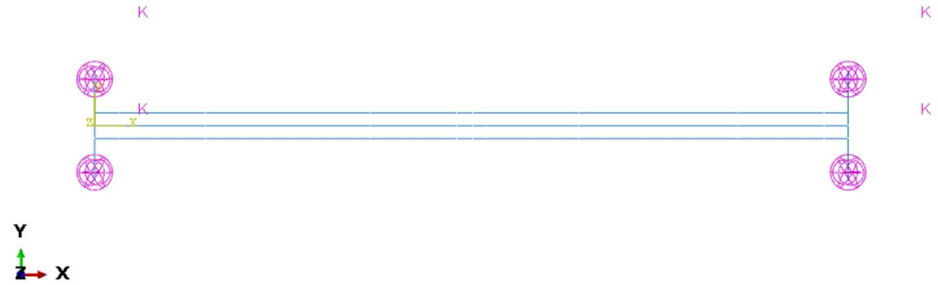

Figure 4.8 Horizontal restraints stiffness at the end columns for the spring model.

The degree of restraint in each support of the 2D plane is shown in Table 4.5 where 0 represents free movement, 1 represents a fixed constraint, x represents the horizontal axis, y represents the vertical axis, and rz represents the out-of-plane axis.

Table 4.5 Degree of restraint in each support of the 2D plane.

Supports	ux	uy	rz
Fixed	1	1	1
Pinned	1	1	0
Roller	0	1	0

4.5 Interaction between reinforcement and concrete

In these models, full interaction between concrete and reinforcing steel was utilized. In full interaction, the assumption is that the reinforcement bars are surrounded by and bonded to the concrete. This implies that there is no relative movement or slip between the reinforcement bars and the surrounding concrete. In ABAQUS, a fully embedded mechanism is created by using a tie constraint where the concrete is a master element whereas the reinforcement bars are secondary elements. This directive constrains each of the nodes on the secondary elements to have the same motion as the node on the master element to which it is closest. Figure 4.9 shows the full interaction between the concrete and top and bottom rebars.

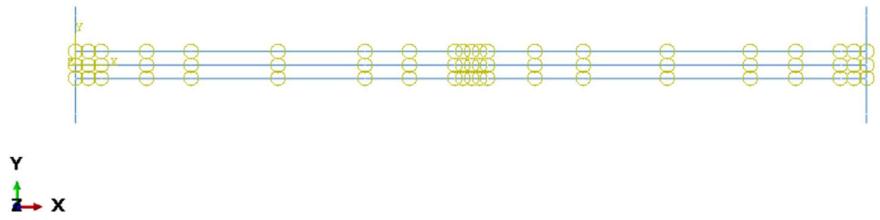

Figure 4.9 Full interaction between the concrete and reinforcing steel.

4.6 Section points

Section points are used to numerically integrate over an element to compute and monitor the various values inside of a FE, for example, stresses, strains, and internal forces inside a beam. In this thesis, the total number of section points for a beam was set to 11 and 1 point is allocated for reinforcing steel. Figure 4.10 and Figure 4.11 show the position of the section points located within the beam element and truss element. The number of section points used

can affect the accuracy and convergence of the FE solution. More section points lead to higher accuracy, however, it increases the computational cost.

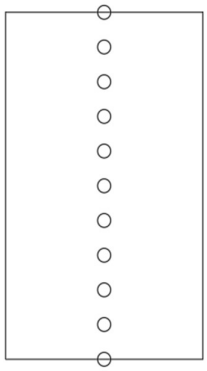

Figure 4.10 11 section points located within the concrete beam.

Figure 4.11 1 section point located in the middle of the reinforcing steel.

4.7 Material model for concrete

This thesis uses the concrete damaged plasticity, CDP model to analyse the behaviour of concrete material. This model incorporates both damage and plasticity in a unified formulation, allowing for a comprehensive investigation using FE analysis.

4.7.1 Concrete damaged plasticity

Concrete damaged plasticity CDP is a beneficial tool for simulating the nonlinear behaviour of RC structures and evaluate their performance under varying load conditions. It assumes that the failure mechanisms are compressive crushing and tensile cracking of the concrete. The CDP model integrates the notion of concrete softening, which is essential for comprehending the formation of microcracks in the concrete component. This phenomenon is noticed when the stress-strain curve decreases from its maximum strength, indicating a decrease in the concrete's load-bearing capacity. As these cracks propagate, they additionally compromise the rigidity of the concrete, gradually reducing its material properties and lowering its strength (Grassl & Jirásek, 2006).

However, concrete may still perform a limited degree of ductility, allowing the structure to experience some deformation before failure. Therefore, concrete would be able to attract some of the applied load through plastic deformation. By incorporating this plastic deformation into the FE analysis, concrete damaged plasticity can be implemented in order to simulate the response of RC structures before failure.

The adopted CDP model describes the process of concrete damage by focusing on the reduction of the material stiffness, namely the elastic modulus of concrete, during the post-peak softening behaviour of the concrete constitutive law. Figure 4.12 depicts the correlation between stress and strain as seen in equation 4.1 for concrete under uniaxial tension or compression.

$$\varepsilon_{(\sigma)} = \varepsilon_{el}(\sigma) + \varepsilon_{in}(\sigma) = \frac{\sigma}{E_{c0}} + \varepsilon_{in}(\sigma) \quad (4.1)$$

Where $\varepsilon_{el}(\sigma)$, $\varepsilon_{in}(\sigma)$, and $\varepsilon_{(\sigma)}$ are the elastic, inelastic, and the total strains, respectively, at the given stress σ. The inelastic strain $\varepsilon_{in}(\sigma) = 0$ when $\sigma < \sigma_y$. E_{c0} represents the initial elastic modulus of undamaged concrete.

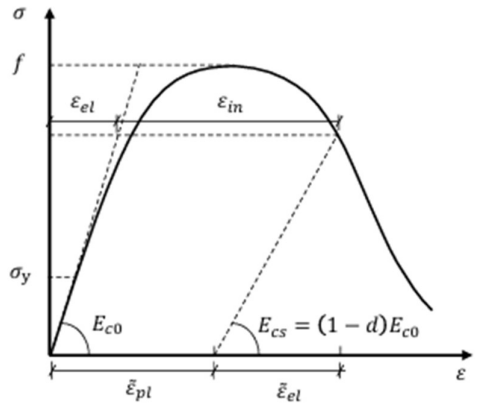

Figure 4.12 Damage evolution and degradation of the material stiffness beyond the peak stress of concrete. By (Mathern & Yang, 2021b).

By considering the damage evaluation beyond the peak stress, the initial elastic strain $\varepsilon_{el}(\sigma)$ changes to $\widetilde{\varepsilon_{el}}(\sigma)$ due to the degradation of the elastic modulus from E_{co} to E_{cs} according to:

$$E_{cs} = E_{co}(1 - d) \quad (4.2)$$

Where, d is the damage factor to be defined for characterizing the damage evolution by:

$$d = 1 - \frac{\sigma}{f} \quad (4.3)$$

Where, f is the concrete tensile strength f_{ct} or compressive strength f_c.

The concrete plasticity parameters to be defined in the CDP model are represented in Table 4.6.

Table 4.6 Plasticity parameters defined in the CDP model.

Categories	Plastic Flow Potential		Yield Surface		Viscosity Parameter
Parameters	Dilation angle φ	Eccentricity ϵ	σ_{b0}/σ_{c0}	k_c	μ
values	35°	0.1	1.16	2/3	1×10^{-5}

The default values of ϵ, σ_{b0}/σ_{c0}, and k_c are determined according to the design manual of ABAQUS. The eccentricity factor, ϵ, is associated with the flow potential, while the factors σ_{b0}/σ_{c0}, and k_c are related to the yield surface as described in Mathen and Yang's analysis. The dilation angle, φ, is one of the parameters defining the concrete plasticity that should be positive and in the range of 0° – 56.3°, (Mathern & Yang, 2021). The dilation angle is the angle between the principal stress direction and the direction of increasing strain during

deformation, which represents the material's tendency to expand as it deforms under loading. In Mathern & Yang (2021), an angle of 35° in the FE analysis showed a suitable result by providing fast convergence and reasonable response compared to the experiment results.

The viscosity parameter μ, can be defined to implement the viscoplastic regularization in the FE analysis in order to overcome the challenging convergence issues in nonlinear concrete problems. The viscoplasticity allows stresses to exceed the yield surface, which enhance the convergence rate for the damaged concrete in the strain-softening regime. A higher value of μ leads a material yield or deform more slowly under the same load. The default value in ABAQUS is taken as 0. A parametric study in Chapter 7 was conducted to determine the appropriate value for the reference FE model by studying the viscosity parameter in the range of 10^{-4} – 10^{-7}, here the value was selected as 10^{-5} in the reference FE model.

4.7.2 Compressive behaviour

Compressive behaviour can be described through the compressive stress-strain relationship. The compressive stress-strain relationship of concrete is nonlinear, starting from a linear initial stiffness until the stress reaches 40% of compressive strength, followed by an ascending branch until reaching the peak stress and descending branch after reaching the peak stress.

The compressive stress-strain relationship was plotted in Yu & Tan (2013) with an acceptable accuracy that matched the result of Maekawa et al. model as shown in Figure 4.13. These stress-strain curves simulated the nonlinear behaviour of concrete under compressive load, including post-peak softening behaviour, which is critical for analysing structural response leading up to failure.

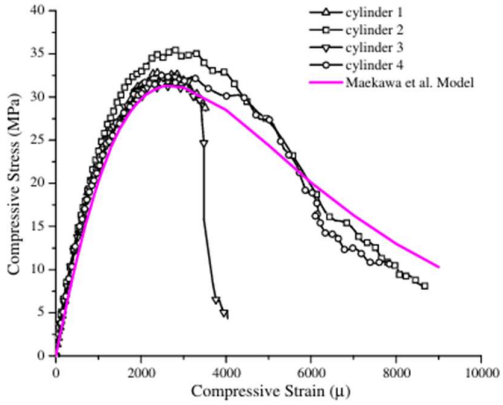

Figure 4.13 Compressive stress-strain relationship extracted from (Yu & Tan, 2013).

Mathern & Yang (2021b) suggest that compressive behaviour after compressive strength should be modified in FE modelling due to strain localization by a factor $\frac{L}{L_{cr}}$ as shown in Figure 4.14 where L is a specimen length, which is 300 mm and L_{cr} denotes a critical fracture zone and it refers to the length or size of the crushing zone in concrete under compression a critical fracture zone. The appropriate value of L_{cr} for concrete compared to the experiment is 10 mm and the appropriate value of L_{cr} is determined in Section 4.8.

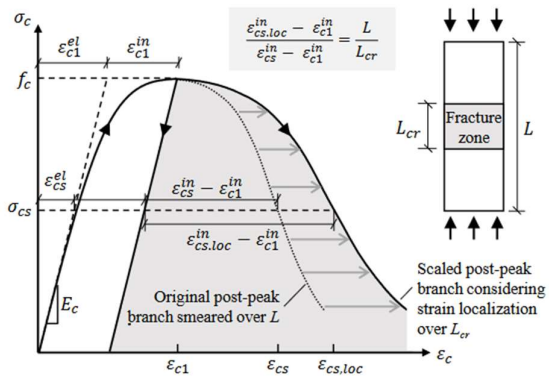

Figure 4.14 Modification of the post-peak softening branch of the constitutive model for concrete in compression originally expressed by the mean strain smearing over the whole length of specimen L to consider the strain localization in the critical fracture zone with the length of L_{cr}. From (Mathern and Yang, 2021b).

Original compressive stress-strain and modified compressive stress-strain relationships are shown in Figure 4.15. As mentioned in the paragraph above, strain values are increased in the post-peak softening region.

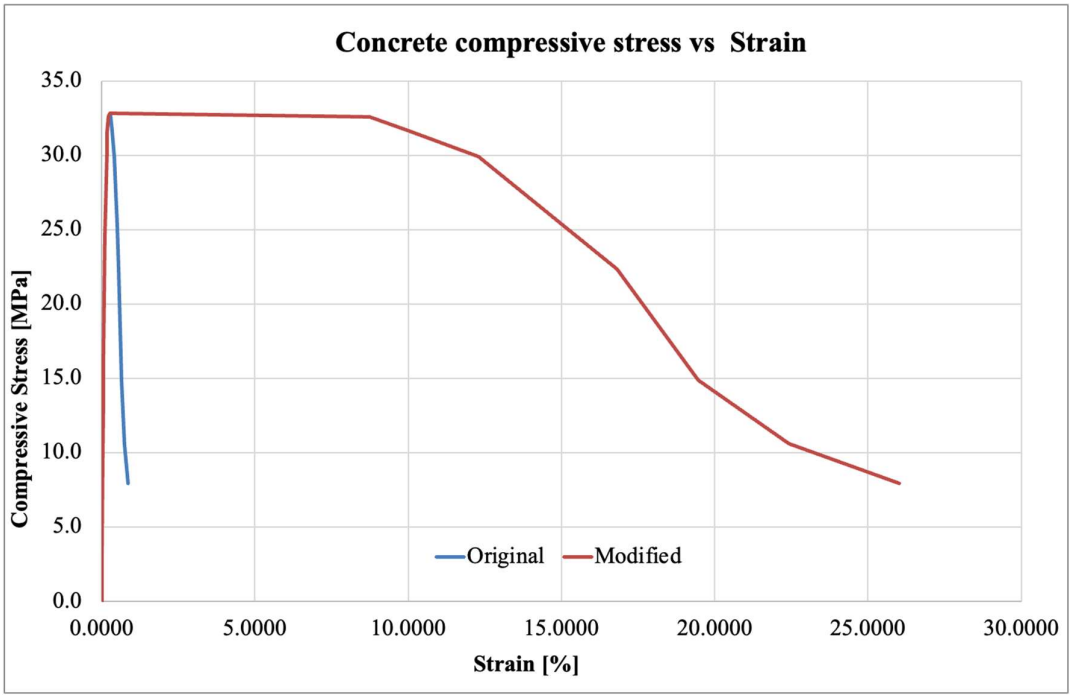

Figure 4.15 Compressive behaviour of the concrete with original stress-strain relationship and modified stress-strain relationship with the consideration of strain localization.

For concrete damaged plasticity in ABAQUS, input data for strain values is inelastic strain, ε_{in} which can be calculated by equation 4.1. Table 4.7 shows original, modified total strain and inelastic strain of the concrete according to the experiment.

Table 4.7 Experimental compressive stress-strain behaviour data for concrete. Shaded areas are input data to provide in ABAQUS.

Compressive stress (MPa)	Original total strain (%)	Modified total strain (%)	Modified inelastic strain (%)
0	0	0	0
2.9	0.01	0.01	0
9.2	0.03	0.03	0
13.1	0.05	0.05	0
16.0	0.06	0.06	0.03
24.5	0.11	0.11	0.03
30.2	0.17	0.17	0.06
31.5	0.18	0.18	0.07
32.6	0.23	0.23	0.11
32.8	0.27	0.27	4.41
32.6	0.29	8.75	5.22
31.6	0.33	10.00	6.58
30.0	0.41	12.29	9.05
25.4	0.50	15.00	12.26
22.3	0.56	16.81	14.39
15.0	0.65	19.46	17.85
10.6	0.75	22.42	21.28
8.0	0.87	26.03	25.17

4.7.3 Tensile behaviour

The tensile failure of concrete is always a discrete phenomenon. Therefore, to describe the tensile behaviour a stress-strain relation should be used for the uncracked concrete, see Figure 2.3a, and a tensile stress, σ_{ct}, - crack opening, w, diagram as shown in Figure 2.3b should be used for the crack section.

For uncracked section, a linear stress-strain relationship as represented in Figure 2.3a, can be applied until the tensile stress reaches the tensile strength. In this relationship, ε_{ct} is the tensile strain, σ_{ct} is the tensile stress in MPa, f_{ctm} is the tensile strength in MPa.

For a cracked section, a bilinear approach for the stress-crack opening relationship, as shown in Figure 2.3b, is applied. This approach involves the fracture energy of concrete, G_f [N/m], which is defined as the energy required to propagate a tensile crack of unit area. The fracture energy is dependent on the mean compressive strength, f_{cm}, and can be estimated using the equation 4.11.

$$\sigma_{ct} = f_{ctm}\,(1.0 - 0.8\frac{w}{w_1}) \qquad \text{for} \qquad w \leq w_1 \tag{4.9}$$

$$\sigma_{ct} = f_{ctm}(0.25 - 0.05\frac{w}{w_1}) \qquad \text{for} \qquad w_1 < w \leq w_c \tag{4.10}$$

$$G_f = 0.73 f_{cm}{}^{0.18} \tag{4.11}$$

where:

$w_1 = \frac{Gf}{f_{ctm}}$ in mm when $\sigma_{ct} = 0.20 f_{ctm}$

$w_c = 5\frac{Gf}{f_{ctm}}$ in mm when $\sigma_{ct} = 0$

According to the experiment by Yu and Tan, 2013, splitting tensile strength, $f_{ctm,sp}$, is given and tensile strength can be calculated providing by EC2 as shown in equation 4.12.

$$f_{ctm} = 0.9 f_{ctm,sp} \tag{4.12}$$

where:

$f_{ctm,sp}$ is splitting tensile strength = 3.2 MPa

Since interaction between concrete and reinforcement is considered to be full interaction or perfect bond, crack band width equals to mean crack distance, s_{rm}, which is calculated based on maximum crack distance, $s_{r,max}$, according to EC2, as shown in equation 4.14. Cracking strain, ε_{cr}, can be determined by dividing crack opening, w, with the crack band width, h_w, which is the length over that the crack localises, see equation 4.15. Converting crack opening (w) to cracking strain (ε_{cr}) is necessary for input data of tensile behaviour.

$$s_{r,max} = k_3 c + k_1 k_2 k_4 \phi / \rho_{p,eff} \tag{4.13}$$

$$s_{rm} = \frac{s_{r,max}}{1.7} \tag{4.14}$$

$$\varepsilon_{cr} = \frac{w}{s_{rm}} \tag{4.15}$$

where:

c is the covering of the concrete

ϕ is the bar diameter

$\rho_{p,eff}$ is the effective reinforcement ratio, $\rho_{p,eff} = \frac{A_s}{A_{c,ef}}$ and $A_{c,ef}$ is the effective area of concrete in tension

$k_1 = 0.8$ for high-bond bars

$k_2 = 0.5$ for pure bending

$k_3 = 3.4$ (recommended value)

$k_4 = 0.425$ (recommended value)

The effective area of concrete in tension can be determined using the provision in the FIB Model Code 1990.

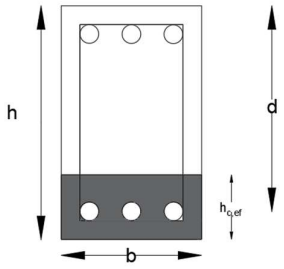

Figure 4.16 Effective area of concrete.

For a beam, the effective area of concrete is calculated by

$$A_{c,ef} = h_{c,ef} \times b \tag{4.16}$$

$$h_{c,ef} = \min\{(h\text{-}x)/3 \; ; \; 2.5(h\text{-}d)\} \tag{4.17}$$

where:

x = depth of the neutral axis

b = width of the beam

Table 4.8 provides the parameters to be used to determine tensile behaviour. Shaded areas represent input data in ABAQUS.

Table 4.8 Parameters in tensile behaviour of the concrete.

G_f [N/m]	s_{rm} [mm]	σ_{ct} [MPa]	w [mm]	ε_{cr}
136.8	103	2.9	0	0
		0.6	0.05	0.0004
		0	0.23	0.0023

Figure 4.17a represents the relationship between tensile stress and crack opening, and Figure 4.17b represents the relationship between tensile stress and cracking strain.

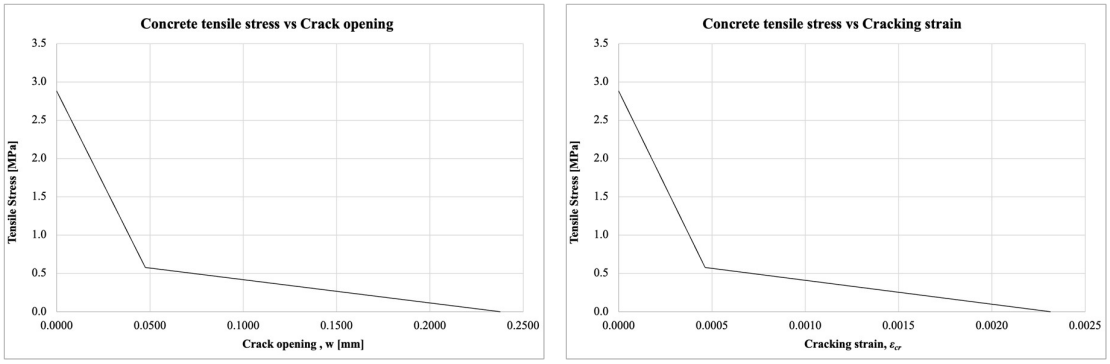

(a) (b)

Figure 4.17 Relationship between (a) concrete tensile stress and crack opening, and (b) concrete tensile stress and cracking strain.

4.8 Material model for reinforcing steel

Plasticity model is applied to the properties of reinforcement bars. Plasticity is defined by providing stress and plastic strain as material input data in ABAQUS. Plastic strain can be calculated by equation 4.18.

$$\varepsilon_{pl} = \varepsilon_{tot} - \varepsilon_{el} \tag{4.18}$$

where:

ε_{tot} is total strain

ε_{el} is elastic strain, $\varepsilon_{el} = \frac{f_y}{E_s}$ where f_y is yield strength and E_s is modulus of elasticity of reinforcing steel.

In a typical tensile test, the data provided is the engineering stress (σ_{eng}) and engineering strain (ε_{eng}) which is assumed that the cross-sectional area remains constant during the test. However, during a tensile test, as the specimen deforms, its cross-sectional area decreases, meaning that true stress is higher than engineering stress which is calculated by the applied load divided by the actual cross-sectional area. According to the ABAQUS manual, when defining plasticity data, true stress and true strain must be used, so it is important to convert engineering stress and strain to true stress and strain. Figure 4.18 illustrates a comparison between engineering and true stress-strain of rebar ϕ10. Stress and strain values are extracted from Figure 4.18 and shown in Table 4.9. It is seen that true stress is higher than engineering stress after the rebar yields.

True stress and true strain can be calculated as follow:

$$\sigma_{true} = \sigma_{eng}\,(1+\varepsilon_{eng}) \tag{4.19}$$

$$\varepsilon_{true} = \ln(1+\varepsilon_{eng}) \tag{4.20}$$

However, true stress after necking can be calculated according to (Ling, 1996) by a power law as shown in equation 4.21

$$\sigma_{true} = K\varepsilon^{n} \tag{4.21}$$

where K and n are empirical constants determined from known true stress-strain data before necking and can be calculated as

$$n = \varepsilon_{u,true} = 0.12$$

$$K = \frac{\sigma_{u,true}}{n^n} = 1065$$

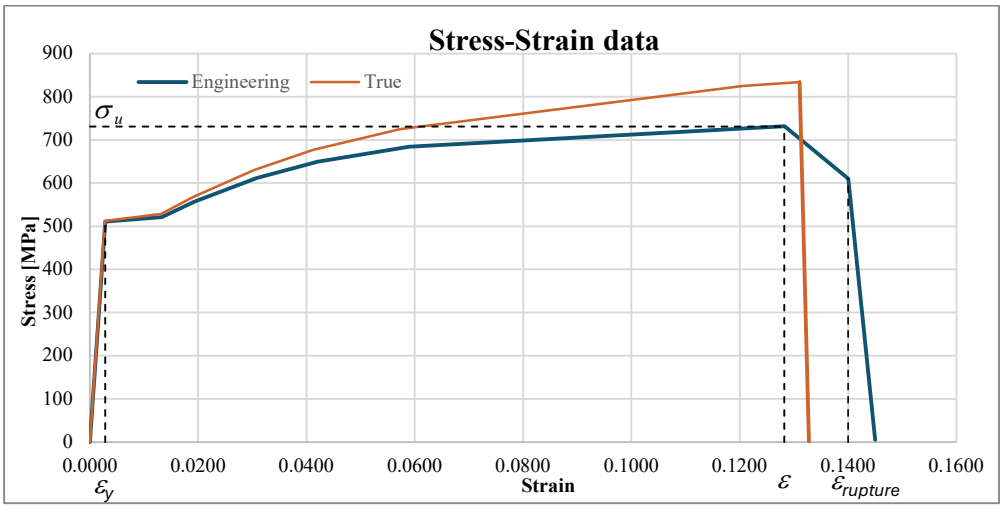

Figure 4.18 Comparison between engineering and true stress-strain.

Table 4.9 Comparison of engineering stress-strain and true stress-strain.

	σ_{eng} [MPa]	ε_{eng}	σ_{true} [MPa]	ε_{true}
	0	0	0	0
Yield	511	0.0028	511	0.0028
	521	0.0133	528	0.0132
	557	0.0193	567	0.0191
	611	0.0308	630	0.0303
	650	0.0420	677	0.0411
	685	0.0590	725	0.0573
Ultimate	731	0.1282	825	0.1207
Rupture	610	0.1400	834	0.1310
	1	0.1420	1	0.1328

The length of specimen (L) is assumed to be 100 mm and the critical length (L_{cr}) due to strain localisation is also considered for reinforced steel in the softening phase. The value of L_{cr} is taken as 25 mm which will be discussed in Section 4.8. Hence, the strain in the softening phase increases with the factor of $\frac{L}{L_{cr}}$.

Table 4.10 provides input data for reinforced steel in ABAQUS. Input data are true stress and true plastic strain. As mentioned above, plastic strain in softening phase is modified with the factor of 4. Shaded areas are input data to be specified.

Table 4.10 Input data of reinforcing steel.

σ_{true} [MPa]	Original ε_{pl}	Modified ε_{pl}
511	0	0
528	0.0104	0.0104
567	0.0163	0.0163
630	0.0275	0.0275
677	0.0383	0.0383
725	0.0545	0.0545
825	0.1179	0.1179
834	0.1282	0.5129
1	0.1300	0.5200

Figure 4.19 compares the applied load against middle joint displacement curves for both engineering and true stress-strain models. It shows that the stress-strain behaviours of reinforcing steel influence the capacity for catenary action. Engineering stress-strain values tend to underestimate this capacity, as shown by the lower applied load curve. In contrast, true stress-strain values result in a higher applied load curve which aligns more closely with experimental results. However, a model with a true stress-true strain curve fails to capture the sudden load drop around 600 mm displacement, which corresponds to the rupture of the top rebars. This may be attributed to the effect of the strain localization, potentially resulting in an overestimation of ductility prior to the rebar reaching its rupture strength. Based on these results, true stress-strain values are used in the material model because it more accurately predicts the overall load-carrying capacity of the system, which is of primary importance in this study.

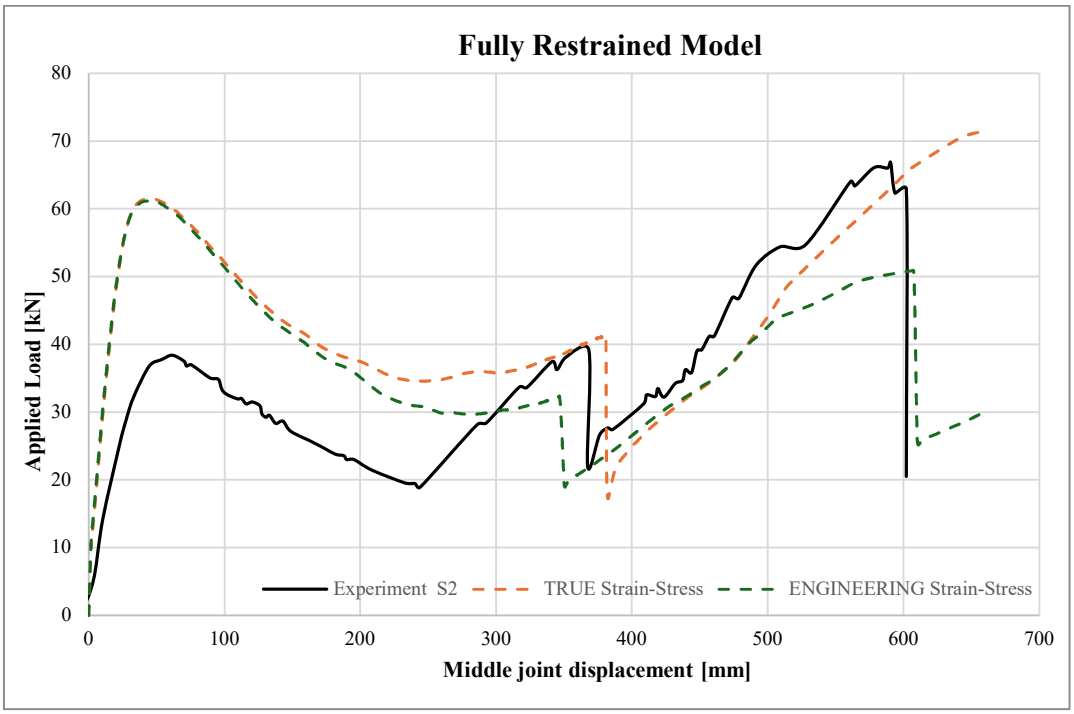

Figure 4.19 Comparison of applied load and middle joint displacement between true stress-strain and engineering stress-strain.

4.9 The critical fracture zone

According to (Mathern & Yang, 2021b), a systematic method is suggested for determining the value of L_{cr} using a logical approach. The assumed value $L_{cr.input}$ which is utilised to change the post-peak branch of the compressive behaviour as input data, should be checked based on the observed length $L_{cr.output}$ of the simulated crushing zone in the numerical result.

However, this approach was employed to determine the appropriate L_{cr} for both concrete, as outlined in appendix A, in accordance with the flowchart devised by Mathern & Yang, see Figure 4.20. The outcome of this analysis was that $L_{cr.output}$ = 150 mm.

Subsequently, the FE modelling utilising the obtained value of $L_{cr} = 150$ mm exhibited a significant disparity in the load-deflection curve, compared to experiment. Therefore, this strategy was deemed invalid for these models. Consequently, another method was implemented, as previously described, to determine an appropriate L_{cr} value.

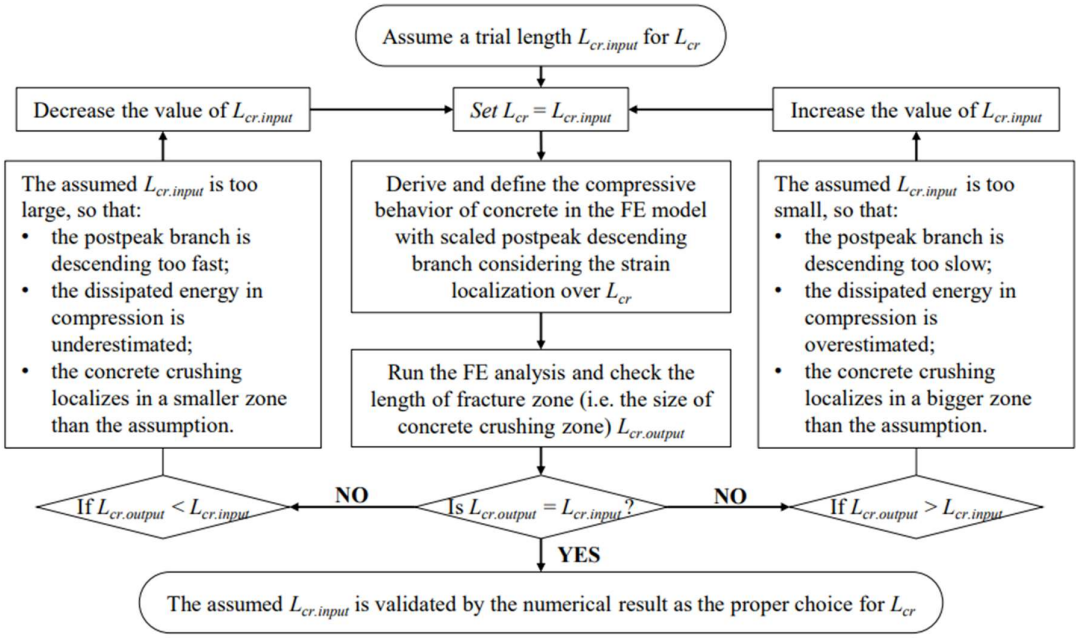

Figure 4.20 Proposed iterative procedure for identifying the reasonable length L_{cr} of the critical fracture zone according to (Mathern & Yang, 2021b).

Nevertheless, as stated in the Section 4.6.2.1, the optimal value of $L_{cr.conc}$ for concrete has been established to be 10 mm. The value has been obtained by doing simulations with various $L_{cr.conc}$ values for concrete, while assuming a fixed $L_{cr.rein}$ value of 25 mm for reinforcement since the length of the specimen is unknown in the experiment, and as the same as the determined mesh size in Chapter 6.

In the current FE study, the load-displacement analysis demonstrates the behaviour of the RC beam with respect to various values of $L_{cr.conc}$. The results in Figure 4.21 indicate that selecting $L_{cr.conc} = 10$ mm is the most appropriate choice regarding the slope of the resultant curve, as it has a greater impact on both the flexural action and CMA compared to experiment, considering that the value of the critical fracture zone L_{cr} can significantly alter these actions. While for the other values of $L_{cr.conc}$ such as 100 and 50 mm, the slopes at descending phase decrease rapidly after the ultimate load capacity within the CMA region.

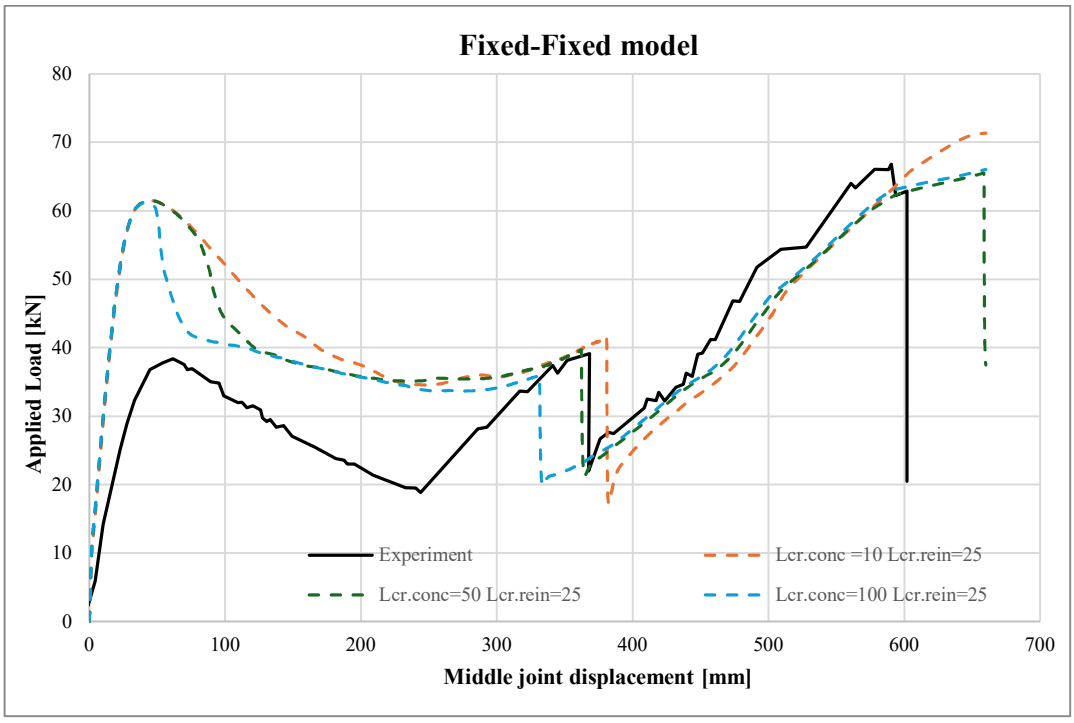

Figure 4.21 Load–displacement curves for FE analyses based on various L_{cr} values for concrete.

4.10 Load application

Load control and deformation control are two methods used in structural analysis and testing to regulate the loading conditions applied to a structure. Load control is the method of increasing the applied load and measuring the corresponding deformations. The test or the structural analysis is completed when the maximum load is reached, (Reinhardt, 2013). In the deformation control, the deformation is increased, and the applied load required to obtain that deformation is measured.

Deformation control is preferable to load control for capturing catenary action in RC beams because it allows for an increase of midspan deformation and allows for the observation of the entire load-deflection response, including the transition from flexural action to CMA, and subsequently to catenary action. Hence, the load capacities for different actions can be captured.

Deformation control is preferable to load control for capturing catenary action in RC beams because it allows for an increase of midspan deformation. Deformation control allows for the observation of the entire load-deflection response, including the transition from flexural action to CMA, and subsequently to catenary action. through a load-deformation curve occurs when a beam deflects under load. By controlling deformation, conditions can be simulated that lead to the development of catenary action, for example, the deformation of the beam and the redistribution of the internal load.

In ABAQUS, desired deformation is specified using boundary condition in the U2 or vertical direction. Deformation is increased linearly until it reaches the desired value. An amplitude refers to a predefined function that defines how a boundary condition or load varies over time. In models where the time-period is defined as 1 second, a tabular amplitude definition can be shown in Table 4.11.

Table 4.11 Tabular amplitude definition.

Time/Frequency	Amplitude
0	0
0.25	0.25
0.50	0.50
0.75	0.75
1	1

4.11 Solution method and time step

The determination of a time step size is based on static analysis, which is usually entails examining structures under constant loading. Therefore, dynamic behaviour or time-dependent phenomena are not considered.

Iterative process is frequently used in ABAQUS to converge to the solution during the problem-solving process, where the magnitude of the time step is utilized in the iterative process effecting the convergence behaviour. Hence, the term "time step" here refers to the incremental modifications made to the solution in each iteration in order to reach convergence.

The time period in this FE modelling in which is how long the step occurs in simulation has been determined to be 1 second for increments in the range of 10000 – 15000. The long the time period in ABAQUS, the more time an increment needs to simulate.

In addition to static analysis, a dynamic analysis has been conducted on these models to examine the behaviour of the beam under dynamic loading conditions, as described in Section 2.2.1. The dynamic FE modelling in ABAQUS demonstrated a highly similar trend line for static, implicit, and explicit dynamic simulations, utilising the preliminary data. This is illustrated in Figure 4.22. Nevertheless, it is important to note that the analysis provided here is only a rudimentary summary, as the focus of this thesis is elsewhere and does not delve deeply into dynamic analysis.

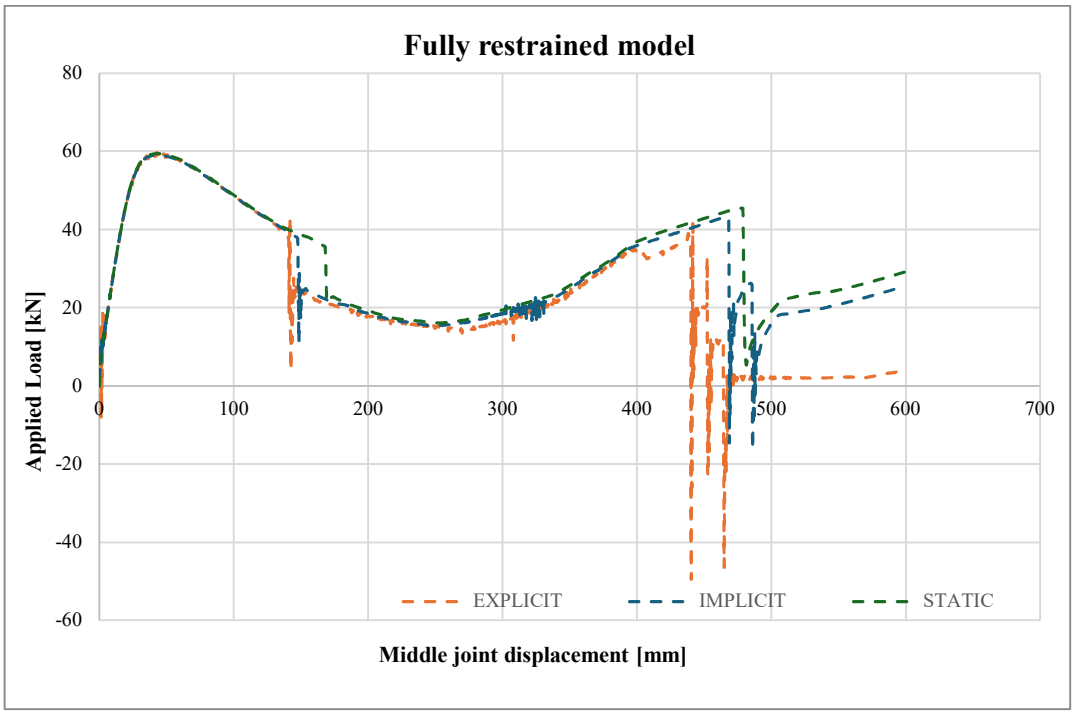

Figure 4.22 Load-deflection curves for different solvers; static, dynamic/implicit, and dynamic/explicit.

5 Analytical Calculations

5.1 Introduction

This chapter presents the analytical calculations focusing on flexural capacity before the onset of CMA and catenary action capacity of the RC beam.

It is important to note that catenary action occurs when the lateral restraint at the supports possesses sufficient capacity to resist additional horizontal reaction forces, for example, if both supports are pinned or fixed. In contrast, if one side of the supports is a roller support, catenary action will not occur since the beam can move freely in horizontal direction.

5.2 Flexural capacity

5.2.1 Modes of failure

There are three possible modes of failure in bending:

1. Concrete crushes first (over-reinforced design)

This failure occurs when the tensile force capacity of reinforcing steel is high so that concrete crushes before steel yields. Because concrete is a brittle material, so it fails without a warning. This type of failure should be avoided.

2. Steel yields first (under-reinforced design)

This type of failure occurs when the tensile force capacity of reinforcing steel is low so that steel yields before concrete crushes. There are two possible failure types for under-reinforced design, either concrete crushes or reinforcing steel ruptures. In both cases, the steel yields first. For the failure type concrete crushing, the strain at the compression edge of the concrete when it reaches the maximum value is typically around 0.0035. The beam continues to deform at constant load. This deformation causes the neutral axis to shift upwards, ultimately resulting in failure when the depth of the compression zone becomes small and insufficient to counterbalance the tensile force in the steel. Additionally, reinforcing steel bars themselves may also fail under the excessive forces. This type of failure is desired since there is a warning before RC beam fails.

3. Simultaneous rupture of steel and concrete

This type of failure involves the simultaneous rupture of steel and concrete. It occurs when the reinforced steel ruptures at the same time as the concrete crushes.

The ultimate flexural capacity is determined through under-reinforcement design principles, in accordance with EC2 guidelines.

5.2.2 Assumptions

1. Strains in both the concrete and reinforcing steel are derived under the assumption that plane sections maintain their planarity.
2. Tensile strength of the concrete is not considered.

5.2.3 Analysis of cross-sections

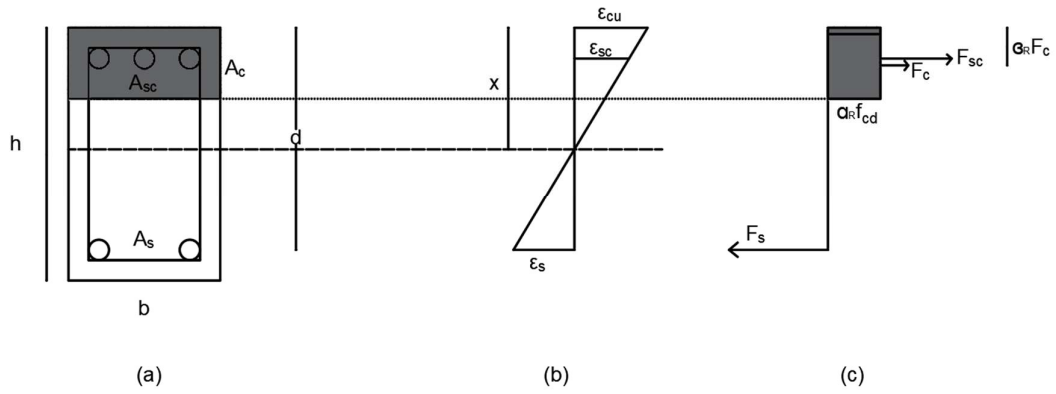

Figure 5.1 (a) Section; (b) strain; (c) stress diagram.

b = *width of the section*
h = *depth of the section*
d = *effective depth*
x = *depth to the neutral axis*
A_c = *area of compressive zone*
A_s = *area of tension reinforcement*
A_{sc} = *area of compressive reinforcement*
F_{sc} = *compressive force in steel*
F_s = *tensile force in steel*
F_c = *compressive force in concrete*
f_{cd} = *designed compressive strength of concrete*
ε_{cu} = *maximum strain in the concrete at failure = 0.0035*
ε_s = *strain in tensile steel*
ε_{sc} = *strain in compressive steel*
β_R = *stress block factor for the location of the stress resultant = 0.416*
α_R = *stress block factor for the average stress = 0.81*
E_s = *modulus of elasticity of reinforced steel*

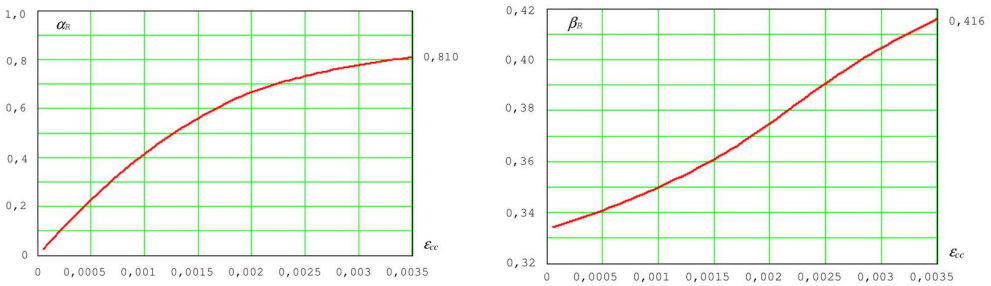

(a) (b)

Figure 5.2 Stress block factors for the simplified stress-strain relationship in normal strength concrete C12/16-C50/60, (a) α_R for stress block resultant, (b) β_R for location of stress block resultant extracted from Engström, 2015.

In typical design, the compressive strength shall be the design strength f_{cd} reduced with regard to sustained loading by a reduction factor α_{cc} and a partial factor γ_c instead of the characteristic strength f_{ck}.

$$f_{cd} = \frac{\alpha_{cc}\, x\, f_{ck}}{\gamma_c} \tag{5.1}$$

where

α_{cc}= 1.0 (recommended value)

γ_c = 1.5 (according to EC2)

The designed tensile strength of the reinforced steel is reduced with a partial factor γ_s

$$f_{yd} = \frac{f_{yk}}{\gamma_s} \tag{5.2}$$

where

γ_s = 1.15 (according to EC2)

According to the assumption that plane sections remain plane before and after bending, the strain ε_s and ε_{sc} in steel is calculated from the strain diagram as shown in Figure 4.18b by

$$\varepsilon_s = \frac{d-x}{x}\,\varepsilon_{cu} \tag{5.3}$$

$$\varepsilon_{sc} = \frac{x-d'}{x}\,\varepsilon_{cu} \tag{5.4}$$

If the strains are greater than the yield strain in reinforced steel, then reinforced steel yields and the value is calculated by

$$\varepsilon_{yield} = \frac{\frac{f_{yk}}{\gamma_s}}{E_s} \tag{5.5}$$

To calculate the ultimate flexural capacity, the equilibrium needs to be fulfilled by equation 5.6 and the ultimate flexural capacity is calculated by equation 5.7. Note that these equations are valid for the case that tensile rebars yield whereas compressive rebars have a linear

response. If compressive rebars also yield, the yield strength of compressive rebars, f'_{yd}, is applied instead of $E_s\varepsilon_{sc}$.

$$\alpha_R f_{cd} bx + E_s\varepsilon_{sc}A_{sc} = f_{yd}\,A_s \tag{5.6}$$

$$M_{Rd} = \alpha_R f_{cd} bx(d\text{-}\beta_R x) + E_s\varepsilon_{sc}A_{sc}(d - d') \tag{5.7}$$

However, to compare the ultimate flexural capacity to the experiment, the partial factors (γ_c and γ_s) used in the analysis are 1.0.

These analytical calculations estimate the ultimate flexural capacity of a RC beam in order to compare with the experimental test by Yu & Tan (2013). Flexural action develops until all plastic hinges occur at the critical sections. In this experiment, because the bottom reinforced steel has a lower amount compared to the top reinforced steel at the middle joint interface, hence, the bottom reinforced steels yield first. Consequently, the plastic hinges first developed at the middle joint interface and follow by the beam-end column stub interfaces.

The positive or sagging moment capacity that occurs at the middle joint interface is denoted as M_f and the negative or hogging moment capacity that occurs at the beam-end column stub interface is denoted as M_s. Figure 5.3c shows a free body diagram of the middle joint and the force equilibrium in the vertical direction is calculated in equation 5.8. Flexural capacity, P_f, is calculated without considering the effect of self-weight, q, and axial force, N, as shown in equation 5.9. Clear span length, l_n, between the support and middle column is considered. The detail of RC beams and capacities are summarised in Table 5.1 and Table 5.2 respectively.

$$P = 2V = 2(M_s + M_f - ND - \tfrac{ql_n^2}{2})/l_n \tag{5.8}$$

$$P_f = 2V = 2(M_s + M_f)/l_n \tag{5.9}$$

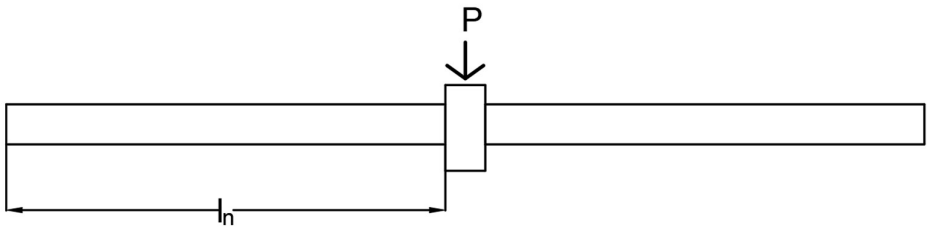

(a)

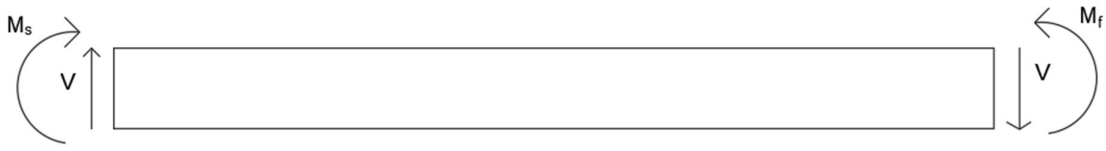

(b)

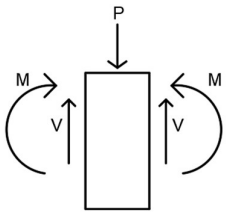

(c)

Figure 5.3 Free body diagrams of RC beam: (a) a beam-column subjected to a concentrated load; (b) left span beam; (c) middle joint.

Table 5.1 Specimen properties from (Yu and Tan, 2013).

Beam size [mm]			Reinforcement at the middle joint		Concrete	Reinforcement	
					f_{ck} [MPa]	f_{yk} [MPa]	f_u [MPa]
h	b	l_n	Top	Bottom			
250	150	2750	3ϕ10	2ϕ10	32.8	511	731

Table 5.2 The calculation of flexural capacity.

M_f [kNm]	M_s [kNm]	P_f [kN]
16.0	23.4	28.7

5.3 Catenary action capacity

The maximum applied load can be calculated with a simplified model and equation as shown in Figure 5.3 and equation 5.10 provided by Yu and Tan, 2013.

$$P = 2N_t sinq \tag{5.10}$$

$$N_t = A_s F_u \tag{5.11}$$

where:

$q = arctan(\frac{\Delta}{l_n})$

Δ = deformation at catenary action capacity regarding to experiment

l_n = clear span length = 2.75 m

N_t = axial force

A_s = top reinforced steel area at the beam end interface

F_u = ultimate tensile strength of top reinforced steel at the beam end interface

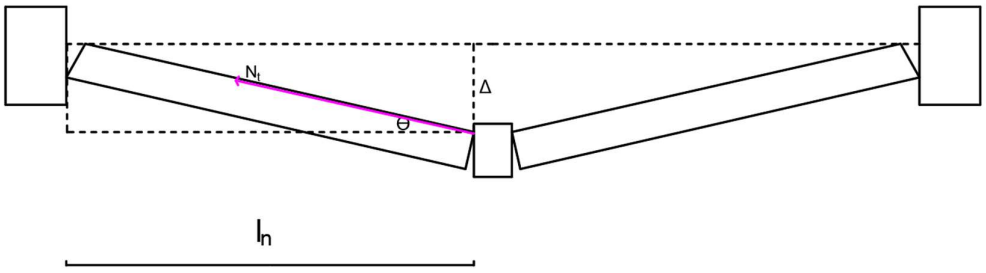

Figure 5.3 Simplified Model for calculation of catenary action capacity.

The analytical calculation of the catenary action capacity from the experiment can be calculated as shown in Table 5.3

Table 5.3 Catenary action capacity.

Deformation, Δ [mm]	Rotation angle, q [degrees]	N_t [kN]	P [kN]
612	12.5	156	68

6 Finite Element Model – Results and Comparison

6.1 Introduction

This chapter presents the outcome from the non-linear element FE-modelling procedure explained in Chapter 4, including the initial analysis to determine an optimal mesh size for the models. Subsequently, a validation procedure of the FE models was undertaken, involving comparison with results obtained from the reference experimental work.

Further study was conducted to examine the influence of various input parameters concerning the geometry of the beam, reinforcement ratios, and some modelling parameters, offering valuable insights into the influence that different parameters have on the structural response. This study will be presented in Chapter 7.

6.2 The choice of mesh size

A mesh size study was carried out to find an appropriate mesh size for the FE model. The study was conducted to analyse the structural response based on the displacement at the midpoint in relation to the applied force. The *fully restrained model* was used in this investigation and the chosen mesh size was then used for all models.

Initially, a comparison was conducted using different meshes, which presented challenges such as the mesh-dependency of the material properties. This study did not provide a clear indication of the optimal mesh size. Consequently, a subsequent approach was adopted, involving a comparison against experimental results to determine the appropriate mesh size.

The nominal mesh sizes used for the study were 25 mm, 50 mm, and 100 mm. The same mesh size was used for both the concrete part and the rebars. Figure 6.1 displays the load-displacement at the middle for two models with varying mesh sizes. The mesh sizes were compared to the experimental deflection-load values at the middle of the beam. A deviation of the numerical results from the experimental result was primarily seen for mesh sizes of 50 mm and 100 mm. Furthermore, the bottom reinforcement at the midspan experienced failure at a later time for a mesh size of 50 mm, while the failure of the bottom reinforcement for a mesh size of 100 mm was not observed. The study showed that the mesh size of 25 mm had higher precision.

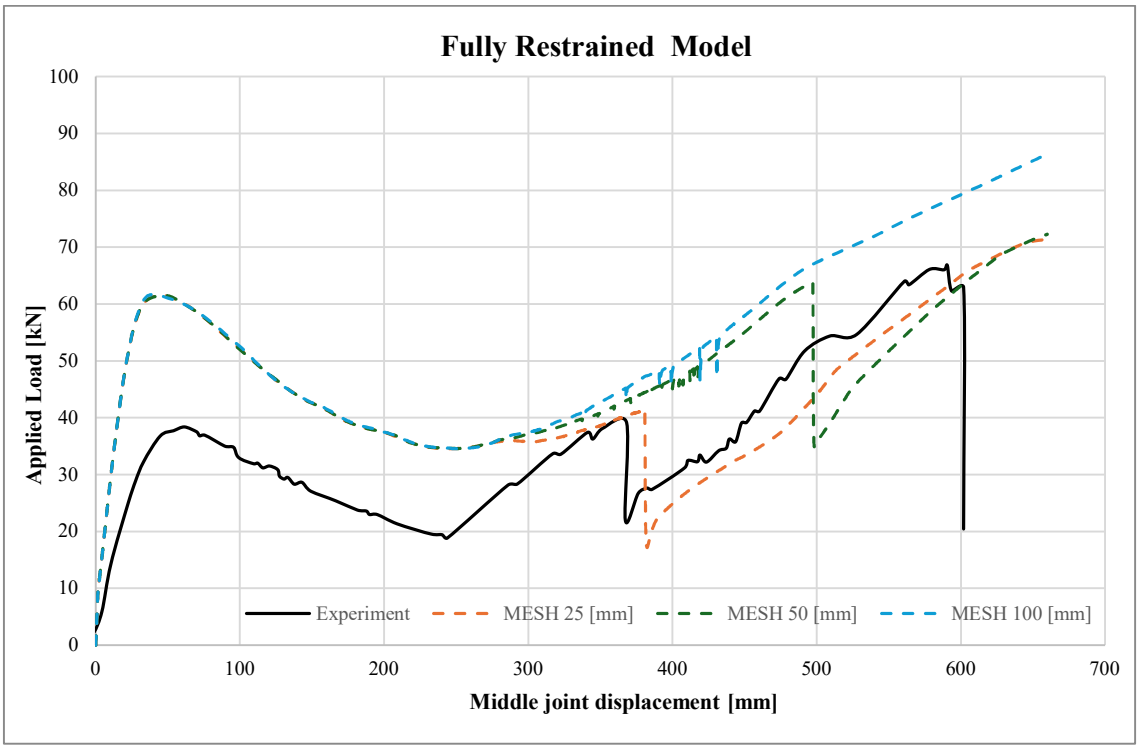

Figure 6.1 *Applied load-Displacement curves for mesh size study. Three different mesh sizes (25 mm, 50 mm, and 100 mm) were analyzed to determine the appropriate mesh size for further simulations.*

6.3 Applied load and horizontal reaction force vs middle joint displacement

An analysis simulating static test was conducted on ABAQUS Model, using the deformation control method outlined in Section 4.8, with a value of 660 mm. The relationships between the applied load, the horizontal reaction force and the middle joint displacement for both models; the *fully restrained model* and the *spring model* are depicted. The static analysis was carried out on the models using a 25 mm mesh size to capture the behaviour of the beam throughout the entire loading process, including beyond the peak CMA capacity.

Figures 6.2 to 6.5 illustrate the load-displacement and horizontal reaction force-displacement curves for the two different models. These figures highlight the classification of three distinct mechanisms, namely flexural action, CMA, and catenary action, based on the relationships between the applied load, the horizontal reaction force and the displacement of the middle joint (MJD). Flexural action continues until plastic hinges form at the critical sections. The presence of CMA can be determined if the horizontal reaction force, N_t, exceeds 10% of the RC beam section's compressive strength ($0.1 \cdot f_c \cdot A_g$). This threshold is used to differentiate flexural action and CMA and used to classify members as beams or columns in ACI 318-05 (Yu & Tan, 2010). The catenary action occurs when the horizontal reaction force shifts direction from compression to tension which can be seen in the relationship between horizontal reaction force and displacement in Figures 6.3 and 6.5. The sudden drop observed between 300 and 400 mm in the graphs of applied load versus MJD indicates the failure of the bottom rebars, where they reach their maximum strain value and rupture. After these critical points, the applied load increases again due to the engagement of the top rebars.

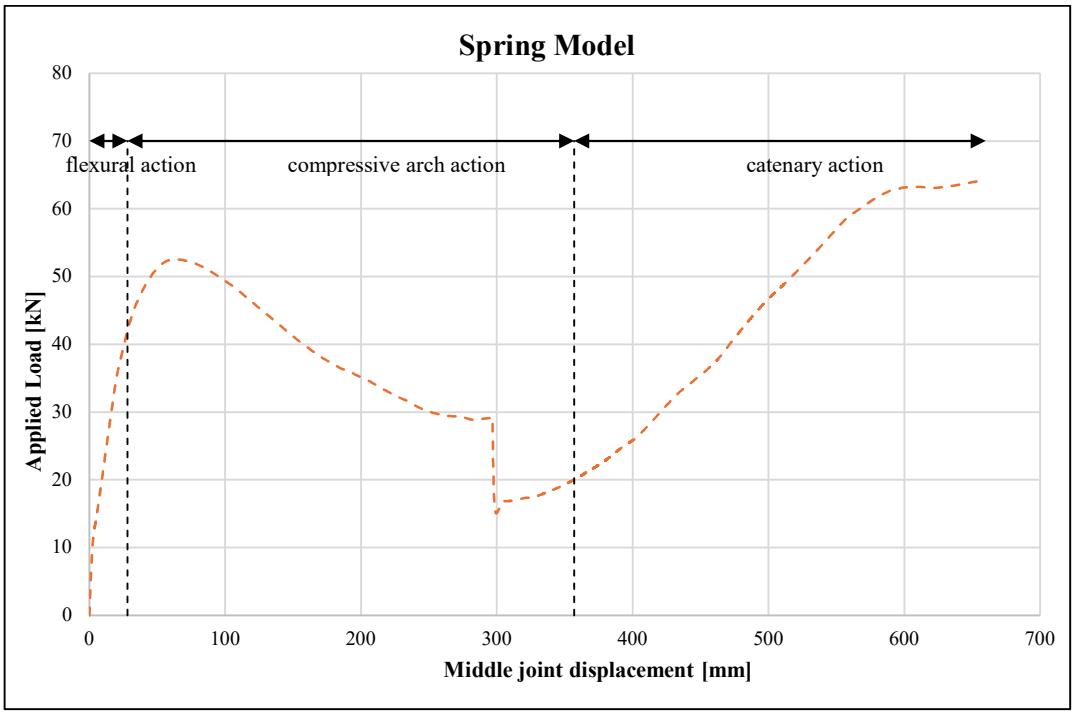

Figure 6.2 *Relationship of the applied force to the middle joint displacement according to the spring model.*

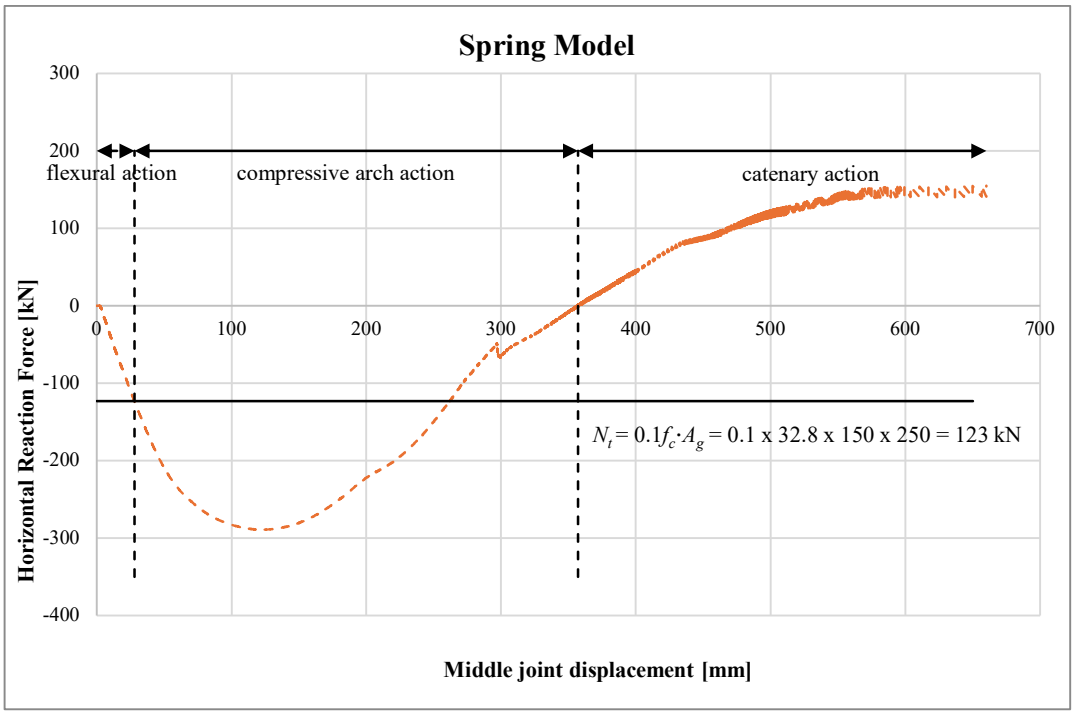

Figure 6.3 *Relationship of the horizontal reaction force to the middle joint displacement according to the spring model where N_t represents the horizontal reaction force used to differentiate flexural action and CMA.*

Figure 6.4 *Relationship of the applied force to the middle joint displacement according to the fully restrained model.*

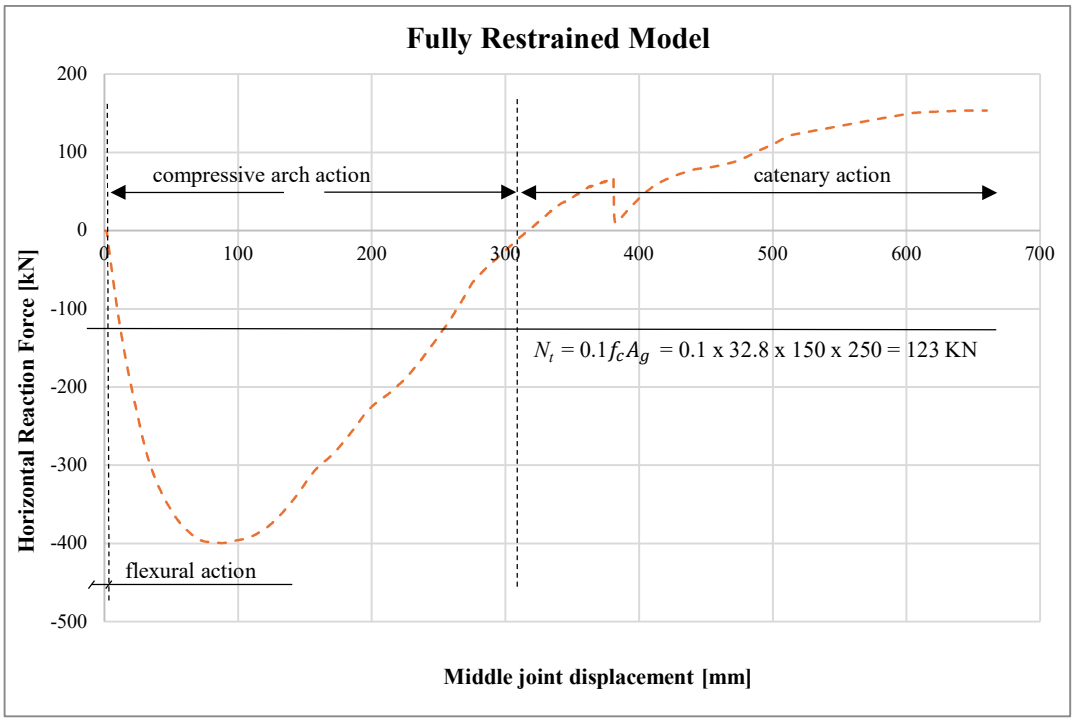

Figure 6.5 *Relationship of the horizontal reaction force to the middle joint displacement according to the fully restrained model where N_t represents the horizontal reaction force used to differentiate flexural action and CMA.*

6.4 Comparison

6.4.1 FEM against experiment

Results obtained from ABAQUS in Figures 6.6 to 6.7 show the comparison between the numerical results with the *spring model* and the experimental observations. Both the applied load and horizontal reaction force from the numerical calculations at the flexural and CMA stages are greater than those observed in the experiment. A potential reason for this deviation might be the equivalent horizontal restrained stiffness at the end columns as mentioned in Section 4.3. The actual horizontal restraint stiffness is lower than the equivalent stiffness as stated in the experiment, leading to differences between the experimental and FEM results. The sudden drop in the applied load due to the fracture of bottom rebars occurred at a different displacement location compared to the experiment. This discrepancy could be attributed to differences in the properties of the rebars, boundary conditions, stiffness of the support, and the value of the critical fracture lengths (L_{cr}). The stiffness of the support appears to have a significant influence at the flexural and CMA stages. Thus, a further study on the influence of support stiffness for the *spring model* will be performed in Chapter 7.

Figures 6.8 and 6.9 show the comparison between the numerical results and the experimental observations for the *fully restrained model*. A greater ultimate load capacity in comparison to the experiment is observed in Figure 6.8. Once more, the rigid boundary conditions are the reason for this observation, resulting in an increased beam stiffness and hence higher load capacity at both flexural and CMA stages. Nevertheless, it exhibits a comparable load-deflection slope both before and after the occurrence of catenary action, as well as a nearly identical failure of the bottom reinforcement at the midpoint of the beam by a sudden reduction of applied load caused by bottom rebars fracture at the middle joint interface.

Several probable factors influence the numerical results, such as the horizontal stiffness mentioned in the previous paragraph, interaction between concrete and reinforcement, strain localization, and the accuracy of material properties and models. The assumption of fully bonded interaction between concrete and reinforcement might affect the response of the RC beams as the reinforcement adds stiffness to the concrete element. Using bond-slip behaviour potentially affect the response differently, for instance, affecting the peak load during the CMA phase and the displacement at which the bottom rebars fracture. Modifying the critical fracture lengths (L_{cr}) for both concrete and reinforcing steel also impacts the response after the post-peak load of CMA, as it increases the original compressive strain values and the rupture strain of the reinforcing steel, resulting in a difference in the displacement at which the sudden load drop occurs, as shown in Figures 6.6 and 6.8. Unlike the experiment, both models did not show the final sudden drop caused by top rebars fracture at one beam end as top rebar did not reach the rupture strain after modification of the post peak strain of reinforcing steel. However, the capacities of catenary action are similar in both the simulations and experiment.

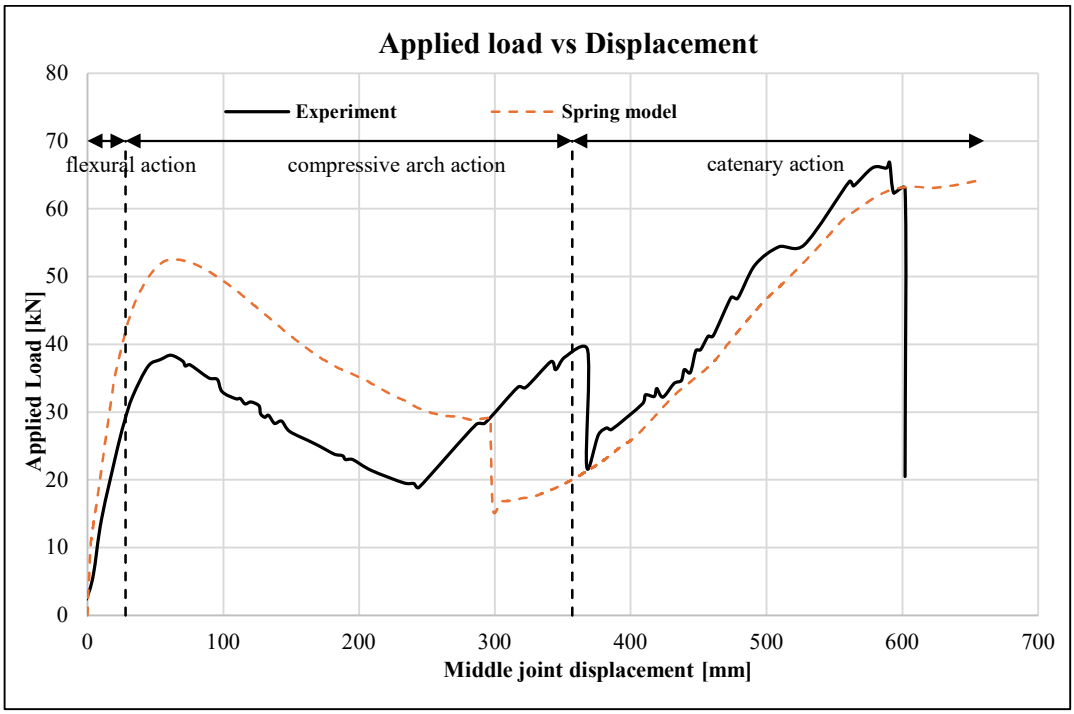

Figure 6.6 *Comparison of the applied force to the middle joint displacement between experiment and the spring model.*

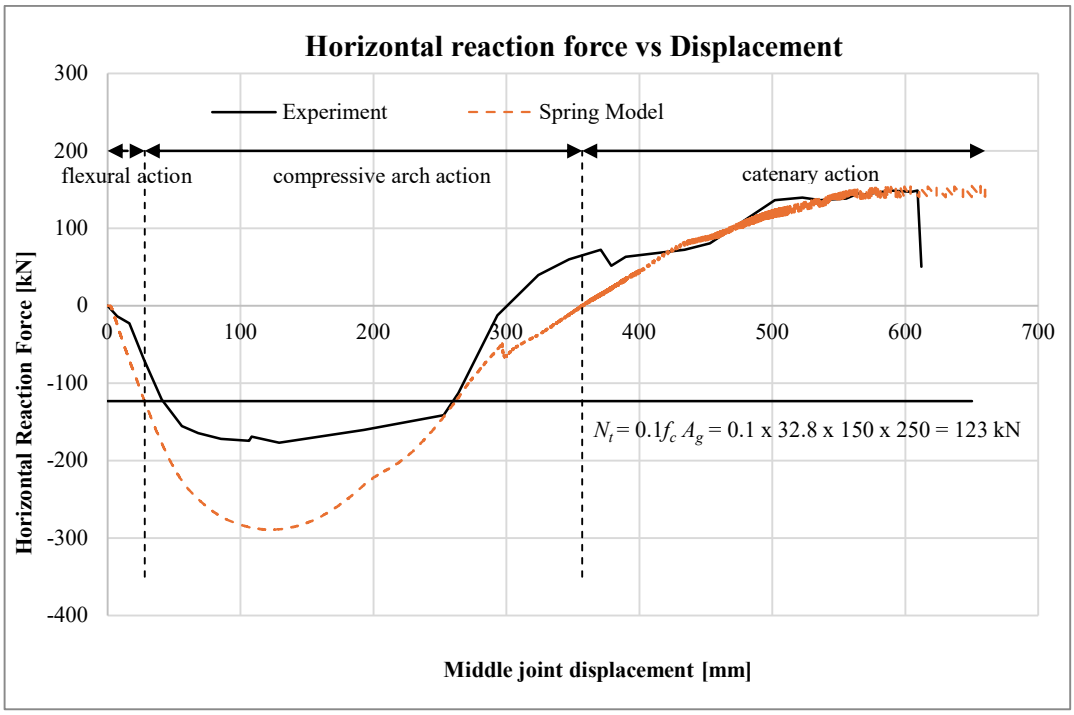

Figure 6.7 *Comparison of the horizontal reaction force and the middle joint displacement between experiment and the spring model where N_t represents the horizontal reaction force used to differentiate flexural action and CMA.*

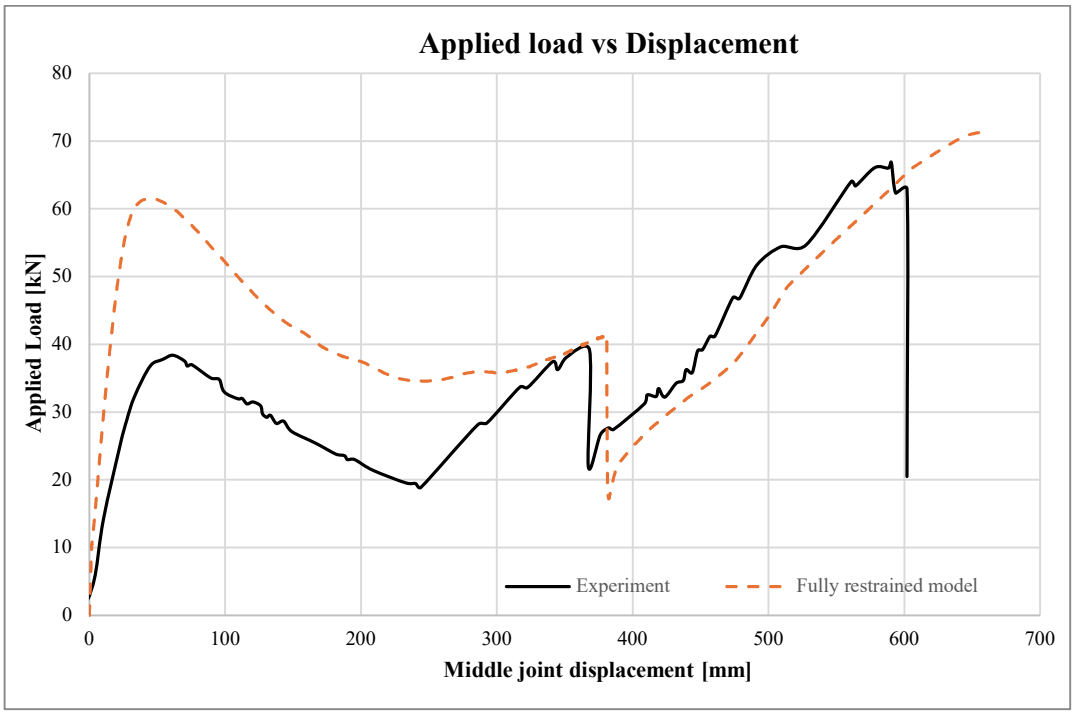

Figure 6.8 *Comparison of the applied force to the middle joint displacement between experiment and the fully restrained model.*

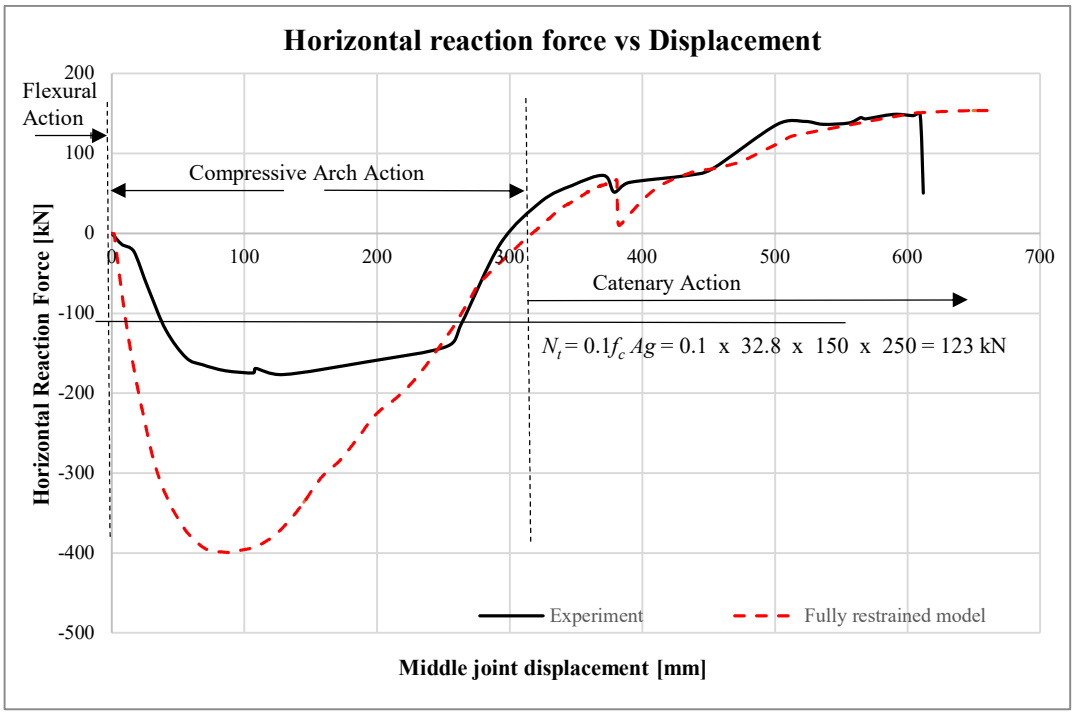

Figure 6.9 *Comparison of the horizontal reaction force and the middle joint displacement between experiment and the fully restrained model where N_t represents the horizontal reaction force used to differentiate flexural action and CMA.*

6.4.2 FEM against analytical calculations

A comparison between analytical calculations and FE results is shown in Table 6.1. The results indicate very good agreement between the capacity under catenary action according to the FE model and the capacity calculated analytically. Table 6.1 shows the comparison between the analytical calculation (according to Section 5.3) and the results from the FE both of *fully restrained* and *spring models* (see Figures 6.2 to 6.5).

Table 6.1 Comparison between FEM results and analytical results.

FEM results		Analytical results		Differences [%]	
Catenary action capacity	Horizontal reaction force	Catenary action capacity	Horizontal reaction force	Catenary action capacity	Horizontal reaction force
[kN]	[kN]	[kN]	[kN]	[%]	[%]
64	154	68	156	6	1

As shown in Table 6.1, while the values obtained for catenary action capacity and horizontal reaction force through analytical calculations are smaller than those obtained from FEM, they still exhibit a good level of agreement.

7 Parametric studies

7.1 Introduction

This chapter presents parametric studies conducted after the numerical models in Chapter 6 were validated. The studies examined the effects of span-depth ratio, horizontal stiffness, viscosity parameter, fracture energy, and reinforcement ratio on structural responses.

7.2 Influence of span-depth ratio

The influence of span-depth ratio (L/d) is investigated in this section. L represents the total span length and d represents the effective depth of a RC beam. Beams with higher L/d ratios refer to high slender beams whereas beams with lower L/d ratios refer to less slender beams. Figure 7.1 presents the applied load-displacement curves for four different L/d ratios. It can be seen from the curves that as the slenderness of the beam increased, both the flexural and CMA capacities decreased. It is obvious that the effect of CMA had minor development in the most slender beam (L/d = 30). In addition, the fracture of the bottom rebars at the midspan occurred earlier as the slenderness of the beam decreased which can be seen from the first sudden drop in the curves. For the beams with $L/d \leq 22$, the second sudden drop which represents the fracture of the top rebars could be captured.

Figure 7.2 represents the horizontal reaction force-displacement curves and it shows that after CMA transitions into catenary action (from negative to positive values), the behaviour of the beam might not be significantly affected by the effect of the slenderness ratio. The bottom rebars at the middle joint tended not to contribute to catenary action for beams with lower slenderness ratios because they had already fractured before catenary action developed. However, for the most slender beam (L/d = 30), the bottom rebars at the middle joint seemed able to contribute to catenary action, as the first sudden drop was delayed further.

Additionally, the area under the curve in Figure 7.1 represents the energy absorption. A larger area under the curve indicates that the RC beam can absorb and dissipate more energy before collapsing. From Figure 7.1, it can be observed that the L/d = 17 (less slender beam) curve shows the largest area under the curve, suggesting that this configuration has the highest energy absorption capacity among the other span-depth ratios. This denotes that the RC beam with the L/d ratio of 17 can dissipate the most energy through deformation before reaching its ultimate capacity. On the other hand, the L/d = 30 (high slender beam) curve shows the smallest area under the curve, indicating the lowest energy absorption capacity. This means that the RC beam with the L/d ratio of 30 would have a reduced ability to dissipate energy through deformation.

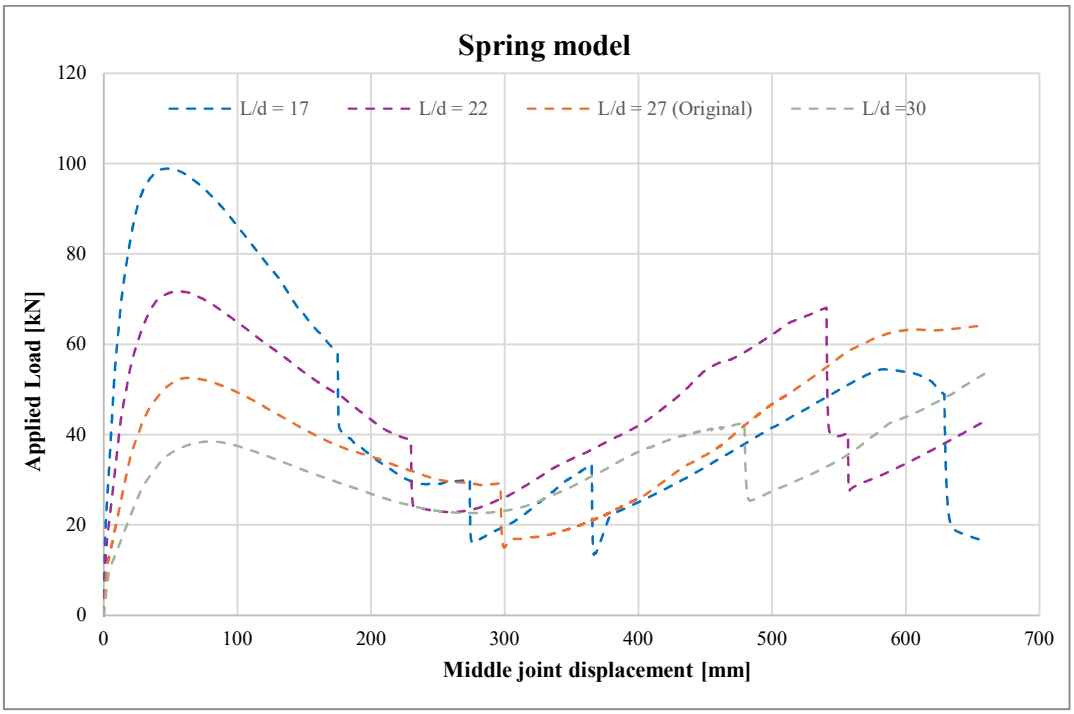

Figure 7.1 *Numerical results for load–midspan deflection relations in the RC beam with the various span-depth ratios.*

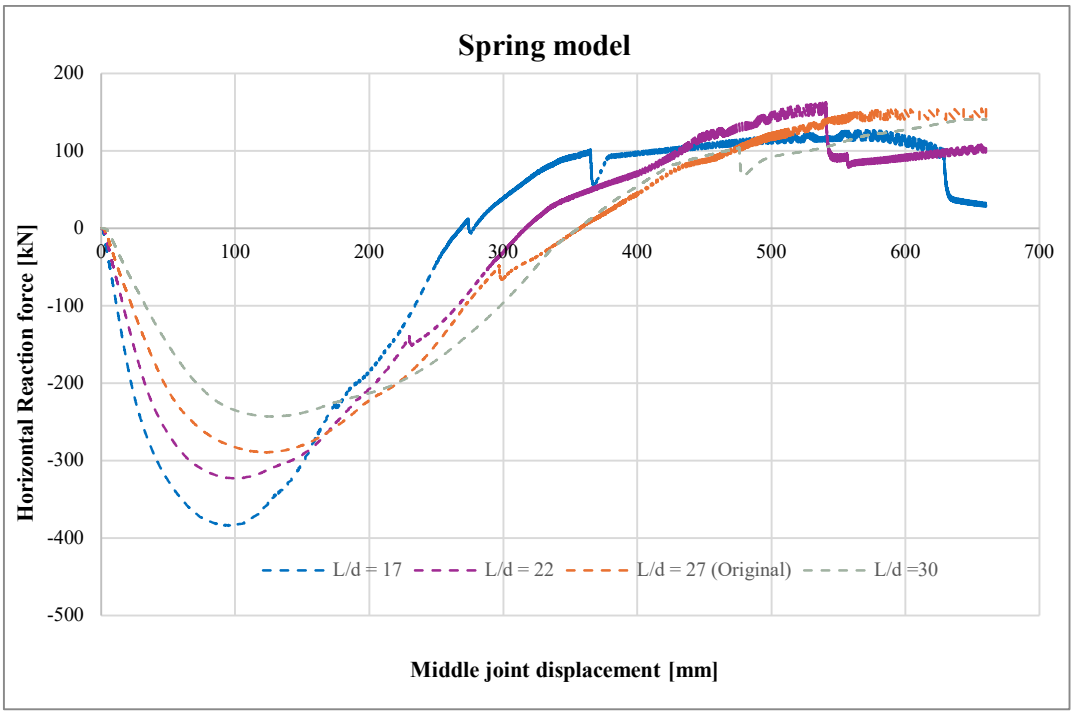

Figure 7.2 *Numerical results for horizontal reaction force–midspan deflection relations in the RC beam with the various span-depth ratios.*

7.3 Influence of horizontal stiffness

Various stiffness of horizontal axial restraints is studied in this section. Equivalent stiffness based on experiment by (Yu & Tan, 2013) is 1×10^5 kN/m. In this parametric study, stiffness is decreased by the factor of 2 and 5 using *spring model* to observe the behaviour of the beam and catenary action capacity. Note that horizontal axial restraints at the end columns are applied by providing spring stiffness in ABAQUS.

Figures 7.3 and 7.4 show applied load-displacement and horizontal reaction force-displacement with three different stiffness of horizontal restraints respectively. It can be seen that the horizontal spring stiffness influences both of applied load and horizontal reaction force during flexural action and CMA. Increased stiffness results in a higher applied force and horizontal reaction force, whereas decreased stiffness leads to lower forces. However, the horizontal stiffness does not influence the catenary action. Catenary action begins at 360 mm when the load shifts from compression to tension. The capacity for catenary action remains similar regardless of variations in horizontal stiffness within the studied range.

While this thesis studied stiffness reductions by factors of 2 and 5, the development of CMA and catenary action could be captured. However, decreasing the horizontal stiffness by a large factor, the beam might not develop CMA and catenary action sufficiently since the adequate restraints are required to obtain these membrane actions. Stiffer horizontal axial restraint might increase the forces in flexural action and CMA. However, after the onset of catenary action, the responses of the beam might not be affected by the horizontal stiffness as it can be seen in Figures 7.3 and 7.4 that the structural responses for all studied cases were similar which means that these studied horizontal stiffness are sufficiently high.

Table 7.1 Parametric study with various horizontal stiffness.

Model	Horizontal stiffness [kN/m]
1	2×10^4
2	5×10^4
3	1×10^5

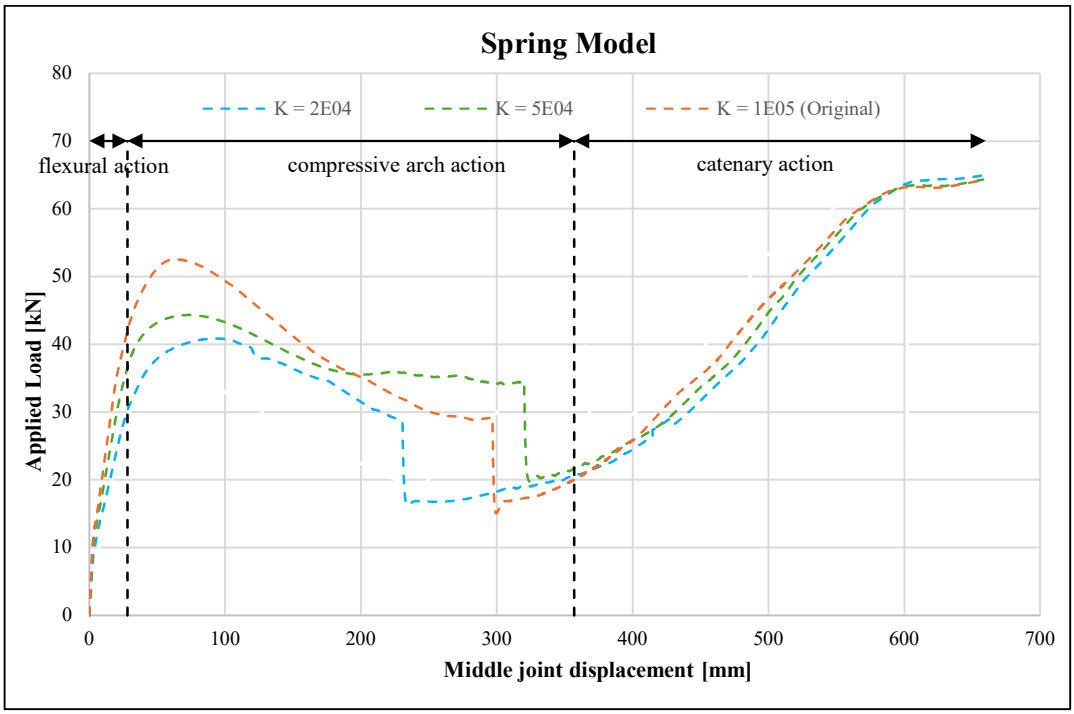

Figure 7.3 *Numerical results for load–midspan deflection relations in the RC beam given the horizontal stiffness K with 1×10^5, 5×10^4, and 2×10^4 kN/m.*

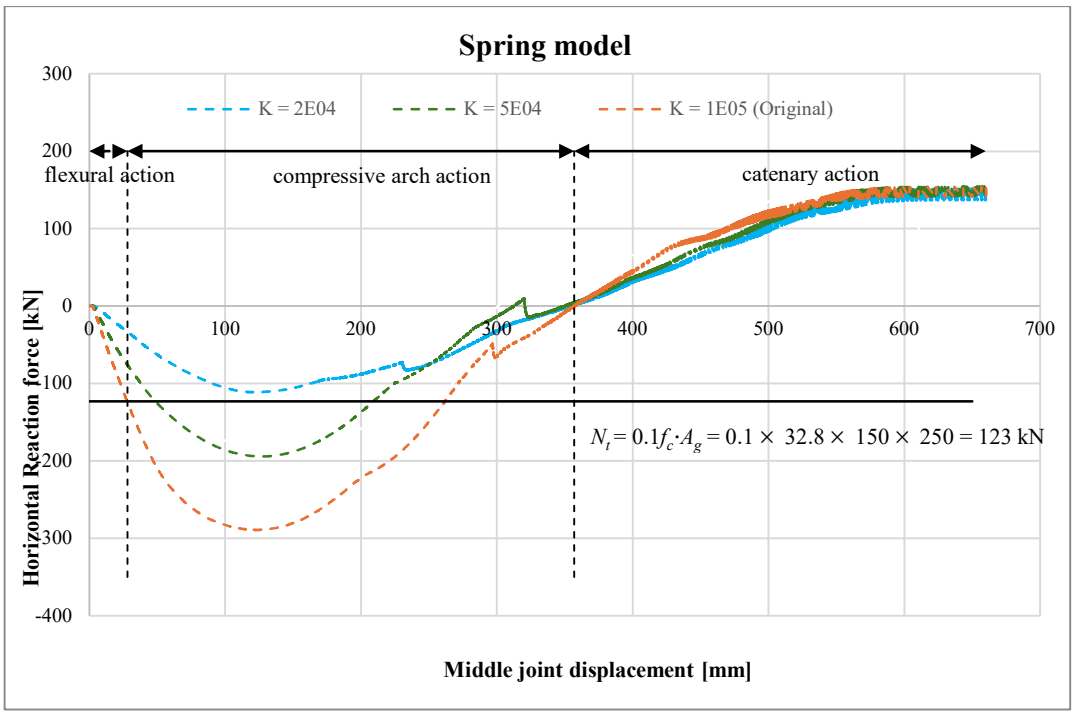

Figure 7.4 *Numerical results for horizontal reaction force–midspan deflection relations in the RC beam given the horizontal stiffness K with 1×10^5, 5×10^4, and 2×10^4 kN/m.*

7.4 Influence of viscosity parameter

As mentioned in Section 4.7.1, the viscosity parameter μ, can be defined to implement the viscoplastic regularization in the FE analysis in order to overcome the challenging convergence issues in nonlinear concrete problems. The viscoplasticity allows stresses to exceed the yield surface, which enhance the convergence rate for the damaged concrete in the strain-softening regime. In order to effectively implement the viscoplastic regularisation while maintaining accurate findings, it is crucial to establish a suitable value for the viscosity parameter. This value should ideally be smaller than the characteristic increment in the step of the nonlinear solution. (Mathern & Yang, 2021b).

A parametric study was conducted to determine the appropriate value for the reference FE model by studying the viscosity parameter in the range of 10^{-4} – 10^{-7}. The load-deflection curves regarding different viscosity values are depicted in Figure 7.5 and Figure 7.6 for the fully restrained and spring model respectively, illustrating how the viscosity value can affect the FE analysis. A value that is too large (e.g. $\mu = 10^{-4}$), tends to diminish the precision of the numerical outcomes, resulting in an overestimation of the structure's response and making it difficult to clearly detect the failure of the reinforcement.

A value that is too small (e.g. $\mu = 10^{-7}$), can lead to a decrease in the convergence rate and potentially even cause the analysis to be aborted. Viscosity values of 10^{-5} or 10^{-6} show a more suitable response regarding the convergence problems and where the reinforcement failure takes a place in the numerical analysis. However, viscosity parameter of 10^{-6} caused the analysis to be aborted for the *spring model*. Hence, the value of viscosity parameter was selected as 10^{-5} in the reference FE models.

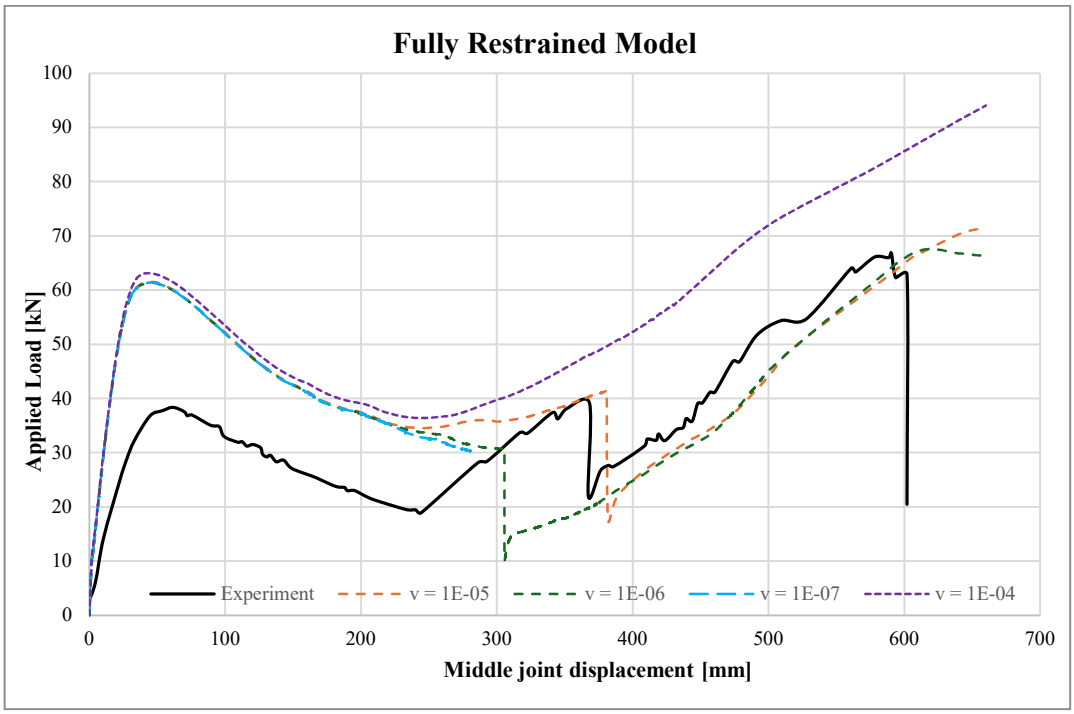

Figure 7.5 *Numerical results for load–midspan deflection relations in the RC beam given the viscosity parameter μ ranging from 10^{-4} to 10^{-7}.*

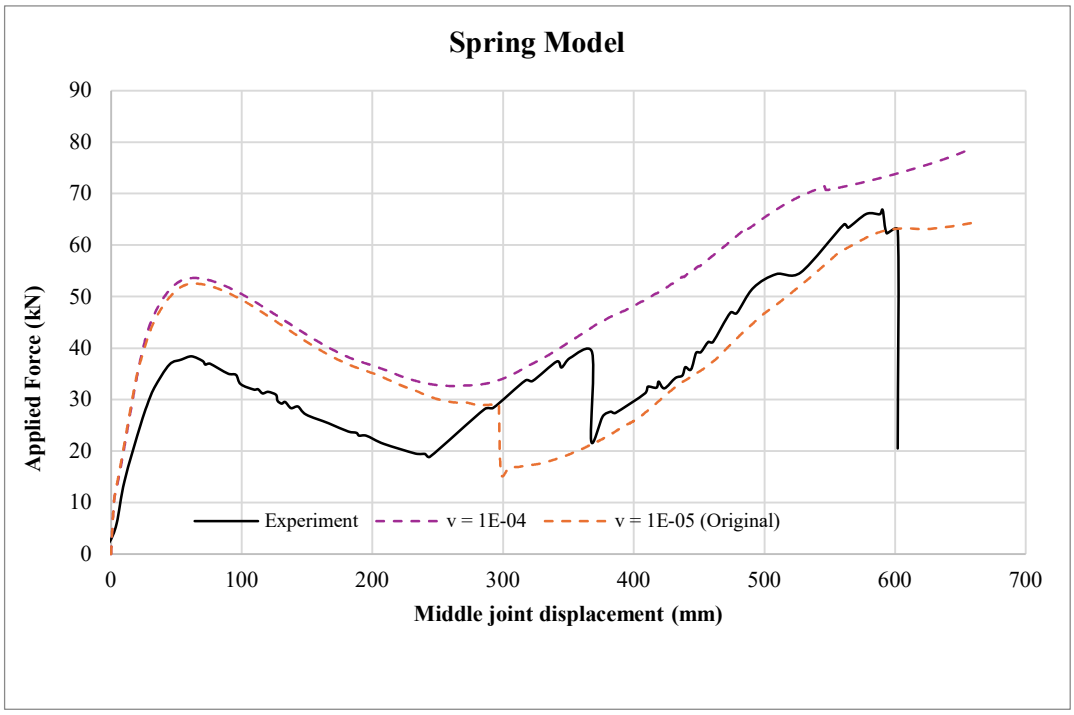

Figure 7.6 *Numerical results for load–midspan deflection relations in the RC beam given the viscosity parameter μ ranging from 10^{-4} to 10^{-5}.*

7.5 Influence of fracture energy

Additionally, a comprehensive analysis was conducted to examine the impact of the concrete fracture energy on the behaviour of the beam. This parameter is closely connected to crack initiation and propagation. The fracture energy, G_f, in the reference model was initially set at 136.8 N/m. However, equation 2.4 allowed for a parametric investigation for other values of the fracture energy (e.g. 100 and 200 N/m) for the concrete, which had a mean tensile strength, f_{ctm}, of 2.88 MPa.

In this investigation, the post-peak softening behaviours and the stress-crack opening model were typically represented by to the bilinear softening model utilised in the reference FE model based on the Model Code 2010, see Figure 2.4. However, the stress-crack opening model indicated that the modelling choice of the fracture energy value has a significant effect on the crack opening width, see Figure 7.7. A higher fracture energy indicates that the concrete has the ability to absorb a greater amount of energy before cracks initiate and spread under tensile loading. This leads to a more ductile behaviour, providing the beam with higher tensile strength that can allow the cracks to develop gradually rather than suddenly.

The load-displacement curves produced from the numerical study for the two models are shown in Figures 7.8 and 7.9. The results show that, overall, the modelling options for the three fracture energy values have minimal impact on the simulated load-deflection curves. Due to its major influence on the tensile behaviour of concrete, fracture energy has a limited impact on catenary action, as increased fracture energy leads to slower crack propagation. The catenary action is mostly influenced by the reinforcement bars rather than the concrete. Therefore, it is expected that the impact of fracture energy on the load-displacement curve and catenary action will be minimal.

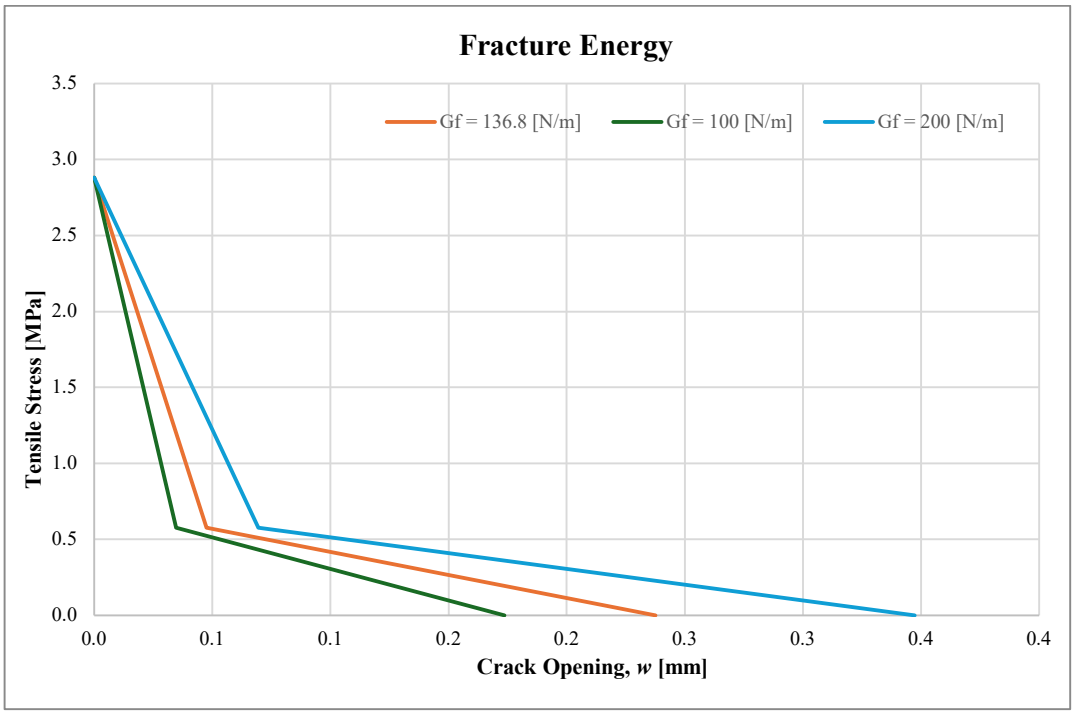

Figure 7.7 *Concrete tensile behaviours considering the uncertainty of the fracture energy G_f.*

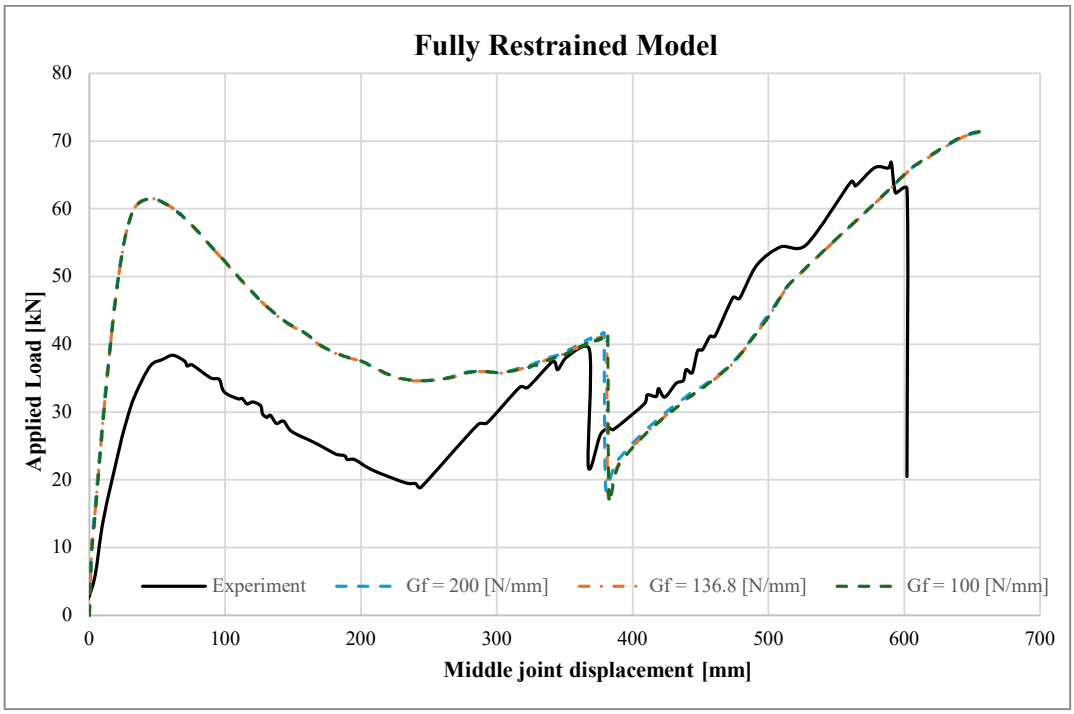

Figure 7.8 Numerical results for the load–midspan displacement relations obtained in the parametric study on the modelling choices for the fracture energy G_f of fully restrained model.

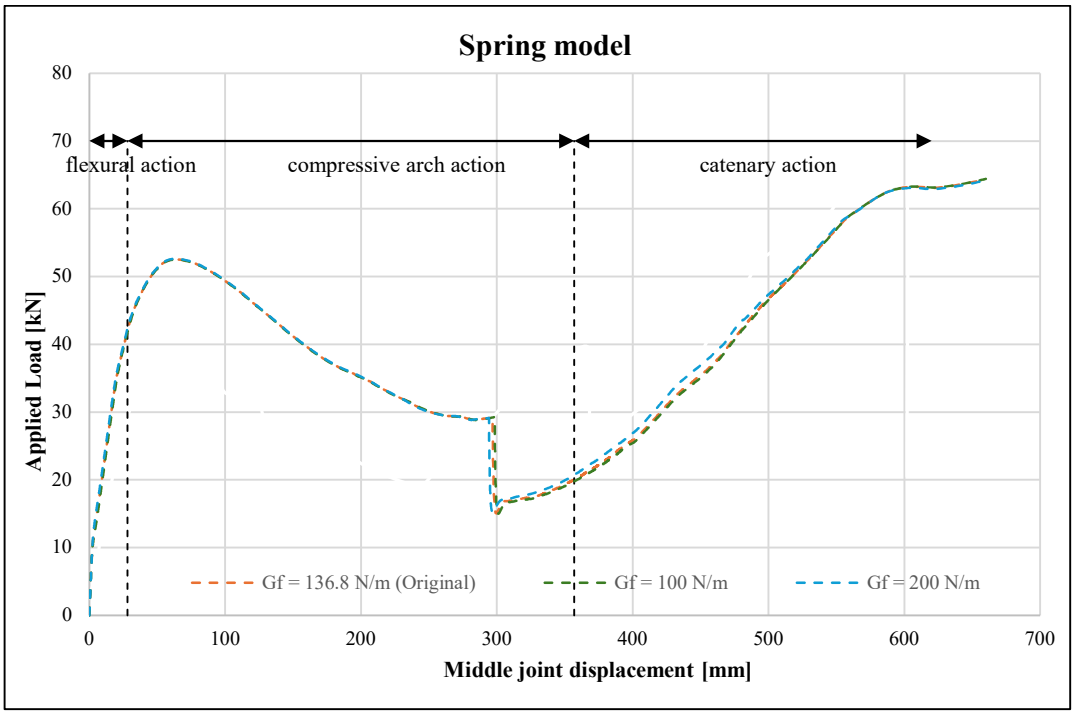

Figure 7.9 Numerical results for the load–midspan displacement relations obtained in the parametric study on the modelling choices for the fracture energy G_f of spring model.

7.6 Influence of reinforcement ratio

This study was conducted using the *fully restrained model* to evaluate the impact of different reinforcement ratios, ρ, under the static response. Figure 7.10 illustrates the relationship between the middle joint displacement and load for various diameters of the reinforcing steel (e.g. ϕ10, ϕ12, and ϕ16) in comparison to the experiment by Yu & Tan (2013). In this study, the experiment utilized the same material properties for the reinforcement. However, only the area of the rebars differed for ϕ10, ϕ12, and ϕ16. The top reinforcement ratios were 0.63%, 1.01%, and 1.81% for ϕ10, ϕ12, and ϕ16, respectively. Nevertheless, the bottom reinforcement ratio was 0.42% for all cases.

It is evident that greater reinforcement ratio of reinforcing steel enhances the load capacities for both flexural action and membrane actions of the RC beam as shown in Figure 7.10. In this study, the width of the beam was not changed, and the effective depths were slightly different. Therefore, increasing the size of the reinforcing steel will result in a greater reinforcement ratio.

Figure 7.10 shows that the top rebars affect the structural responses before and after the rupture of the bottom rebars at the middle joint. The bottom rebars affect the responses only before their rupture at the middle joint and they might not contribute to catenary action.

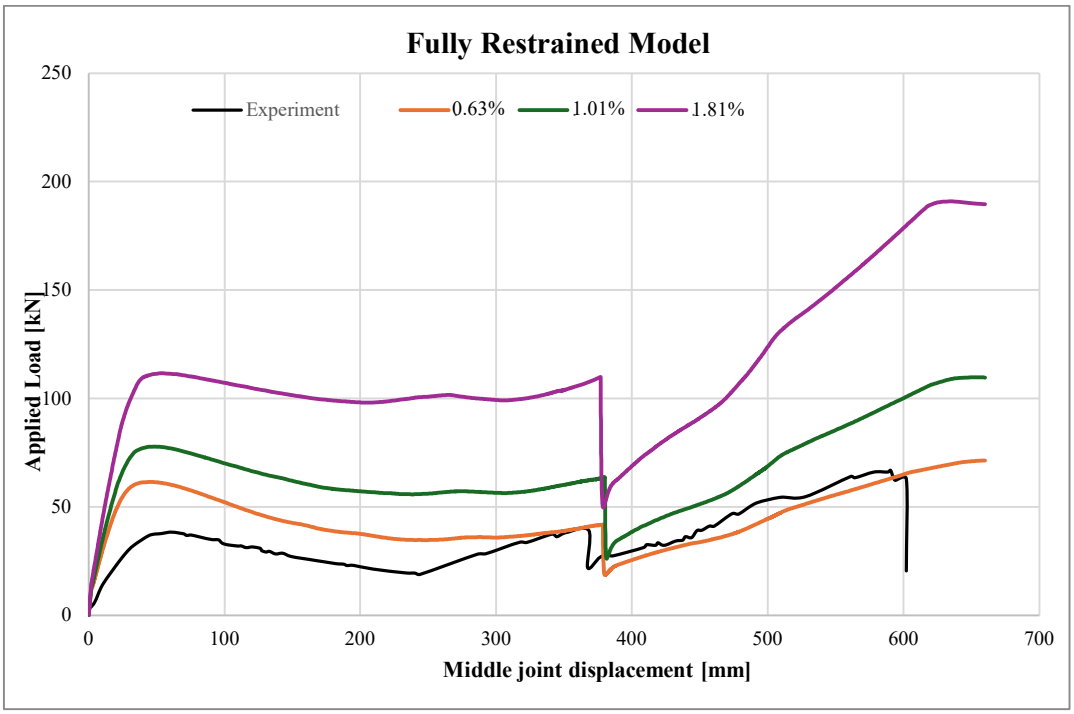

Figure 7.10 Numerical results for the load–midspan deflection relations for different ratios of the reinforcing steel.

8 Discussion and Conclusions

8.1 General

This chapter presents a brief overview and discussion of the relevant findings collected during the thesis development. The discussion focuses on the findings obtained from the non-linear finite element analyses.

8.2 General description

The thesis utilised Finite Element Analysis (FEA) software, specifically ABAQUS, to simulate and study catenary action in RC beams. These analyses are important for comprehending the behaviour of RC beam when subjected to large deformations caused by the removal of the central support, which was imitated by a point load at the middle span of the beam.

The research significantly highlighted the development of catenary action in beams. This condition happens when the beam exceeds its usual bending and compression limits and starts to primarily resist loads through tension in the reinforcement instead of compression in the concrete. The FEA results provided a comprehensive analysis of the conditions that start the catenary action and the resulting impact on the structural load capacity.

8.3 Finite element analysis results

The static analysis was conducted utilising the RC beam models with various boundary conditions. FEA results revealed some inconsistencies with the experimental benchmarks, specifically in terms of the applied load capacities and the displacement characteristics. The FE model predicted comparable deflections to the experimental observations when loads were applied at midspan. However, the applied load in the FE model was larger than the observed load in the experiments. This difference may be attributed to the simplifications made in the boundary conditions of the beam. Nevertheless, the load-displacement curves obtained from the static analysis generally aligned with the experimental data, suggesting that the models well-described the overall structural responses.

As the deformation increased, there was a noticeable transition from flexural action to CMA, and subsequently catenary action. This shift is characterised by a transition from compressive forces to tensile forces. This signifies the initiation of catenary action as the principal load-bearing mechanism of the beam once other support mechanisms, such as flexural action and CMA, have been depleted. The catenary action could significantly withstand due to the top rebars which played a significant role in enabling this mechanism since after the fracture of bottom rebars at the middle joint, the structural response depended on the top rebars. These top rebars were under tension in all sections when the beam was in the catenary action stage.

Analysis of sensitivity revealed that the precision of the model was greatly influenced by the size of the mesh size of the material. Modifications to these parameters resulted in enhancements in the level of agreement between the simulated findings and the experimental results, specifically with regard to the load-displacement relationship and the catenary action.

The FEM approach followed the methodology proposed by Mathern & Yang (2021) that the stress-strain relationship for the compressive behaviour of the concrete and for reinforcement shall be modified by increasing post-peak strain, considering strain localization to improve the accuracy of the numerical models. However, the input critical fracture length, L_{cr} , which was intended to provide a similar output did not match the slope in the crushing zone of the concrete compared to the reference experimental results since the slope decreased more

rapidly in the post-peak branch, indicating a more brittle behaviour of the concrete in the crushing zone. This discrepancy could be attributed to the simplifications in the model. Specifically, stirrups were not included in the model. Stirrups enhance the ductility of the concrete through confinement, leading to a more gradual decrease in the post-peak branch of the compressive stress-strain curve. Hence, the output L_{cr} differed from the input L_{cr}. The output value was 10 mm whereas the input value for the concrete was 150 mm.

Parametric studies explored several critical parameters affecting the load-displacement relationships of the RC beam through the FE analysis. The study of the viscosity parameter determined that a value of $\mu = 10^{-5}$ is an optimal setting for balancing accuracy and convergence rate. It was shown that high viscosity value ($\mu = 10^{-4}$) resulted in a decrease in the accuracy of the numerical results and delayed the ability to clearly identify the failure of the reinforcement whereas the models were aborted due to the convergence issue when using low viscosity values ($\mu = 10^{-6}$ to $\mu = 10^{-7}$).

The span-depth ratio (*L/d*) is one of the critical factors for determining the behaviour and load capacity of RC beams. This ratio represents the slenderness of the beam, with higher *L/d* ratios indicating more slender beams and lower *L/d* ratios indicating less slender beams. From the results, less slender beams showed higher load capacities in the flexural action and CMA, as well as higher energy absorption capabilities. However, they tended to have a lower catenary action capacity compared to highly slender beams. In contrast, highly slender beams had lower load capacities in the flexural action and CMA. Nevertheless, they were more likely to develop catenary action because of the large deflections which are important to cause this mechanism. The contribution of bottom rebars also varied with beam slenderness. In less slender beams, bottom rebars at the middle joint typically fractured before the onset of catenary action, limiting their contribution to this mechanism. Conversely, in the most slender beam (*L/d* = 30), the bottom rebars appeared to contribute to catenary action, as evidenced by the delayed occurrence of the first sudden drop in load capacity. It's worth noting that after the transition from CMA to catenary action, the behaviour of the beams appeared to be less influenced by the slenderness ratio.

The horizontal stiffness had an impact on the flexural action and CMA. Higher horizontal stiffness values resulted in higher load capacities and horizontal reaction force during flexural action and CMA. However, with these different values of the horizontal stiffness, the system was sufficient to develop CMA and catenary action. After the onset of catenary action, the studied horizontal stiffness values did not influence the structural response. It should be noted that sufficient restraints at the supports are needed to obtain membrane actions.

The parametric study of the fracture energy, G_f, aimed to assess the impact of variations in the concrete's ability to absorb energy influence crack propagation and the RC beam's overall ductile behaviour. The study indicated that fracture energy largely affects the growth of cracks rather than the overall capacity to bear loads.

An investigation was conducted to assess the influence of varying reinforcement ratios of the fully restrained RC beam. Increasing the reinforcement ratio was discovered to increase the load capacities. In addition, it was found that top rebars affected the structural responses before and after the rupture of the bottom rebars at the middle joint.

8.4 Analytical analysis results

The catenary action capacity calculated using the simplified equation was close to the capacities obtained from numerical models and experiment, approximately 68 kN. The ultimate strength and the area of top rebars at the supports were chosen to calculate the

capacity in the simplified equation. The rotation angle at catenary action capacity from analytical calculations was 12.5 degrees, which closely aligns with the DoD limit of 12 degrees. Notably, the analytical calculations do not take shear reinforcement into account, whereas the DoD guidelines require lacing reinforcement. For a conservative design, yield strength of the rebars might be used instead of the ultimate strength and the minimum area of top rebars shall be adopted.

8.5 Conclusions

In this study, the behaviour of the RC beams under the catenary action was investigated and able to simulate using ABAQUS. The contributions of this thesis are summarized as follows:

- Catenary action using the simplified geometry and approach under static condition could be captured in FE modelling with acceptable results.
- Sufficient lateral restraints have a significant effect on the development of catenary action. In other words, catenary action is unable to develop effectively if the boundary conditions allow for lateral movement since lateral restraint is crucial for mobilizing this mechanism.
- The vertical displacement where the bottom rebars fracture occurred might not be predicted accurately by the numerical models but it ranged between 1 to 1.5 times of the height of the beam.
- The higher reinforcement ratio provided higher catenary action capacity.
- Span-depth ratio influences the flexural action and CMA, as well as the energy absorption. After the onset of the catenary action, the behaviour of the beam might not be significantly affected by the effect of the slenderness ratio.
- The fracture energy, G_f, had minor effects on the load-displacement curve.
- Modified post-peak softening branch considering the strain localization is essential to improve the numerical models as proposed by Mathern & Yang (2021). However, the concrete beam and reinforcing steel modelled by using 1D beam element might not provide the good values of the critical fracture length (L_{cr}). Hence, the input critical fracture length was adjusted to accurate the numerical models.
- Viscosity parameter, μ, as an input in concrete damaged plasticity model in ABAQUS should be set to a sufficiently small value to capture the reasonable simulation results and prevent convergence issues during the simulation.
- The stress-strain relationship of the reinforcement used in ABAQUS should be the true stress-strain. It is essential to convert engineering stress-strain to true stress-strain values before inputting data because engineering stress-strain provided the lower stress values as it assumes that area of the rebar remain constant during the tensile test. Consequently, this assumption lowered the catenary action capacity.

The transition from linear to nonlinear behaviour, followed by the development of a yielding plateau and ultimately the catenary action, illustrates the complex interplay between material properties, geometry, and loading conditions. The development of catenary forces and the associated increase in load capacity before failure provide valuable insights into the post-yield behaviour of RC structures.

8.6 Future studies

While this thesis focused on the numerical modelling of tensile membrane action in reinforced concrete beam under static loading conditions using a 1D beam element, further studies and investigations could be suggested as follows:

- Future theses could extend the numerical modelling approach to incorporate other numerical solvers, i.e. dynamic/implicit and dynamic/explicit solvers.
- Future theses could analyse the development of three dimensional (3D) numerical models using solid element for the concrete. This would allow for a more comprehensive representation of the beam's geometry and boundary conditions and provide the results more accurate compared to using a 1D beam element.
- The bond-slip behaviour between the concrete and reinforcement bars could be considered since it more accurately represents their interaction.
- Future theses could involve more reference experiments to validate the modelling approaches and assumptions. Different load types could be considered, for example, uniformly distributed load.
- The detailing of the reinforcement, especially the top rebars could be studied since they impact the catenary action mechanism.

References

Bischoff, P. H., & Perry, S. H. (1991). Compressive behaviour of concrete at high strain rates. *Materials and Structures*, *24*(6), 425–450. https://doi.org/10.1007/BF02472016

CEB-FIB (1991). *CEB-FIB Model Code 1990*. Comité Euro-International du Béton.

CEB-FIB (2013). *CEB-FIB Model Code 2010*. Fédération nternationale du Béton.

CEN (2004). EN 1992-1-1 Eurocode 2: Design of concrete structures - Part 1-1: General rules and rules for buildings. European Committee for Standardization.

Dassault Systémes. ABAQUS Version 6.6 Documentation.

DoD (Department of Defense) (2008). Unified Facilities Criteria (UFC) 3-340-02. Structures to Resist the Effects of Accidental Explosions. DOD, Washington, DC, USA.

Engström, B. (2015). *Design and analysis of continuous beams and columns*.

Gouverneur, D., Caspeele, R., & Taerwe, L. (2013). Experimental investigation of the load–displacement behaviour under catenary action in a restrained reinforced concrete slab strip. *Engineering Structures*, *49*, 1007–1016. https://doi.org/10.1016/j.engstruct.2012.12.045

Grassl, P., & Jirásek, M. (2006). Damage-plastic model for concrete failure. *International Journal of Solids and Structures*, *43*(22–23), 7166–7196. https://doi.org/10.1016/j.ijsolstr.2006.06.032

Johansson, M. (2000). *Structural Behaviour in Concrete Frame Corners of Civil Defence Shelters*.

Mathern, A., & Yang, J. (2021). A Practical Finite Element Modeling Strategy to Capture Cracking and Crushing Behavior of Reinforced Concrete Structures. *Materials*, *14*(3), 506. https://doi.org/10.3390/ma14030506

Mendoza, F. L., & Aphram, J. M. (2017). *Concrete Beams Subjected to Drop-Weight Impact and Static Load*.

Park, R. (1964). Tensile membrane behaviour of uniformly loaded rectangular reinforced concrete slabs with fully restrained edges. *Magazine of Concrete Research*, *16*(46), 39–44. https://doi.org/10.1680/macr.1964.16.46.39

Smith, P. P. (2016a). *An Investigation into Tensile Membrane Action as a Means of Emergency Load Redistribution*.

Yu, J., & Tan, K.-H. (2013). Experimental and numerical investigation on progressive collapse resistance of reinforced concrete beam column sub-assemblages. *Engineering Structures*, *55*, 90–106. https://doi.org/10.1016/j.engstruct.2011.08.040

Yu, J., & Tan, K.-H. (2010). Progressive collapse resistance of RC beam-column sub-assemblages. *Design and analysis of protective structures*

Zhang, C., & Abedini, M. (2023). Strain Rate Influences on Concrete and Steel Material Behavior, State-of-the-Art Review. *Archives of Computational Methods in Engineering*, *30*(7), 4271–4298. https://doi.org/10.1007/s11831-023-09937-6

Appendix A Strain Localization

This section presents determination of the strain localization. According to Matthern & Yang (2021), the input critical fracture length (L_{cr}) must be equal to the output critical fracture length. However, the initial output value did not provide the good result as mentioned in section 4.9, requiring further modification of the critical fracture length, which was then applied in the post-peak branch of the compressive behaviour of concrete and the tensile stress-strain response of the reinforcing steel.

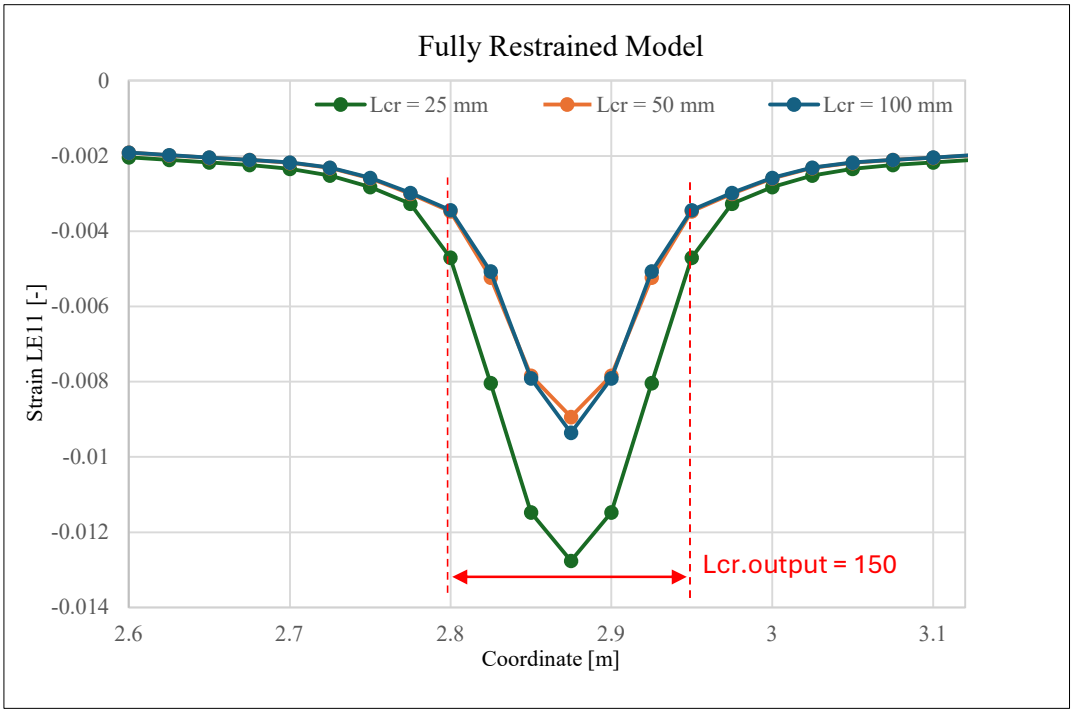

Figure A.0.1 Strain-coordinate at the centre of the beam at top edge for mesh size 25 mm.

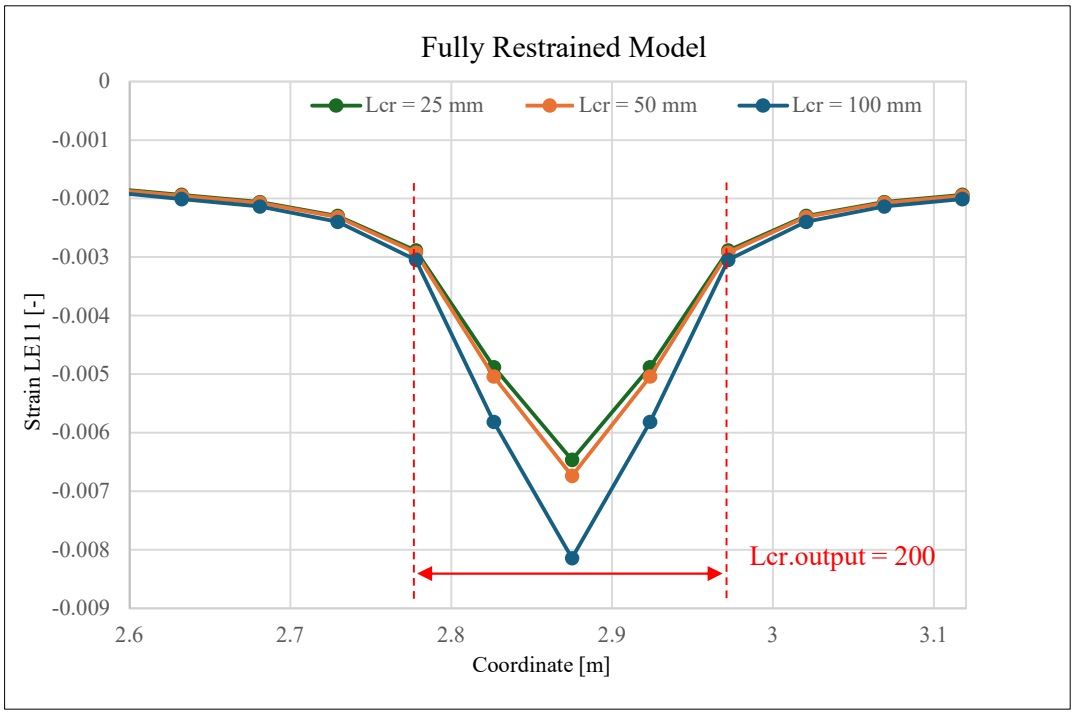

Figure A.0.2 Strain-coordinate at the centre of the beam at top edge for mesh size 50 mm.

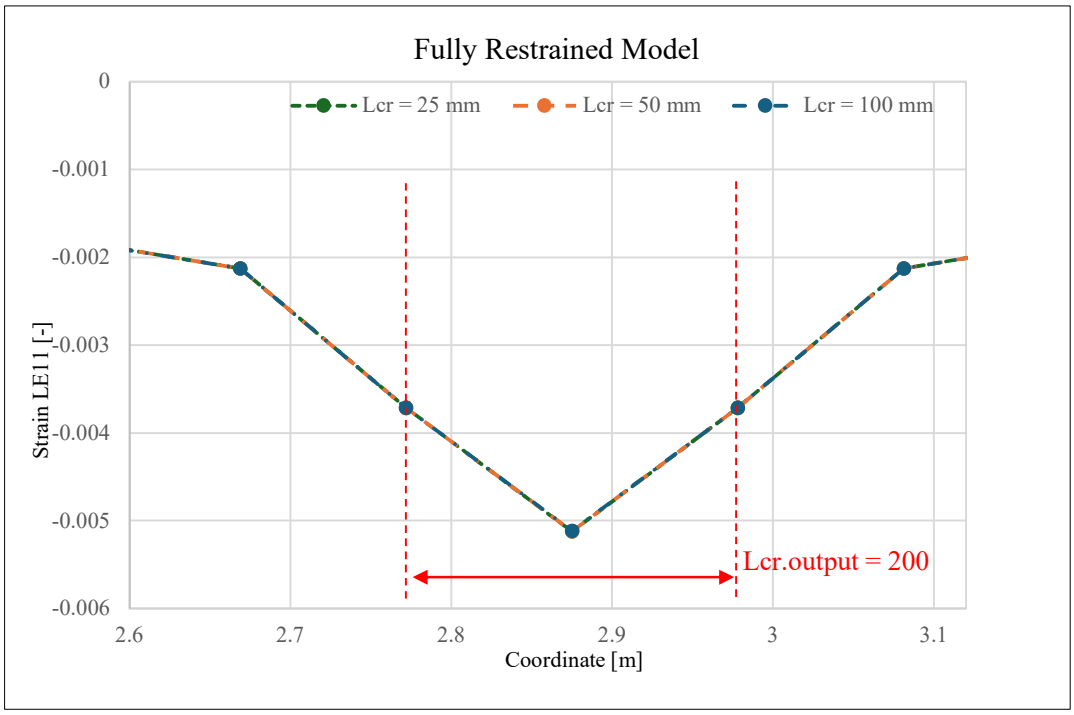

Figure A.0.3 Strain-coordinate at the centre of the beam at top edge for mesh size 100 mm.

Appendix B Analytical Calculation of Ultimate Flexural Capacity

This section presents the calculation of ultimate flexural capacity based on Eurocode 2.

```
%% Input
clc; clear;
syms x;


b = 0.15;                   %width of beam in m
h = 0.25;                   % depth of beam in m
c = 0.02;                   %covering in m

%Dimensions of compressive rebars, 1st layer
diaComp_1 = 9.53;           %diameter in mm
noComp_1 = 2;               %amount of reinforcement

%Dimensions of compressive rebars, 2nd layer
diaComp_2 = 10;             %diameter in mm
noComp_2 = 0;               %amount of reinforcement

%Dimensions of tensile rebars, 1st layer
diaTen_1 = 9.53;            %diameter in mm
noTen_1 = 3;                %amount of reinforcement

%Dimensions of tensile rebars, 2nd layer
diaTen_2 = 10;              %diameter in mm
noTen_2 = 0;                %amount of reinforcement

%Concrete properties
f_ck = 32.8e6;              %Characteristic Compressive strength in 28 days
E_con = 27.663e9;           %Young's Modulus of concrete

f_cd = f_ck/1;              %Designed compressive strength

%Steel properties
f_yk = 511e6;               %Characteristic yield strength
E_steel = 182.611e9;        %Young's Modulus of steel

f_yd = f_yk/1;          %Designed yield strength
yieldStrain = f_yd/E_steel;

%Effective depth tensile layer

%First layer
d1_Ten = h-c-diaTen_1/2000;

%Second layer
if noTen_2 ~= 0
   d2_Ten = h - c - diaTen_1/1000 - c - diaTen_2/2000;
else
   d2_Ten = 0;
end
```

```
%Effective depth compressive layer

%First layer
d1_Comp = c + diaComp_1/2000;

%Second layer
if noComp_2 ~= 0
   d2_Comp = c + diaComp_1/1000 + c + diaComp_2/2000
else
   d2_Comp = 0;
end

areaComp_1 = noComp_1*pi/4 *(diaComp_1/1000)^2

areaComp_2 = noComp_2*pi/4 *(diaComp_2/1000)^2

areaTen_1 = noTen_1*pi/4 *(diaTen_1/1000)^2

areaTen_2 = noTen_2*pi/4 *(diaTen_2/1000)^2


%% Analysis of section
%Assume compressive rebars don't yield
alpha = 0.81;
beta = 0.416;
eqn = alpha*f_cd*b*x + E_steel*(x-d1_Comp)/x *3.5*10^-3*areaComp_1  == f_yd*areaTen_1;

% Solve the initial equation to find x
sol = solve(eqn, x);
x_initial = double(sol);
xu = max(x_initial)
es_comp = (xu-d1_Comp)/xu *3.5*10^-3

%Moment capacity
M_Rd = alpha*f_cd*b*xu*(d1_Ten-(beta*xu)) + E_steel*es_comp*areaComp_1*(d1_Ten-d1_Comp)
```